AN ABSTRACT OF THE THESIS OF

Salvador Martin Aceves-Saborio for the degree of Doctor of Philosophy in Mechanical Engineering presented on November 14, 1989.

Title: Evaporator Analysis for Application to Water-Source and Ice-Maker Heat Pumps

Abstract Approved: Redacted for Privacy
Gordon M. Reistad

Water-source and ice-maker heat pumps share many characteristics. However, each presents different technical difficulties that have prevented them from being used more widely. In a water-source heat pump a very important consideration is to reduce water consumption, while in an ice-maker heat pump a major concern is to reduce the number of deicing cycles while keeping a high performance.

Previous research by this author has indicated that the use of the flow reversal method (reversing periodically the water flow direction in the evaporator) has the effect of partly deicing the evaporator, reducing pressure drop and enhancing heat transfer. This thesis shows the development and application of analytical and numerical models to study the effect of different evaporator parameters on heat pump efficiency, as well as the possible

advantages of using the flow reversal method in a water-source or ice-maker heat pump.

The conclusion reached from these studies is that periodic water flow reversals inside an evaporator with freezing help improve the performance of a heat pump system in two different ways. First, periodic water flow direction reversals serve to enhance heat transfer in the evaporator. Second, reversing the water flow direction also delays ice blockage in the evaporator, or totally prevents blockage from happening. Delaying ice blockage represents a substantial improvement for ice-maker heat pumps, since these may then operate for a longer time without deicing. Preventing ice blockage represents a substantial improvement for water-source heat pumps, since these may then operate at lower water flow rates.

Suggestions for future work include further testing of the flow reversal method for different evaporator geometries, as well as an experimental evaluation of the flow reversal method.

Evaporator Analysis for Application to Water-Source and Ice-Maker Heat Pumps

by

Salvador Martin Aceves-Saborio

A THESIS

submitted to

Oregon State University

in partial fulfillment of
the requirement for the
degree of

Doctor of Philosophy

Completed November 14, 1989

Commencement June 1990

APPROVED

Redacted for Privacy

Professor of Mechanical Engineering in charge of major

Redacted for Privacy

Head of Department of Mechanical Engineering

Redacted for Privacy

Dean of Graduate School

Date thesis is presented November 14, 1989

ACKNOWLEDGEMENTS

I would like to express my heartfelt gratitude to my major advisor, Dr. Gordon M. Reistad, for the interest, the guidance and the support given throughout the duration of my studies. I also want to thank Dr. Steve Binney, Dr. David Burch, Dr. Lorin Davis and Dr. James Welty, for serving as my committee members.

I am also grateful to Dr. Hajime Nakamura, Dr. Jai-Hyo Lee, Dr. Jatila Ranasinghe and Abel Hernandez for the help that they gave me during the development of this thesis. I also wish to express my gratitude to the University of Guanajuato and CONACYT for all their help and support during my studies abroad.

Most importantly, I would like to thank my parents for their never wavering moral support of my pursuits. They provided me with the greatest source of motivation, and my main goal is in pleasing them.

Finally, I am grateful to my cousin Miryam for her help in producing the final copy of this thesis.

TABLE OF CONTENTS

TABLE OF CONTENTS - CONT.

TABLE OF CONTENTS - CONT.

LIST OF FIGURES

LIST OF FIGURES - CONT.

LIST OF FIGURES - CONT.

LIST OF TABLES

NOMENCLATURE

a	maximum ice thickness, Equation (2.7)
A	area
Bo	boiling number
C	cost
Co	convection number
COP	coefficient of performance
Cp	specific heat
D	diameter
e_{det}	energy per unit area required for deicing
E	heat exchanger duty
EX	exergy
f	friction factor
F	interface position
Fr	Froude number
g	acceleration of gravity
G	mass velocity
h	heat transfer coefficient
I	irreversibility generation rate
i_{fg}	enthalpy of vaporization
k	thermal conductivity
l	evaporator circuit length
L	latent heat of solidification
m	mass flow rate
n	coordinate normal to the ice-water interface
N	number of evaporator circuits in parallel
Nu	Nusselt number

NOMENCLATURE - CONT.

p	pressure
P	power cost
P_h	heat transfer perimeter
Pr	Prandtl number
q	heat transfer rate per unit area
Q	heat transfer rate
r	radial cylindrical coordinate
R_i	internal tube radius
R_o	external tube radius
s	adimensional ice thickness
S	area cost
t	time
t_{ap}	application life
t_{block}	time for duct blockage
t_{cycle}	operation cycle length
T	temperature
T_d	reservoir temperature
U	fluid velocity
V	volumetric flow rate
v_2	accelerational pressure drop factor
W	power consumption
x	ice thickness
x_r	refrigerant quality
z	axial coordinate
α	thermal diffusivity

NOMENCLATURE - CONT.

μ	fluid viscosity
ρ	density
ϕ	polar transversal coordinate
ϕ_o	half of the angle between consecutive fins
ϕ_{fo}	frictional pressure drop factor
σ	heat transfer coefficient multiplier
Φ	exergetic efficiency

SUBSCRIPTS

a	area parameter
air	air property
avg	average value
c	freezing condition
can	compressor can condition
comp	compressor condition
cond	condenser condition
det	condition for deice or ice detachment
disln	discharge line condition
dp	caused by pressure drop
dT	caused by heat transfer
e	evaporator condition
exp	expansion device condition
f	liquid property
g	gas property
i	ice property

SUBSCRIPTS - CONT.

in	inlet condition
liqln	liquid line condition
m	material exergy property
o	initial condition
opt	optimal condition
out	outlet condition
pump	pump condition
r	refrigerant condition
s	solid wall property
sucln	suction line condition
tp	two-phase condition

SUPERSCRIPTS

*	non-dimensional variable

EVAPORATOR ANALYSIS FOR APPLICATION TO WATER-SOURCE AND ICE-MAKER HEAT PUMPS

I. INTRODUCTION

1.1 General

A heat pump is a system that extracts thermal energy from a region of low temperature (low temperature reservoir) and makes it available for use at a higher temperature (high temperature reservoir). Heat pumps are classified according to their low temperature reservoir as earth, water or air-source heat pumps. Heat pumps recover and utilize the thermal energy stored in these three sources, and also make low-grade waste heat sources more usable. They are truly an energy conserving and, many times, a cost conserving technology.

The heat pump cycle is illustrated in Figure 1.1. The cycle consists of four basic operations: evaporation, compression, condensation and expansion. A heat pump accomplishes its task of transferring energy from a low temperature reservoir to a high temperature space by using a refrigerant. Space heating is accomplished by transferring energy from the low temperature reservoir (water, earth or ambient air) to the liquid refrigerant. The refrigerant evaporates by the effect of the thermal energy transferred to it. Work is then done on the vapor by a compressor.

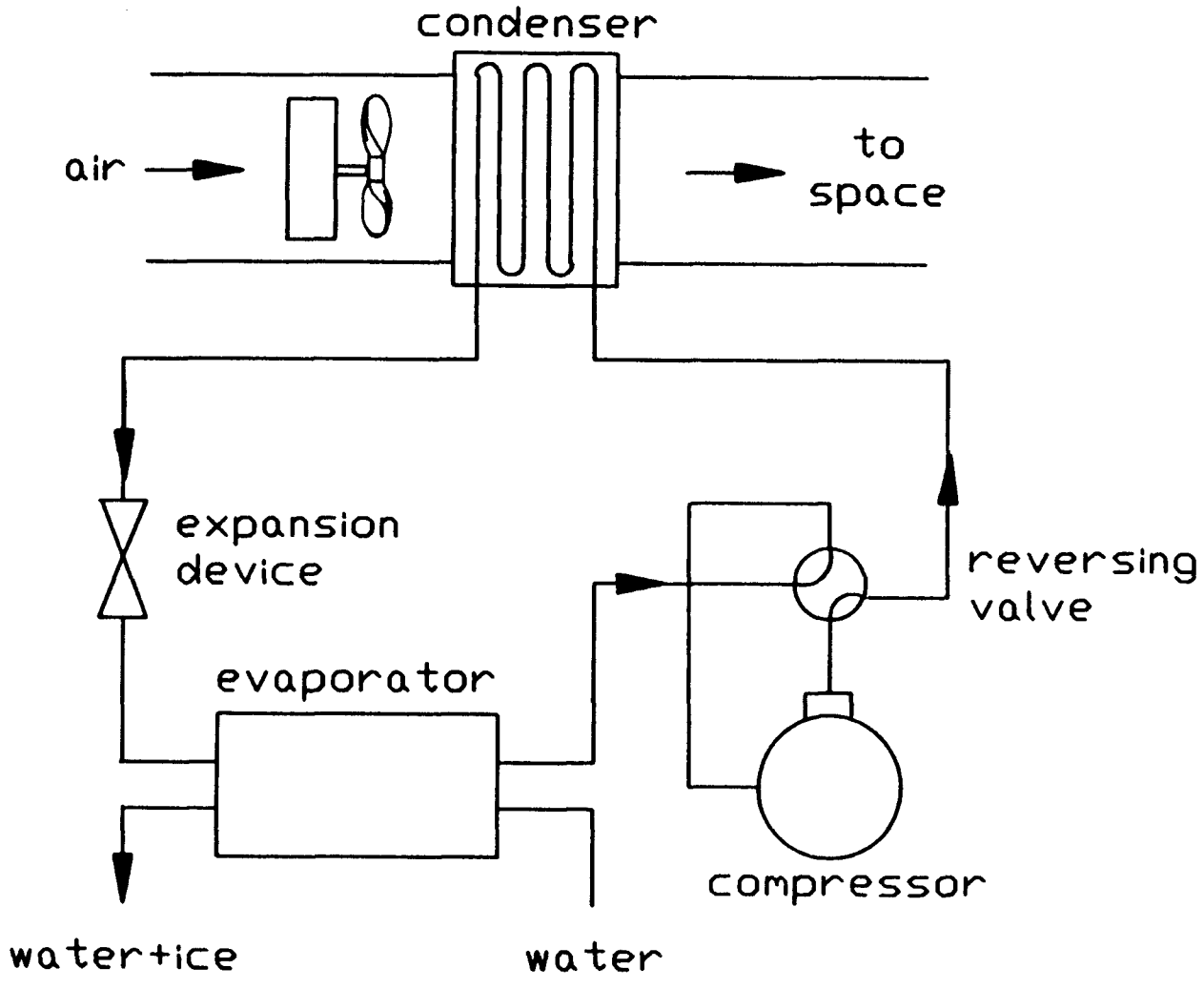

Figure 1.1 Schematic of an ice-maker heat pump operating in the heating mode

This increases the temperature and pressure of the vapor. The vapor is then condensed and the heat of condensation is released to the heated space. The advantage of this type of heating is that more energy is made available for heating than just the work required to operate the heat pump.

A heat pump cycle can be reversed to provide space cooling during the summer months. To accomplish this, most heat pumps have a four-way valve as shown in Figure 1.1. A movement of this valve transforms the indoor heat exchanger into the evaporator, while the outdoor heat exchanger acts as the condenser.

Air is the most commonly used low temperature reservoir for heat pump operation, because ambient air is readily available and free. However, air-source heat pumps present the following major deficiencies:

1. The efficiency and capacity of air-source heat pumps decrease as ambient temperature drops. This condition requires the use of expensive backup heating when the heating demand exceeds capacity.
2. At low ambient temperatures, frost forms on the surfaces of the evaporator. Frost formation insulates the surfaces and impedes air flow through the evaporator, making it necessary to use additional energy for defrosting.
3. Defrosting is usually accomplished by reversing the heat pump cycle. Therefore, no heating energy is delivered from the heat pump to the heating space during the defrosting

cycle, requiring the use of backup heating. Defrost cycles are also a major cause of reliability problems with heat pumps.

Water-source heat pumps obtain thermal energy from water (either surface or ground water) rather than from ambient air. Therefore, they are not subjected to frost formation in the evaporator surfaces. Water-source heat pumps are the ideal choice when a well or a stream with warm water is available. However, the temperature of water in high latitudes is generally low, so that the amount of energy that can be obtained from the water before cooling it to the freezing point may be very small. A very large volume of water would be needed to meet the heating demand of the heated space, and the cost of this water may make the use of a heat pump uneconomical.

Ice-maker heat pumps are a special kind of water-source heat pump that take advantage of the latent heat of solidification of the water to satisfy the heating demand. For this, they freeze part of the water circulating through the evaporator. The purpose of freezing part of the water in the evaporator is to reduce the water consumption by increasing the amount of energy obtained per unit mass of water. The ice formed must be removed from the surfaces periodically, to allow additional ice formation. This need to remove the ice from the evaporator in ice-maker heat pumps introduces the disadvantage of requiring a periodic interruption of the cycle to

deice the surfaces.

It must be observed that a water-source heat pump in which freezing occurs, but where the ice is either not removed from the evaporator or totally melted, cannot be considered to be an ice-maker heat pump, because under these conditions there is no water savings due to the freezing.

The following sections continue the discussion on heat pumps by first presenting an historical background. Next, a section presents a literature survey on the main topic of interest in this thesis, namely, water-source heat pumps and ice-maker heat pumps that use non-conventional water-saving or deicing techniques. The last section gives a precise statement of the problem studied in this thesis.

1.2 Historical Background

Heat pumps have their origins in the early years of the 19th century. The growing understanding of physical processes led to interest in the possibility of pumping heat energy to a higher temperature. Sadi Carnot described in 1824 the theoretical concept of the heat pump. William Thomson (Lord Kelvin), 1852, was the first in proposing a "heat multiplier", as he called the heat pumps.

The first heat pump applications were considered in the 1920s, with improvements on Thomson's paper by Krauss, 1921. Haldane, 1930, analyzed data from a number of refrigerating plants. From his analysis, Haldane was able to

recommend the heat pump as an efficient device for building heating.

In the early 1960s, reversible domestic air-to-air heat pumps achieved an appreciable sales success in the U.S.A. Unfortunately, they were not reliable, because it had not been recognized that a reversible heat pump needs to be more than just an air conditioner with a refrigerant reversing valve added. The models built broke down easily as the heating load increased. These experiences almost destroyed the heat pump industry.

From 1973 to date, heat pump production has experienced a constant growth. This is mainly the result of the increased awareness of the world's limited available energy, high energy costs, and the design and construction of more efficient and reliable heat pump systems.

1.3 Water-Source and Ice-Maker Heat Pump Literature Review

This section presents a literature review on water-source and ice-maker heat pumps, with special emphasis on techniques that aid in reducing water consumption in water-source heat pumps, and techniques that reduce deicing penalty losses in ice-maker heat pumps.

Water-source heat pumps are a well-established technology, with analyses, simulations and experimental results appearing in the literature with some frequency. In most cases, water-source heat pumps use ground water during operation (EPRI, 1985). Ground water has the

advantage over ambient air and surface water that it keeps a more constant temperature throughout the year. Ground water in the United States has temperatures that range from 25°C in the south to 4°C in the northernmost latitudes, with most of the country having temperatures of at least 8°C (EPRI, 1985). This temperature is high enough for water-source heat pumps to operate with a good thermal efficiency. However, ground water water-source heat pumps require the drilling of one or more wells to provide an adequate water supply. Well drilling is expensive, and the investment required may make a water source heat pump uneconomical.

Even if there is no need to drill a new well (because there is one in existence or because surface water is being used), a water-source heat pump may be uneconomical due to the high volume of water necessary. Only 33.6 kJ/kg of energy can be obtained from water at 8°C without freezing some of the water, and usually only a fraction of this amount can be extracted, because ice can form on the evaporator walls well before the water bulk temperature reaches the freezing point. High volumes of water mean high pumping power or high economical cost, in cases where it is necessary to pay for the water. Mei, 1983, determined experimentally the coefficients of performance (COP) of a commercially available water-source heat pump. His results indicate that the power required to pump the water from a well (46 m head) makes a low water flow rate

heat pump preferable to a high flow rate heat pump, even though the COP of a high flow heat pump is better when the pumping power is not taken into account. Reistad et al., 1984, obtained results similar to those obtained by Mei. They compared a water-source heat pump with an air-source heat pump and a dual-source heat pump (air and water). The results indicate that, although water-source heat pumps have the highest COP, they can many times be uneconomical due to the high costs of water and pumping power.

Some alternatives exist in the literature. One is to use an earth-coupled heat pump, where the cold water going out of the evaporator is circulated through a ground coil (a water-to-earth heat exchanger). The ground coil reheats the water, making it possible to use the same water over and over. The water circulated by the ground coil can also be blended with water extracted from the well to get a semi-open circuit that reduces water consumption (Rackliffe and Schabbel, 1986). Reistad et al., 1984, and Lee, 1989, have studied dual-source heat pumps. A dual-source heat pump operates as a regular air-source heat pump for ambient temperatures higher than a certain changeover point and switches to a water-source heat pump when the ambient temperature goes under the changeover point. A dual-source heat pump has a good COP even for low ambient temperatures, since groundwater temperature is fairly constant throughout the year. Water consumption is also substantially decreased, because water is only used when

the ambient temperature is lower than the changeover point.

Still, even a dual-source heat pump requires the use of fairly warm water (6°C or more). For water temperatures under 6°C, like those existing in surface water or in ground water in the northern latitudes, a heat pump cannot operate efficiently without freezing part of the circulating water. Ice-maker heat pumps freeze some of the circulating water to take advantage of the latent heat of solidification of the water and reduce the water consumption. Ice-maker heat pumps give the possibility of using the ice obtained for cool storage, and provide a good economic alternative to other heating methods (Fischer and Nephew, 1976).

However, ice formation in the evaporator surfaces of ice-maker heat pumps reduces the heat pump efficiency, making it necessary to interrupt the heating cycle to deice the surfaces. Therefore, ice-maker heat pumps present similar capacity losses and reliability problems associated with deice cycles as those found in air-source heat pumps.

Insulation of evaporator surfaces caused by ice or frost formation is an important problem in the operation of ice-maker and air-source heat pumps, respectively. Deicing of the surfaces can be accomplished in a number of ways, but it always reduces the effectiveness of the heat pumps, because energy is consumed to deice the surfaces. In addition to this, the heating cycle is usually interrupted during the deicing period.

Baxter (1978, 1980, 1981) studied different methods for ice-maker heat pump evaporator deicing. The results showed that the method of reversing the heating cycle and circulating a stream of warm refrigerant through the evaporator introduces the highest performance penalty. The best method proved to be a dual-fluid deicing system. This system subcools the condensed refrigerant and stores the thermal energy in a secondary fluid until it is needed for harvesting. Harvesting is done by circulating the warm secondary fluid through parallel circuits in the evaporator plates.

Some alternative methods for deicing with reduced energy consumption have been studied in the past. Rinaldi et al., 1977, tried to supercool water in the evaporator without freezing it. The supercooled water was supposed to flow out of the evaporator to a reservoir where ice would form from the supercooled water. This method would provide steady-state operation of the heat pump without the need of interrupting the cycle for deicing. Their experimental work consisted of measuring the maximum supercooling attainable with water flowing over the evaporator surfaces. The surfaces were coated with different substances to reduce the chances of ice formation on the wall. However, the results indicated very low water supercooling (the maximum value recorded was 2.5^{o}C), so that the amount of ice obtained in the reservoir would be negligible, if any. There is also the possibility of having ice build-up in the

evaporator, which would translate into a drop in effectiveness.

Stewart and Dona, 1988, studied the effect of surface coatings in the freezing of electrolytic solutions. They froze the electrolyte in an immersed plate coated with an adhesivity-reducing substance. The result was the self-release of the ice, due to the buoyancy force, after it reached a critical thickness (6 mm). However, the experiments were carried out in a tank with no flow, and their application to flow systems remains to be shown.

Juhola, 1988, introduced an ice-maker heat pump in which ice production takes place away from the evaporator surfaces. In this heat pump, the water inlet flows into a vacuum chamber whose pressure is less than the vapor pressure of the water at $0^{o}C$. Therefore, part of the water evaporates while the rest of the water freezes. The water vapor is then circulated through the evaporator, while the ice can be used for cool storage or just dumped away. Although the idea reduces substantially the ice buildup in the evaporator, the added hardware required (a vacuum pump and a vacuum chamber) will probably limit the applicability of this method.

Aceves-Saborio et al., 1989a, studied a water-source heat pump evaporator with a tube-in-tube configuration (Figure 1.2). The water temperature was low enough for some ice to form in the evaporator. Water was allowed to flow in one direction for a period of time long enough to

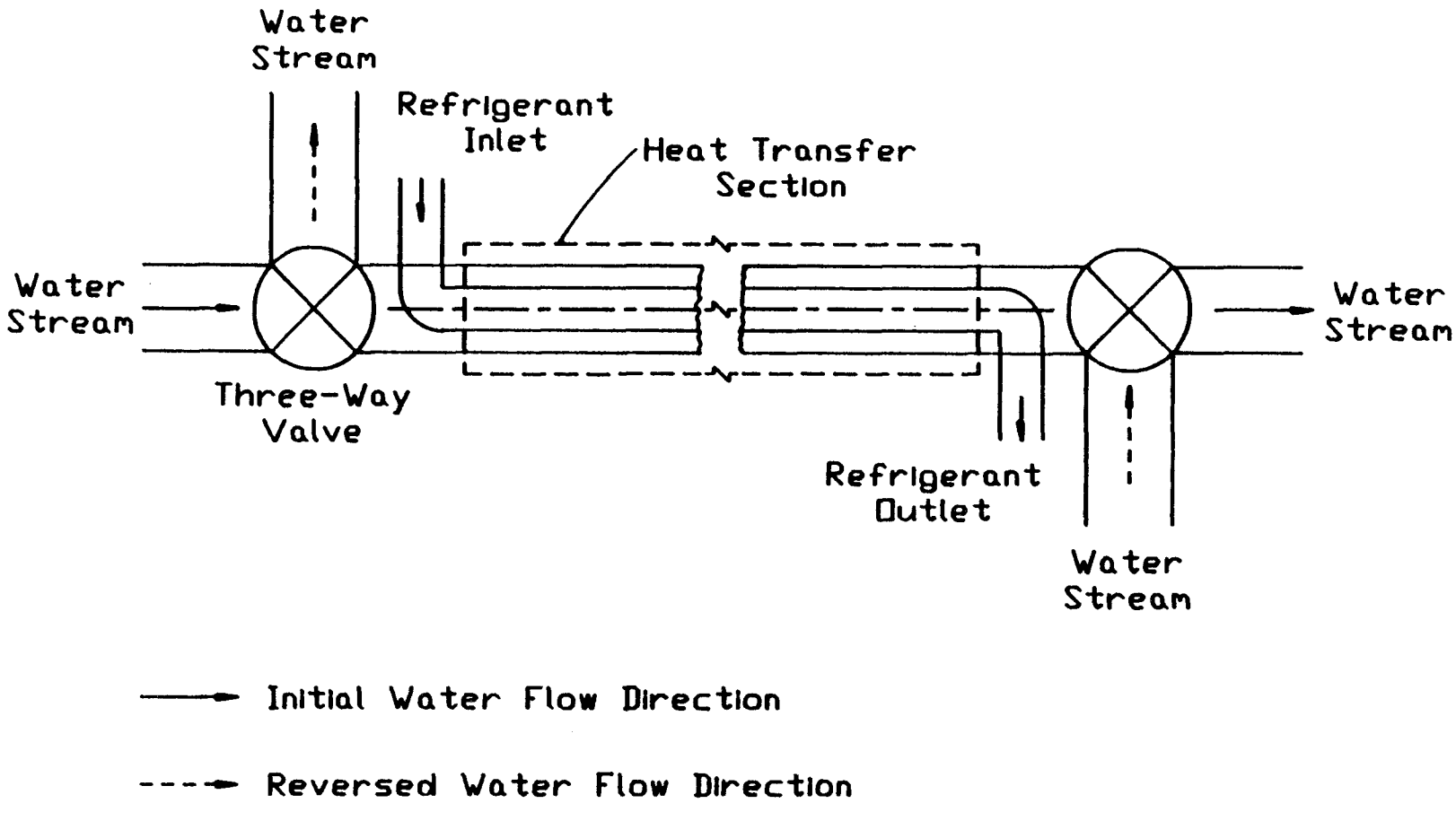

Figure 1.2 General schematic of an evaporator operating under the flow reversal method.

obtain substantial ice formation. Then, the water flow direction was suddenly reversed. The results indicated that reversing the water flow direction improves the heat exchange performance of the evaporator by melting or detaching part of the ice that insulates the surfaces. Therefore, although a total surface deicing was not obtained, there was a substantial improvement when the performance was compared to the performance obtained without reversing the water flow direction (continuous water flow in one direction). Nakamura et al., 1989, also studied the effect of periodic water flow reversals on ice formation inside a duct. The study showed that periodic water flow reversals enhance heat transfer and reduce pressure drops in the duct.

1.4 Problem Statement

Most of the analyses described in the previous section were done for relatively high water temperatures, typical of mid-latitude groundwater. For low water temperatures, such as those usually found in surface water or high-latitude groundwater, it is impossible to obtain a good amount of energy from the water without freezing some of it. Therefore, the only technologies available are either ice-maker heat pumps or water-source heat pumps designed especially to allow some freezing in the evaporator. Both of these require a careful evaporator design.

This thesis contains a study of low-temperature

water-source and ice-maker heat pumps. The study centers on finding evaporator properties that allow water-source and ice-maker heat pumps to operate efficiently at low temperatures.

Water-source and ice-maker heat pumps share a lot of characteristics. However, each presents different technical difficulties that have prevented them from being used more widely. In a water-source heat pump a very important consideration is to reduce water consumption, while in an ice-maker heat pump a major concern is to reduce the number of deicing cycles while keeping a high performance.

The purpose of this thesis is to search for evaporator designs and operation modes that help reduce the water consumption in a water-source heat pump, and help reduce the frequency of the deicing cycles in ice-maker heat pumps. The approach used consists of studying the effect of different evaporator parameters on heat pump efficiency, as well as the possible advantages of using the flow reversal method in a water-source or ice-maker heat pump.

To accomplish the objective just stated, this thesis includes the following.

1. A theoretical analysis that describes qualitatively the desired evaporator characteristics and the different trade-offs that appear when working with low-temperature water-source and ice-maker heat pumps. The theoretical analysis is complemented by a heat pump simulation. The results of

the simulation extend the conclusions obtained in the theoretical analysis.

2. A detailed description of a simulation model to study the transient behavior of a water-source evaporator with freezing, to be used in an extensive heat pump simulation.

3. A description of an existing steady-state heat pump model. This model is used to simulate the high-pressure side of the heat pump. The description gives all the options available for modelling every heat pump component, as well as the options selected for the present study.

4. The details on how the interaction between the time-dependent evaporator model and the steady-state heat pump model takes place, and the conditions under which the steady-state heat pump model predicts accurately the transient heat pump behavior.

5. A heat pump optimization that uses the exergetic efficiency as objective function. Optimizations are carried out for ice-maker heat pumps (heat pumps where deicing is required after a period of time), and water-source heat pumps with freezing (some ice forms in the evaporator, but no deicing is ever required).

6. A detailed discussion on how the different evaporator parameters and the use of the flow reversal method affect the heat pump performance.

7. An irreversibility analysis of the water-source heat pump studied in this thesis.

8. General conclusions and suggestions for future work.

II. ANALYSIS OF ICE-MAKER EVAPORATORS

2.1 Introduction

This chapter presents an analytical and numerical study of ice-maker evaporators. The study is mainly analytical, but it is complemented with the results of a heat pump simulation. The theoretical analysis is carried out for a flat-plate heat exchanger, this configuration being chosen due to its mathematical simplicity. The numerical analysis is done for a tube-in-tube evaporator. The evaporator model is incorporated into a heat pump model to simulate the overall system behavior.

The study presents first the theoretical analysis. This includes heat transfer results with and without deicing, an optimization of an ice-maker evaporator in which the ice self-releases from the surfaces after a critical thickness is reached (deicing with no penalty), and the effect of a deicing penalty in the optimum heat exchanger. The theoretical analysis is followed by the simulation results. The simulation uses detailed models of a tube-in-tube evaporator (Chapter 3) and a heat pump (Chapter 4). The simulation results are used to test the generality of the conclusions reached in the theoretical analysis. The last section in the chapter gives the final conclusions obtained from the analysis.

2.2 Theoretical Analysis

This section presents a theoretical analysis of a flat-plate ice-maker evaporator. This section first describes the evaporator model used for the simulation, and then shows a procedure to calculate evaporator performance with and without deicing.

2.2.1 The Evaporator Model: The evaporator under analysis is shown in Figure 2.1. This is a flat-plate, submerged evaporator. The tank temperature is kept at a constant, and uniform, value, T_d, by adding an adequate amount of mass at a temperature T_o and having good mixing of the water in the tank. The evaporator duty and temperature are constant, and equal to E and T_e respectively. The evaporator temperature Te is negative (the centigrade scale, with the freezing point, T_c, equal to 0^oC, is used for simplicity). Therefore, some ice builds on the evaporator.

Assume a constant heat transfer coefficent equal to h between the liquid water and the ice. The equation for the ice growth is,

$$L \rho \frac{dx}{dt} = q_{out} - q_{in} \qquad (2.1)$$

where,

$$q_{in} = h (T_d - T_c) = h T_d \qquad (2.2)$$

and

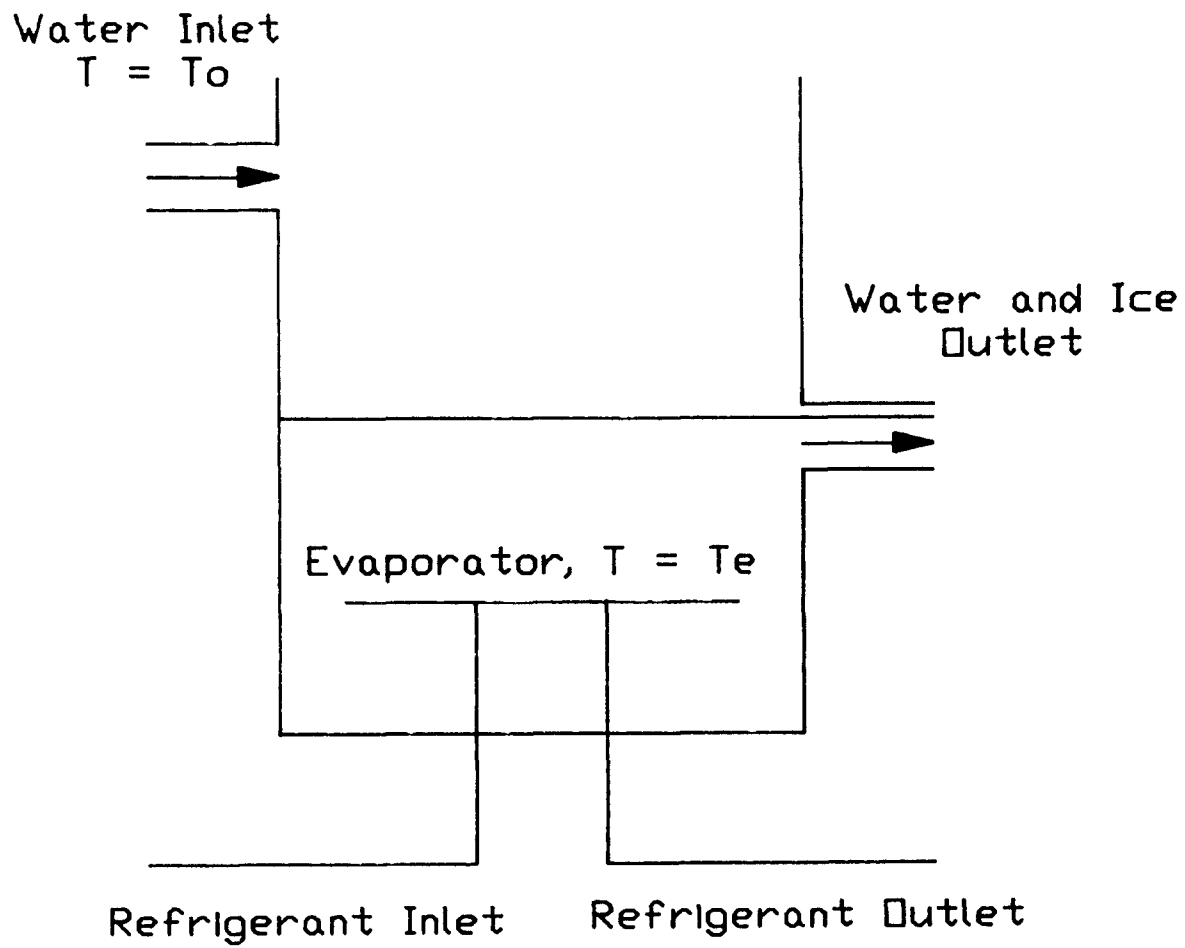

Figure 2.1 Schematic of an immersed, flat-plate, ice-maker evaporator.

$$q_{out} = -k_i \frac{dT}{dx} \tag{2.3}$$

are respectively the heat flux entering and leaving the ice-water interface. L is the latent heat of solidification, ρ is the ice density, x is the ice thickness and k is the thermal conductivity.

The temperature profile in the ice, necessary to calculate the derivative in Equation (2.3), can be obtained as the solution to a complex unsteady-state problem (Carslaw and Jaeger, 1959). However, the ice growth is very slow compared to the heat transfer process. Therefore, the effect of the ice growth can be neglected. This is a usual assumption in this type of problem (Sampson and Gibson, 1981), and is commonly known as the quasi-steady-state assumption. Neglecting the ice growth results in a linear temperature profile across the ice, with $T = T_c = 0$ at the interface and $T = T_e$ at the evaporator surface. Therefore,

$$q_{out} = - \frac{k_i \, T_e}{x} \tag{2.4}$$

and

$$L \, \rho \, \frac{dx}{dt} = - \frac{k_i \, T_e}{x} - h \, T_d \tag{2.5}$$

Now, separating variables and integrating yields an implicit expression for the ice profile as a function of time,

$$t^* \equiv \frac{t\ h\ T_d}{a\ L\ \rho} = -(\ x/a + \ln(1 - x/a)) \qquad (2.6)$$

where,

$$a \equiv -\frac{k_i\ T_e}{h\ T_d} \qquad (2.7)$$

is the maximum thickness reached by the ice. The non-dimensional thickness x/a is easily obtained from Equation (2.6), and the result is used to evaluate the heat transfer rate per unit area into the evaporator,

$$q = -k_i \frac{T_e}{x} = \frac{h\ T_d}{x/a} \qquad (2.8)$$

Figures 2.2 and 2.3 show respectively plots of x/a and the non-dimensional heat flux $q^* \equiv q/hT_d$ as a function of the non-dimensional time t^*. As Figure 2.2 shows, the ice thickness grows fast for a short period after start-up. The rate of growth then decreases, until finally the ice thickness reaches its steady-state value (x=a). Figure 2.3 shows that the heat transfer decreases rapidly as a function of time until it reaches a steady-state, where there is no more ice formation, but only heat transfer due to convection (except for the T_d=0 case, where there is no convection, but the ice keeps growing thicker, without ever reaching a steady-state value).

It is clear from Figure 2.3 that it is disadvantageous to work in steady-state. The low values of q indicate that a large area is required to meet the heat exchanger duty E. From this, it seems obvious that a periodic deicing should

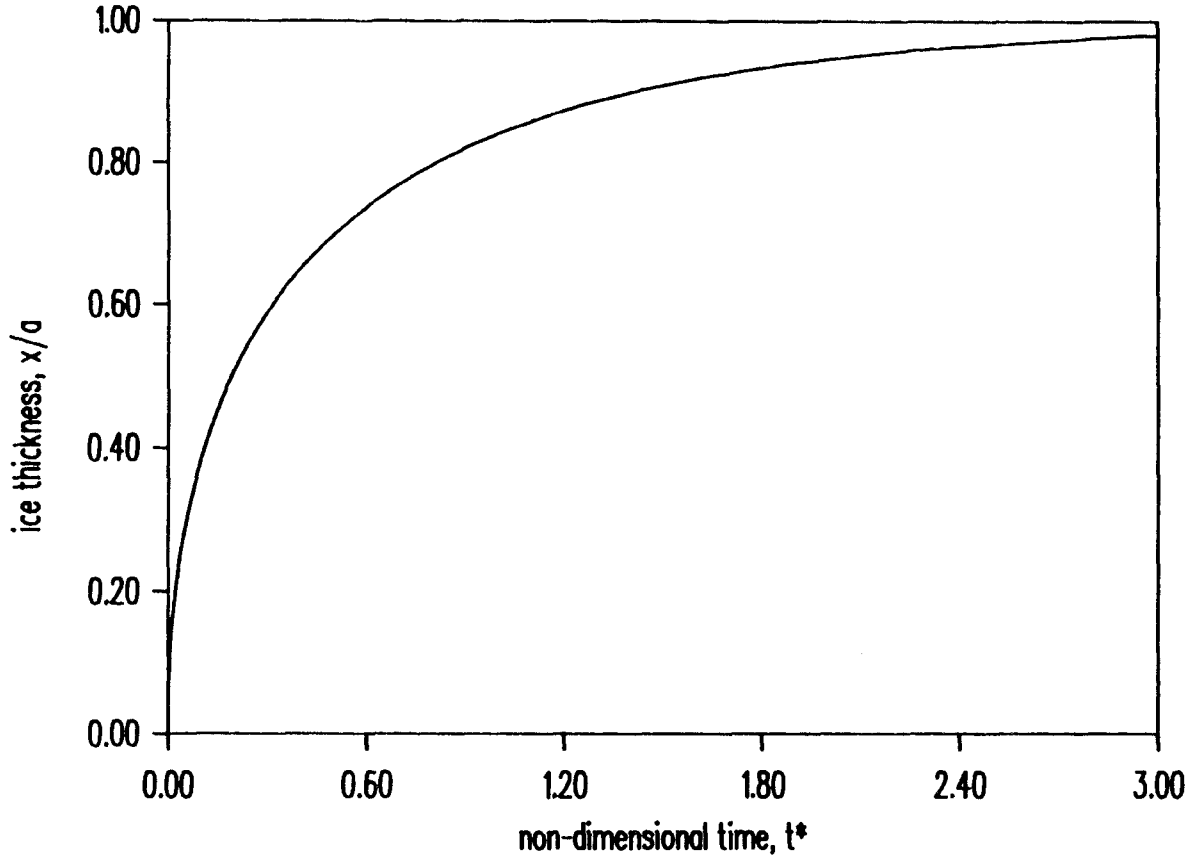

Figure 2.2 Ice thickness as a function of the non-dimensional time for the flat-plate evaporator.

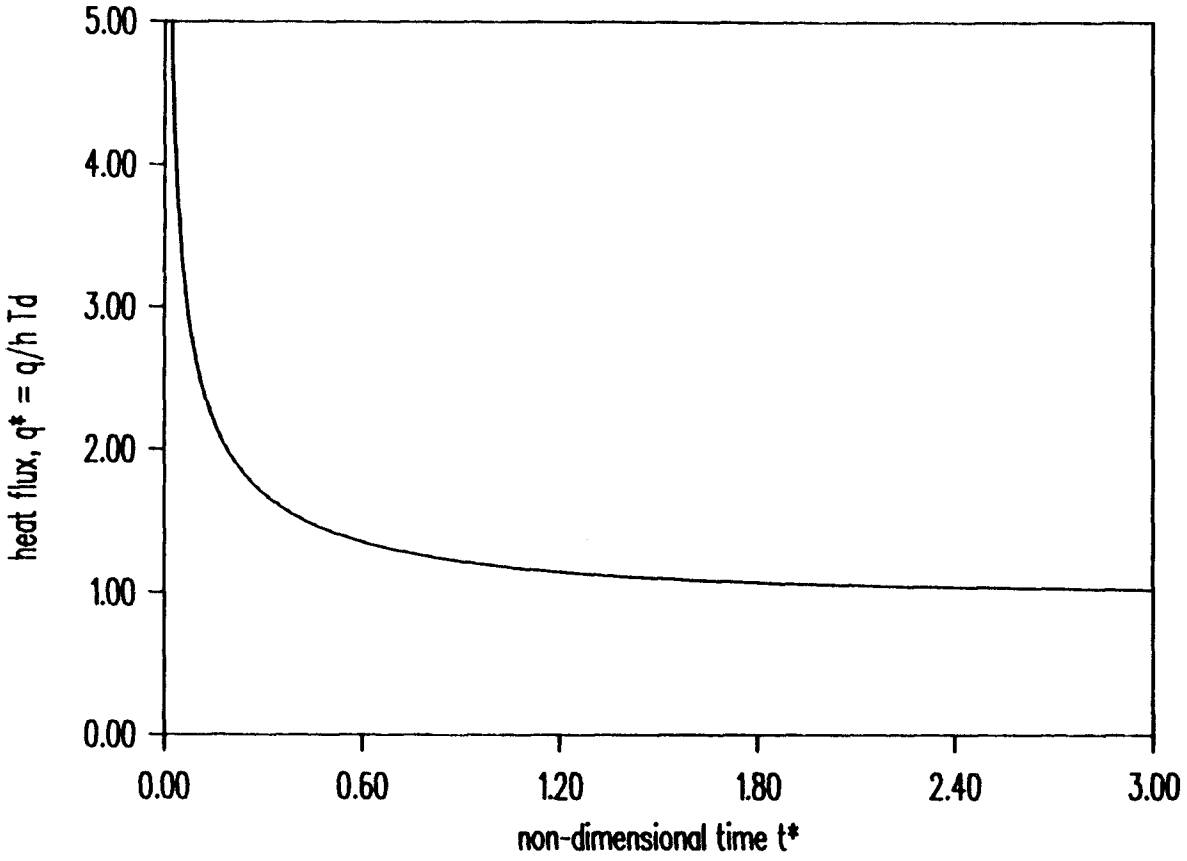

Figure 2.3 Non-dimensional heat flux as a function of the non-dimensional time for the flat-plate evaporator.

be considered. Deicing the evaporator periodically results in a heat transfer rate as shown in Figure 2.4. Each period starts from the no-ice condition. From this point, the heat transfer flux changes in the same form as shown in Figure 2.3 until it reaches some pre-established point at which the deicing takes place. Deice periods are generally of short duration, but usually there is no heat transfer during the period.

At first glance, it seems that it would be convenient to deice the evaporator very frequently. However, there is a penalty for every deice period. This penalty exists because a deice period reduces the heat pump performance and creates reliability problems with the compressor. Therefore, the time for deicing, t_{det}, is a design parameter that can be obtained from an optimization that balances the cost of area against the cost of the penalty associated with deicing.

However, a recent study (Stewart and Dona, 1988) tried to find situations in which the ice that forms in the evaporator self-releases from the surfaces, yielding a no-penalty deicing. Their study focused mainly on the possibility of using the buoyancy force (caused by the difference in density between ice and liquid water) to obtain ice self-release. To understand the possibility of obtaining ice self-release due to buoyancy force, consider a submerged layer of ice facing upwards. There are two forces acting over this layer. The first is the adhesion

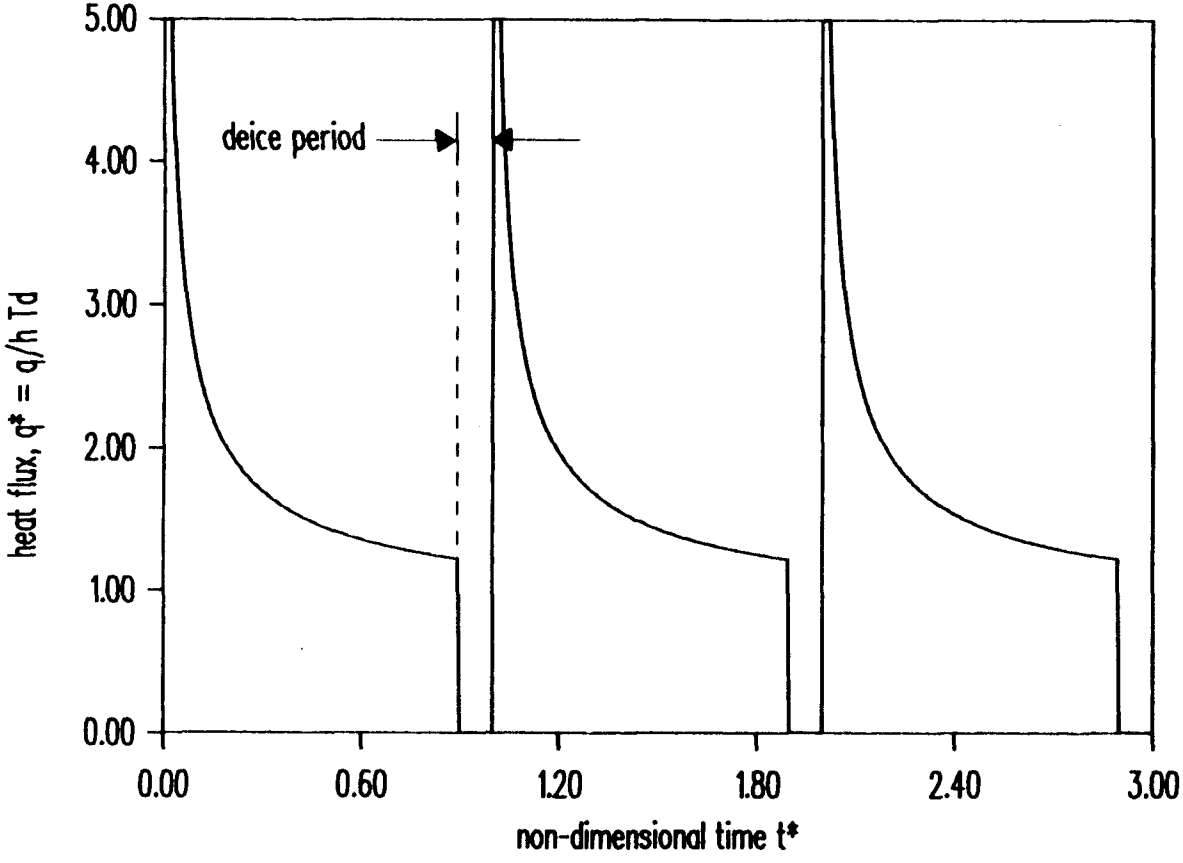

Figure 2.4 Non-dimensional heat flux as a function of time for an evaporator with periodic deicing. The length of the deicing cycle is indicated by the arrows.

force that keeps the ice attached to the surface, and the second is the buoyancy force that tends to detach the ice from the surface and make it float to the surface. The buoyancy force is proportional to the ice thickness. Therefore, it can be expected that there is a critical thickness at which the buoyancy force overcomes the adhesive force, causing a self-release of the ice.

Although this critical thickness is in general too large for practical applications, Stewart and Dona, 1988, obtained ice self-release for small thicknesses (6 mm), by using electrolytic solutions and adhesion-reducing coatings on the surfaces.

The concept of ice self-release is applied in the following section to an evaporator optimization. The analysis assumes that the ice self-releases from the evaporator when it reaches a critical thickness. The deicing penalties are included in a later analysis.

2.2.2 Evaporator Optimization with Ice Self-Release:
Consider once more the evaporator shown in Figure 2.1. The evaporator is a fixed-duty heat exchanger and its temperature T_e is constant. The heat transfer into the evaporator has two parts. The first part is a latent part, related to the amount of ice formed on the evaporator. The second part is a sensible part, and is equal to the energy lost by the water due to convection. The sum of these two contributions over the heat exchanger area A must equal the heat exchanger duty E. The temperature of the water

reservoir T_d has opposite effects in both terms. An increase in T_d causes an increase in the convective heat transfer, but a decrease in the amount of ice formed. Therefore, it is likely that there is an optimum T_d at which the area required to meet the heat transfer duty is a minimum. The following analysis calculates this minimum area and the optimum temperature T_d. The analysis is based on the hypothesis that ice self-release can consistently be obtained when the ice reaches a thickness equal to x_{det}.

Related to the critical thickness, x_{det}, there is a time for self-release, t_{det}. This time can be obtained for a given value of x_{det} from Equation (2.6) or from Figure 2.2. As shown in Figure 2.4, the heat transfer varies rapidly during each cycle. This analysis assumes that the heat exchanger duty E has to be met in the average throughout each cycle. Therefore, the average heat transfer must be equal to E/A, where A is the total evaporator area.

$$E/A = q_{avg} = \frac{L \rho x_{det}}{t_{det}} + h T_d \qquad (2.9)$$

The first term in Equation (2.9) is the latent energy, while the second term is the sensible energy. This equation shows clearly the different effects that T_d has in the two terms, since both t_{det} and the convective term increase as T_d increases. The time for detachment t_{det} is substituted from Equation (2.6) into (2.9). The result is,

$$E/A = - \frac{k_i T_e}{x_{det}} \frac{s \ln (1-s)}{s + \ln (1-s)} \tag{2.10}$$

where,

$$s \equiv x_{det}/a = Nu\ T_d^* \tag{2.11}$$

$$Nu \equiv h\ x_{det}/k_i \tag{2.12}$$

$$T_d^* \equiv -T_d/T_e. \tag{2.13}$$

Solving for the total area and writing it in non-dimensional form,

$$A^* \equiv - \frac{A\ h\ T_e}{E} = Nu \frac{s + \ln (1-s)}{s \ln (1-s)} \tag{2.14}$$

This equation can be used to find a minimum area that meets the fixed duty condition. Figure 2.5 shows a plot of the area A^*/Nu as a function of s. This figure shows that A^* is a monotonically increasing function in the range $0 \leq s \leq 1$, and therefore the optimum point corresponds to s=0. A value of s=0 corresponds to T_d=0. Then, the optimum operating condition for an evaporator with ice self-release is with water at the freezing point and no sensible heat transfer.

For values of s larger than one in Figure 2.5, there is no ice self-release, because the ice never reaches the critical detachment thickness ($a<x_{det}$), and therefore all the heat transfer is due to convection. The disadvantage of operating on this mode is obvious, being necessary to go to very high temperatures in order to obtain a good performance.

The optimum area can be obtained by evaluating

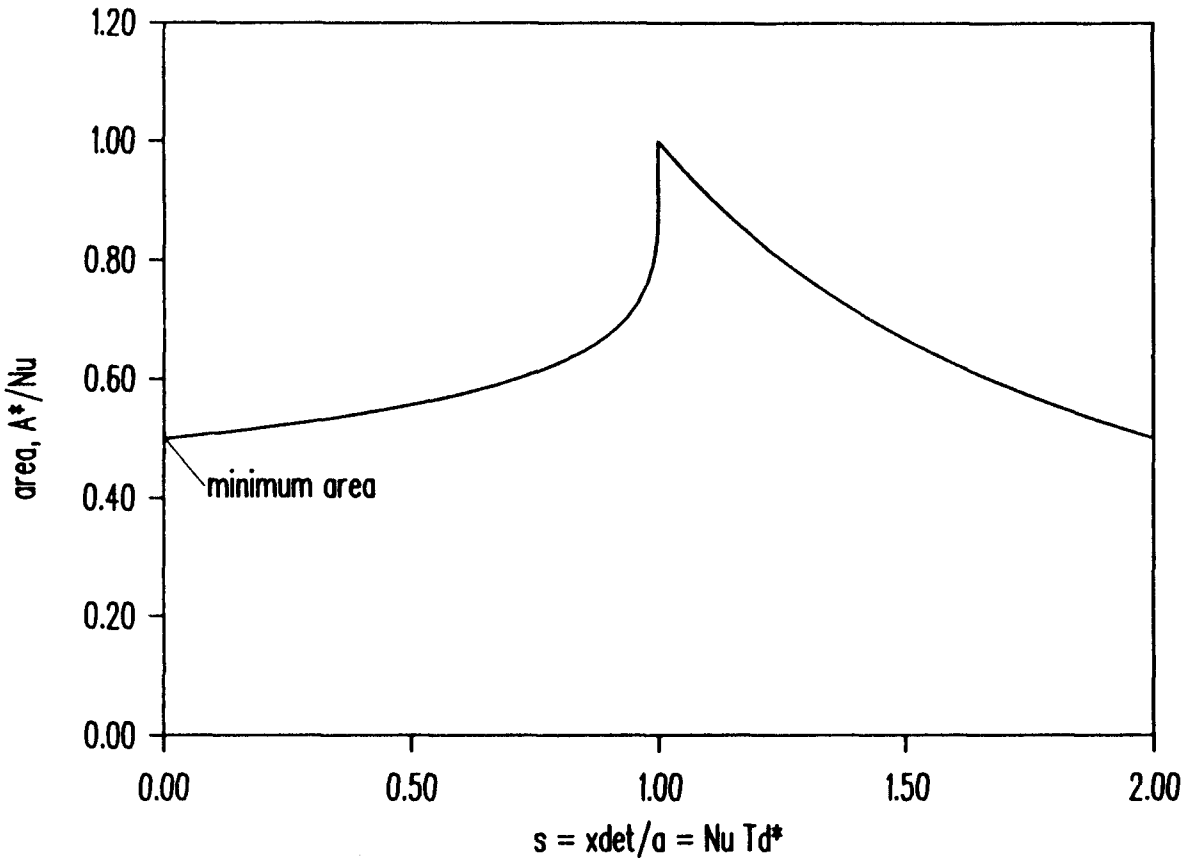

Figure 2.5 Non-dimensional area as a function of the non-dimensional ice thickness for detachment s.

Equation (2.14) at the limit when s goes to zero. The result is,

$$A_{opt} = - \frac{2\ E\ x_{det}}{k_i\ T_e} \qquad (2.15)$$

and is independent of the heat transfer coefficient.

Now, this result can be used to compare the performance of the ice-maker evaporator with an air-source evaporator. The problem can be stated as follows. Consider two possibilities for operating a heat pump. One is to use water at 0^oC as a source and the other is to use air at a temperature T_{air} as a source. Although thermodynamics indicates that it is always better to use a higher temperature for a low-temperature reservoir, heat transfer to water is more active than heat transfer to air. Therefore, less area is required in the water-source case, and this may overcome some of the thermodynamic advantage of operating with a higher air temperature.

For this simplified analysis, consider the case in which the temperature of the air-source evaporator is T_e, equal to the water-source evaporator temperature and below the freezing point. Neglect defrosting losses in the air-source evaporator and assume again ice self-release in the water-source evaporator. The heat transfer coefficient from the air to the evaporator is h_{air} and the temperature of the air is T_{air}. The area required to meet the heating duty E in the air-source heat exchanger is,

$$A_{air} = \frac{E}{h_{air}\,(T_{air}-T_e)} \qquad (2.16)$$

As the duties and temperatures of the two evaporators are the same, the best evaporator is the one that meets the duty with the least area. Therefore, the water-source heat pump performs better than the air-source heat pump whenever $A_{opt}<A_{air}$, with A_{opt} given by Equation (2.15) and A_{air} given by Equation (2.16). This inequality yields,

$$Nu_{air} < \frac{1}{2\,(T_{air}^{*}+1)} \qquad (2.17)$$

with $Nu_{air} \equiv h_{air}\,x_{det}/k_i$, and $T_{air}^{*} \equiv -T_{air}/T_e$.

The condition given by the expression (2.17) is satisfied when the water-source heat pump performs better than the air-source heat pump. The inequality sets an upper bound to the value of Nu_{air} (or to the value of x_{det}, since h_{air} and k_i are taken as constants) for each value of the air temperature. Then, for each value of the air temperature, there is a critical value of the self-release thickness x_{det} under which it is more convenient to operate a water-source heat pump. For an example, take k_i=2.2 W/m^{o}C and a typical value of h_{air}=60 W/m^{2o}C. Figure 2.6 shows the critical value of x_{det} as a function of the non-dimensional temperature T_{air}^{*}. Any value of x_{det} under the curve at the corresponding temperature indicates that operation of the water-source heat pump is advantageous compared to an air-source heat pump. Now consider a typical ice-maker evaporator temperature of -5^{o}C and a

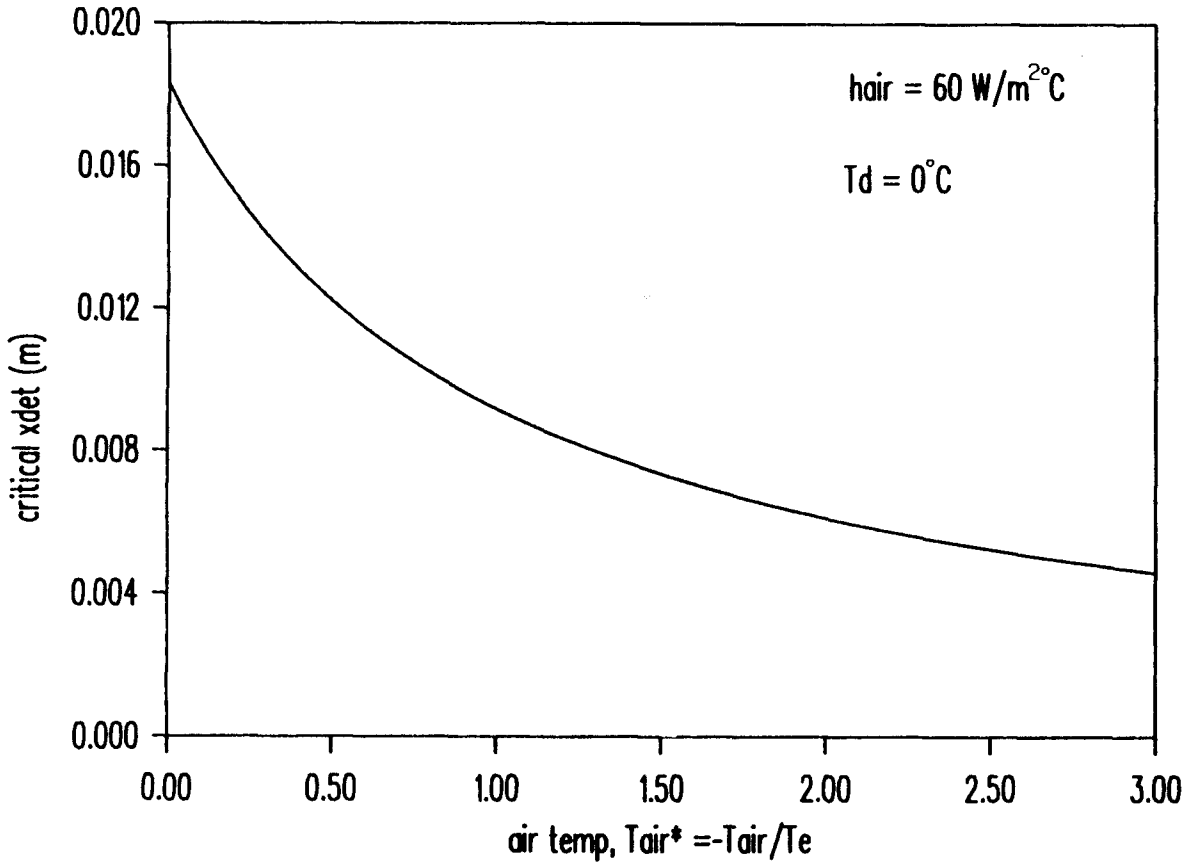

Figure 2.6 Critical self-release ice thickness as a function of the non-dimensional air temperature. An ice-maker heat pump performs better than an air-source heat pump for all the temperature-thickness conditions that fall under the curve.

detachment thickness of 6 mm. For these conditions, the graph indicates that an ice-maker heat pump has an advantage compared to the air-source heat pump for air temperatures less than approximately 11°C. Therefore, ice self-release gives a big advantage to ice-maker heat pumps as compared to alternative heat pumps.

2.2.3 Analysis With Deicing Penalties: It is unlikely that a convenient self-release thickness can always be obtained. Therefore, it is necessary to consider the need for deicing the evaporator periodically. This section presents an evaporator optimization in a case in which there is a deice penalty. The analysis is done in terms of the costs of the area and the energy required to deice the evaporator. The geometry considered is still the one presented in Figure 2.1.

Assume that an evaporator deice cycle is started every time that the ice thickness reaches a specified value, x_{det}. As this problem is completely analogous to that studied in Section 2.2.2, Equation (2.6) can be used to relate x_{det} to the time elapsed between consecutive deicing periods, t_{det}.

Deicing an evaporator requires an energy investment that is proportional to the total area of the evaporator. Take e_{det} as the energy required to deice a unit area of evaporator. The power invested to deice the evaporator can then be calculated as the total energy invested, $e_{det}A$, divided by the time elapsed between deice periods, t_{det}.

The cost[1] of this power is equal to the power multiplied by a constant, P, that represents the unit cost of the power. The cost of the evaporator area is assumed to be proportional to the total area, and given here as A S, where S is the cost of a unit of area. Therefore, the total cost of operating the evaporator is,

$$C = A\ S + \frac{P\ e_{det}\ A}{t_{det}} \tag{2.18}$$

Now, using Equations (2.6) and (2.14) and writing the equation in terms of non-dimensional variables, Equation (2.18) becomes,

$$C^* = \frac{s + \ln(1-s)}{s\ \ln(1-s)} - P^* \frac{s}{\ln(1-s)} \tag{2.19}$$

with,

$$C^* \equiv - \frac{C\ h\ T_e}{S\ Nu\ E} \tag{2.20}$$

$$P^* \equiv - \frac{P\ e_{det}\ h^2\ T_e}{S\ L\ \rho\ k_i\ Nu^2} \tag{2.21}$$

The first term in the right hand side of Equation (2.19) has been shown to be a monotonically increasing function of s in the range $0 \leq s \leq 1$. On the other hand, the second term is a monotonically decreasing function of s, for any positive value of P^*. Therefore, the value of s for minimum overall cost can be expected to be a function

---

[1] Costs here indicate cost rates (costs per unit of time). The expressions given represent therefore heat exchanger operation expenses during a unit of time. Total costs of operation can be obtained by multiplying the cost rates by the application life of the evaporator.

of P^*.

Indeed, an analysis shows that three different situations appear depending on the value of P^*. The first situation appears for small values of P^* ($0 \leq P^* \leq 1/6$). For this range of values, the optimum value of s is s=0, exactly the same as in the case where no deicing penalties exist. For values of P^* in the range $1/6 \leq P^* \leq 1.0$, the optimum values of s are in the range $0 \leq s \leq 1$, which correspond to periodic evaporator deicing with a water reservoir temperature above the freezing point ($T_d > 0$). Values of P^* in the range $P^* > 1$ yield no optima in the range $0 \leq s \leq 1$, and therefore deicing never occurs.

The three situations just described are illustrated in Figures 2.7, 2.8 and 2.9. Each of these figures show the two right-hand-side terms from Equation (2.19) as a function of s, as well as the sum of the two terms (the total cost). Figure 2.7 is obtained by using $P^*=0.1$, and therefore shows a case in which the optimum value of s is s=0. Figure 2.8 is generated with $P^*=0.70$, and therefore shows an optimum cost for a value of s in the range $0 \leq s \leq 1$. A value of $P^*=1.10$ yields curves as shown in Figure 2.9. For this case, no optimum exists in the range $0 \leq s \leq 1$ (deicing is so expensive that the evaporator should never be deiced).

For values of P^* between 1/6 and 1 there is an optimum value of s corresponding to each value of P^*. This optimum value of s can be calculated, and is illustrated in Figure

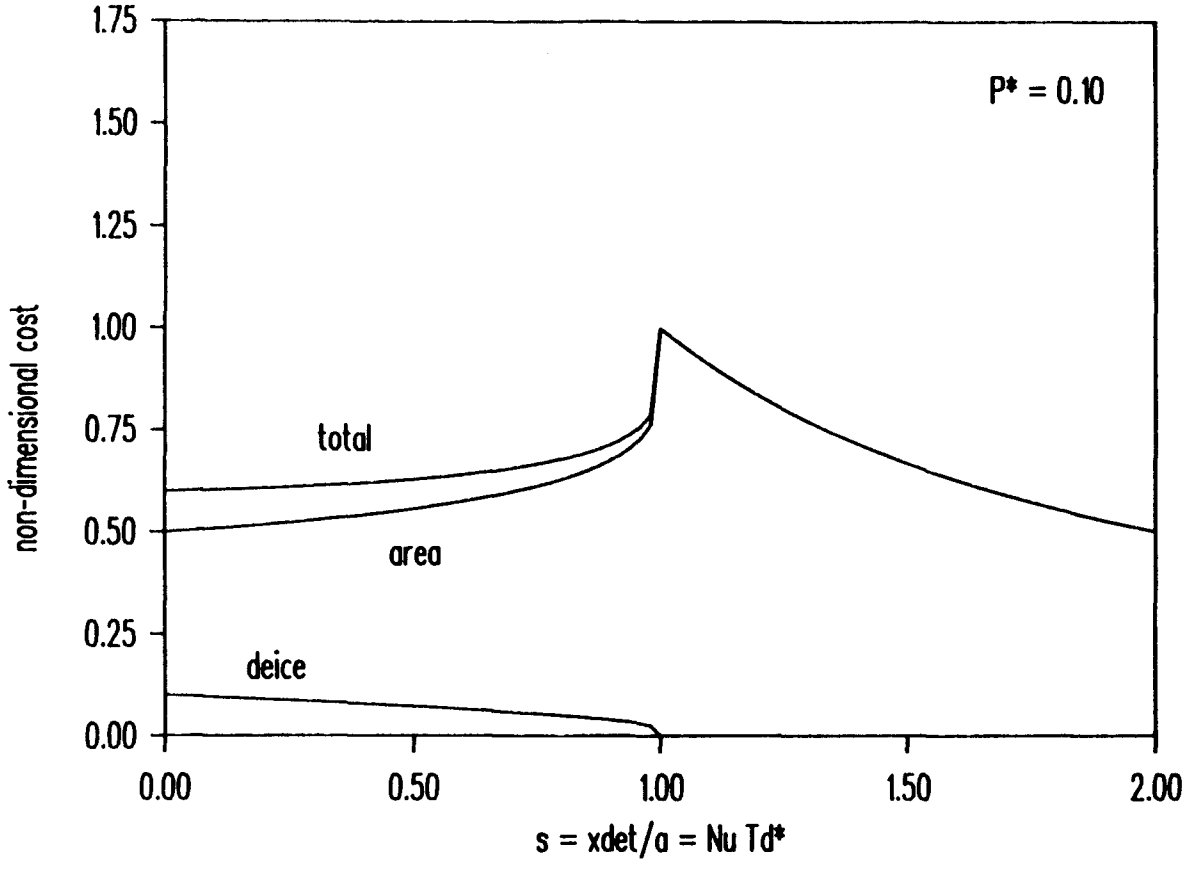

Figure 2.7 Deice, area and total costs for an ice-maker evaporator. The figure shows the first case, in which the optimum condition is to operate with a water temperature of 0°C. A value of P^*=0.10 is used to generate the figure.

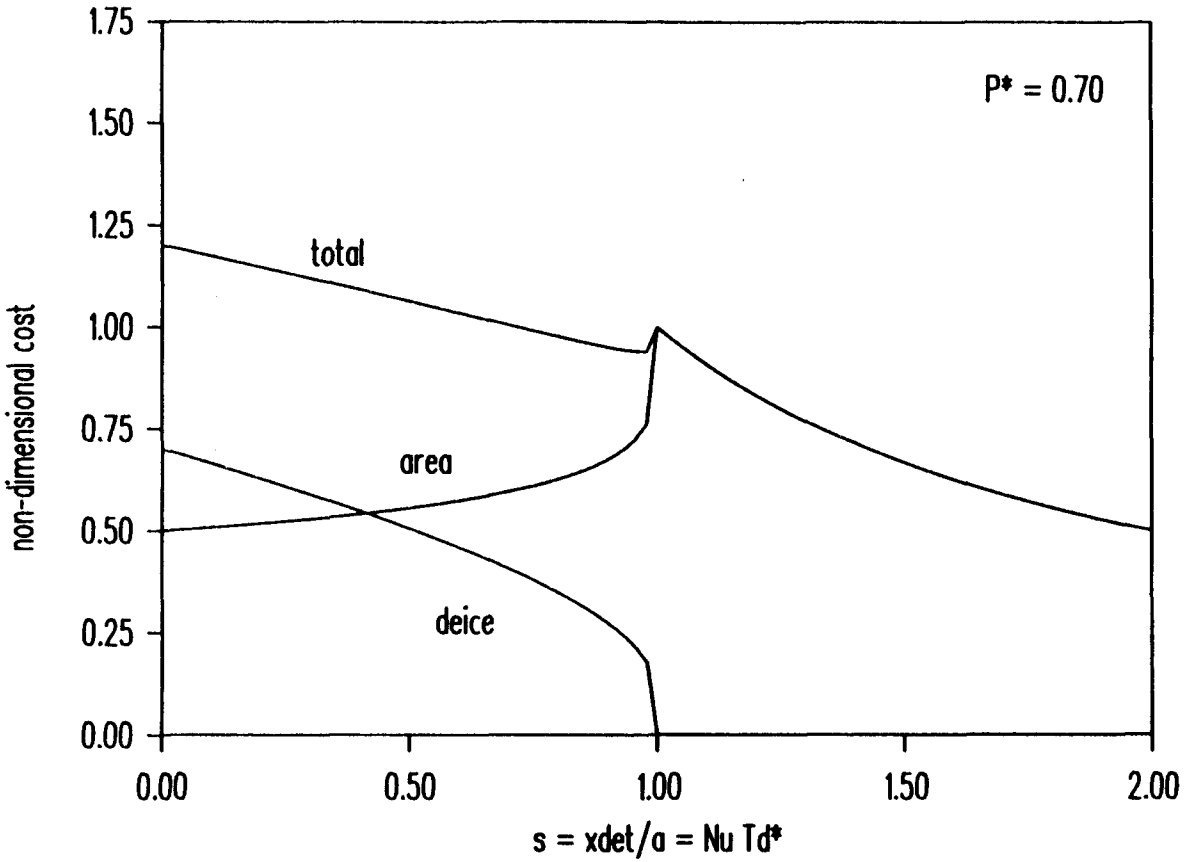

Figure 2.8 Deice, area and total costs for an ice-maker evaporator. The figure shows the second case, in which the optimum condition is to operate with a water temperature above the freezing point, and it is convenient to deice the evaporator periodically. A value of P^*=0.70 is used to generate the figure.

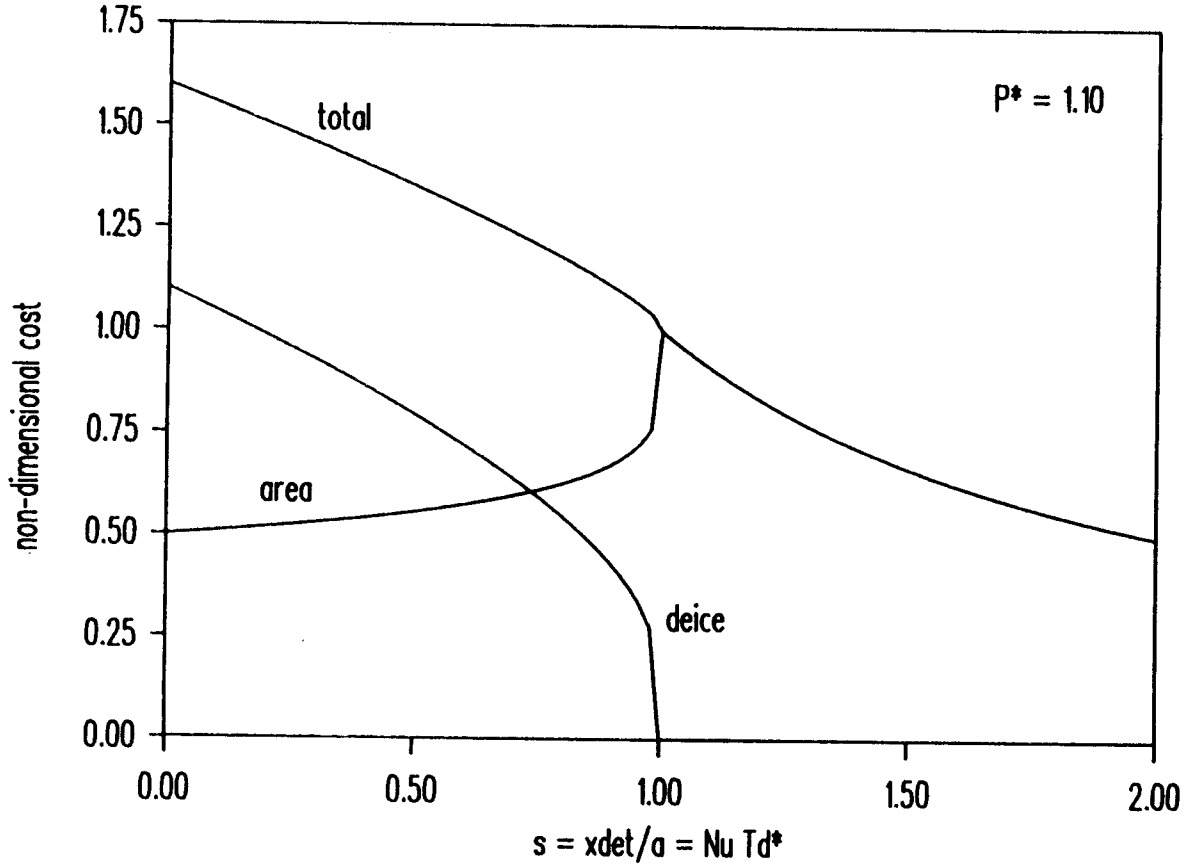

Figure 2.9 Deice, area and total costs for an ice-maker evaporator. The figure shows the third case, in which the optimum water temperature is high, and it is not convenient to deice the evaporator. A value of $P^*=1.10$ is used to generate the figure.

2.10 as a function of P^*. The figure shows an optimum value of s=0 for $P^*<1/6$. From this point, the value of s increases rapidly and then levels off at a value near 1.0. Figure 2.10 can be used to obtain an optimum value of s once the value of P^* is known. However, P^* is a function of many factors, including economical factors, and therefore it is difficult to obtain an accurate estimate of its value. If the value of P^* cannot be calculated accurately, but its order of magnitude can be estimated, Figure 2.10 can still be used to choose a value of s. The figure indicates that small values of P^* ($0\leq P^*\leq 0.2$) correspond to an optimum of s approximately equal to zero, while $s\approx 1$ gives a good approximation for the optimum for larger values of P^* within a wide range ($0.4\leq P^*\leq 1.0$). Intermediate values of s are the optima for only a small range of values of P^* ($0.2<P^*<0.4$), and therefore should be avoided, unless P^* is known with good accuracy and its value falls in the given range. Therefore, this analysis recommends either $s\approx 0$ (water reservoir temperature nearly at the freezing point), or $s\approx 1$ (almost no deicing or no deicing at all in the evaporator), depending on whether the value of P^* is small or large.

The case s=0 corresponds to an ice-maker heat pump evaporator. This evaporator requires frequent deicing, and therefore this mode of operation is only recommended when deicing costs are low. The s=1 alternative corresponds to a water-source heat pump, and is attractive for high

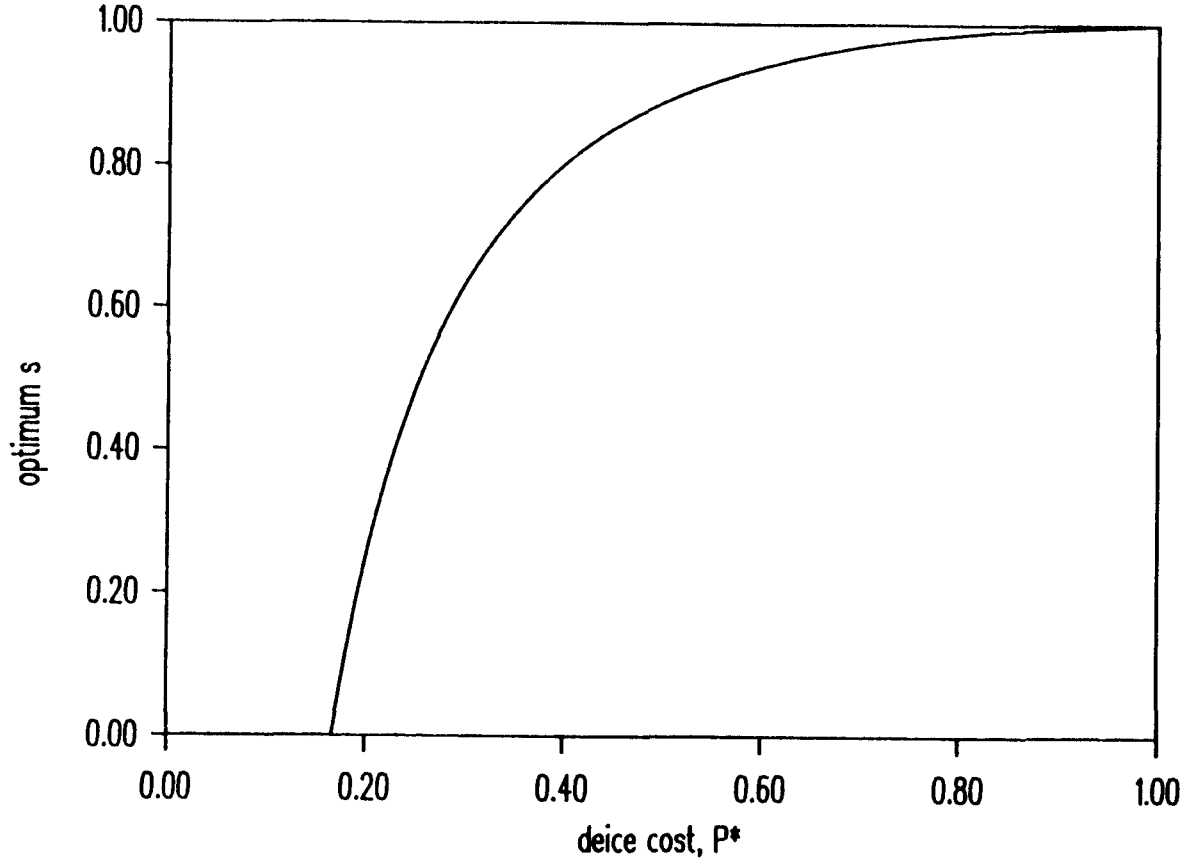

Figure 2.10 Optimum value of s (non-dimensional reservoir temperature multiplied by the Nusselt number) as a function of the non-dimensional deicing cost P^*.

deicing costs. However, the applicability of the s=1 case to a heat pump may be limited by the availability of water at high enough temperatures (remember that $s \equiv -Nu\ T_d/T_e$, with a value of $Nu \equiv hx_{det}/k_i$ that is typically small, so that s=1 may imply a high value of T_d). Therefore, two parameters, deicing costs and water temperature are the determining factors to find if it is more convenient to operate a heat pump as a water-source or as an ice-maker heat pump.

This completes the theoretical calculations. The following section complements the theoretical results with a simulation of a water-source/ice-maker heat pump. The simulation code is used to calculate the optimum heat pump operation cycle length.

2.3 Evaporator Simulation

This section presents the results of a heat pump simulation. The heat pump is a water-to-air unit. The heat pump evaporator is a set of tube-in-tube heat exchangers. The refrigerant and water temperatures are low enough for some freezing to occur. A complete description of the evaporator and the heat pump can be found in Chapters 3 and 4.

In this section, the heat pump simulation model is used to perform a calculation that is equivalent to the theoretical calculation shown in the previous section. The purpose of this is to compare the results obtained in the

theoretical analysis with the results from a detailed heat pump simulation. This comparison is helpful to test the generality of the conclusions obtained in the previous section.

The heat pump calculations start by presenting an optimization of the overall heat pump system. This optimization is carried out for evaporator inlet water temperatures of 1,2,3,4,5,6,7 and 8°C. This section also illustrates the effect of temperature on heat pump performance. Later, the heat pump efficiencies are calculated as a function of the energy required to deice the evaporator.

2.3.1 Heat Pump Optimization: The optimization presented here follows closely the procedure used for the overall heat pump optimization (Chapter 5). The objective function is the exergetic efficiency,

$$\Phi = \frac{EX_{air}}{W_{comp} + W_{fan} + W_{pump}} \qquad (2.22)$$

with the exergy of the cold water flowing out of the evaporator not taken into account, because this exergy is not applied to anything useful.

The exergetic efficiency (2.22) is calculated for different lengths of the operation period (time period between deicings) and for steady-state. The length of the operation period determines whether the heat pump operates as an ice-maker heat pump or as a water-source heat pump. Ice-maker heat pumps obtain most of their energy from

freezing the water, and require frequent deicings. Water-source heat pumps operate only as water chillers and do not require deicing. In this analysis, the exergetic efficiency is calculated for operation periods lasting 1800 s, 3600 s, 7200 s, and 14400 s. The exergetic efficiency is also calculated in steady-state. Heat pumps operating with short periods (1800 s, 3600 s) correspond closely to ice-maker heat pumps, while heat pumps operating in steady-state are water-source heat pumps. Heat pumps with intermediate operation cycle lengths (7200 s, 14400 s) operate partly as a water-source heat pump (because they obtain most of their energy from cooling down the water) and partly as an ice-maker heat pump (because they require periodic deicings).

The optimization is carried out with the operation period as a parameter. Also, the optimization is done for different evaporator inlet water temperatures (1,2,3,4,5,6,7 and 8°C).

The decision variables and constraints are almost identical to those used in Chapter 5, except that a maximum limit to the water mass flow rate is imposed. The decision variables and constraints used here are,

water volumetric flow rate, V, 10^{-4} m^3/s	$2 \leq V \leq 6$
number of evaporator circuits in parallel, N	$4 \leq N \leq 8$
evaporator circuit length, l, m	$1 \leq 20$
evaporator circuit external radius, R_o, cm	$1 \leq R_o \leq 2$

The internal radius of the evaporator duct is always

half of the external radius.

Table 2.1 presents the results of the optimization. The objective function is a performance figure and does not take into account the cost of area. Therefore, all the optimum designs have the maximum duct length (20 m) and the maximum number of evaporator circuits (8). The evaporator radius is not always the maximum. A small duct radius is sometimes convenient because a small flow area increases the water velocity and enhances the heat transfer.

It can be noticed that the table shows no optimum heat pump for small temperatures (1 and 2°C), and long operation cycles. This is because the evaporator freezes solid before reaching the required operation cycle length for any allowed value of the water flow rate.

The results of Table 2.1 also show that the efficiency always decreases as the operation cycle becomes longer. This result is a consequence of using Equation (2.22) as objective function, because Equation (2.22) does not take into account any deicing penalties that would reduce the efficiency of the heat pumps requiring periodic deicing. Section 2.3.2 shows the effect of including a deicing penalty in the heat pump performance.

Figures 2.11 and 2.12 show respectively the effect of inlet water temperature on exergetic efficiency and COP. Both figures show the performance of the optimum heat pump at the given temperature (obtained from Table 2.1), for two different conditions. The two conditions are: deicing

Table 2.1 Optimum heat pump designs as a function of water inlet temperature and operation cycle. All the heat pump designs in the table have N=8 and l=20 m. No indication of a blockage time means that the evaporator under the given condition never gets blocked with ice.

t_{cycle} s	R_o cm	$\dot{V}$ (10^{-4} m^3/s)	t_{block} s	Φ	COP
Temperature = 1°C					
1800	1.5	2.0	3650	0.270	2.917
3600	2.0	2.0	5750	0.263	2.861
Temperature = 2°C					
1800	1.5	2.0	3850	0.261	2.924
3600	1.5	2.0	3850	0.256	2.876
7200	2.0	5.2	7400	0.216	2.442
Temperature = 3°C					
1800	1.5	2.0	4100	0.252	2.932
3600	1.5	2.0	4100	0.248	2.899
7200	2.0	3.5	7400	0.225	2.651
14400	2.0	6.0	--	0.202	2.378
steady	2.0	6.0	--	0.162	1.921
Temperature = 4°C					
1800	1.5	2.0	4450	0.244	2.941
3600	1.5	2.0	4450	0.241	2.912
7200	2.0	2.6	7350	0.227	2.771
14400	2.0	4.4	17500	0.210	2.560
steady	1.5	5.0	--	0.206	2.504

Table 2.1. Cont.

Temperature = 5°C

t_{cycle} s	R_o cm	V (10^{-4} m^3/s)	t_{block} s	Φ	COP
1800	1.0	2.0	2450	0.236	2.951
3600	1.5	2.0	4900	0.232	2.924
7200	2.0	2.0	7500	0.224	2.853
14400	1.5	3.9	--	0.211	2.669
steady	1.0	4.2	--	0.210	2.633

Temperature = 6°C

t_{cycle} s	R_o cm	V (10^{-4} m^3/s)	t_{block} s	Φ	COP
1800	1.0	2.0	2800	0.227	2.966
3600	1.5	2.0	5250	0.224	2.937
7200	2.0	2.0	8150	0.218	2.882
14400	1.0	3.5	--	0.211	2.755
steady	1.0	3.5	--	0.210	2.746

Temperature = 7°C

t_{cycle} s	R_o cm	V (10^{-4} m^3/s)	t_{block} s	Φ	COP
1800	1.0	2.0	3300	0.219	2.978
3600	1.5	2.0	5950	0.216	2.971
7200	1.5	2.4	7800	0.210	2.882
14400	1.0	2.9	--	0.208	2.835
steady	1.0	3.0	--	0.207	2.826

Temperature = 8°C

t_{cycle} s	R_o cm	V (10^{-4} m^3/s)	t_{block} s	Φ	COP
1800	1.0	2.0	3900	0.210	2.990
3600	1.0	2.1	4250	0.207	2.957
7200	1.5	2.1	7850	0.205	2.932
14400	1.0	2.6	--	0.203	2.895
steady	1.0	2.6	--	0.202	2.888

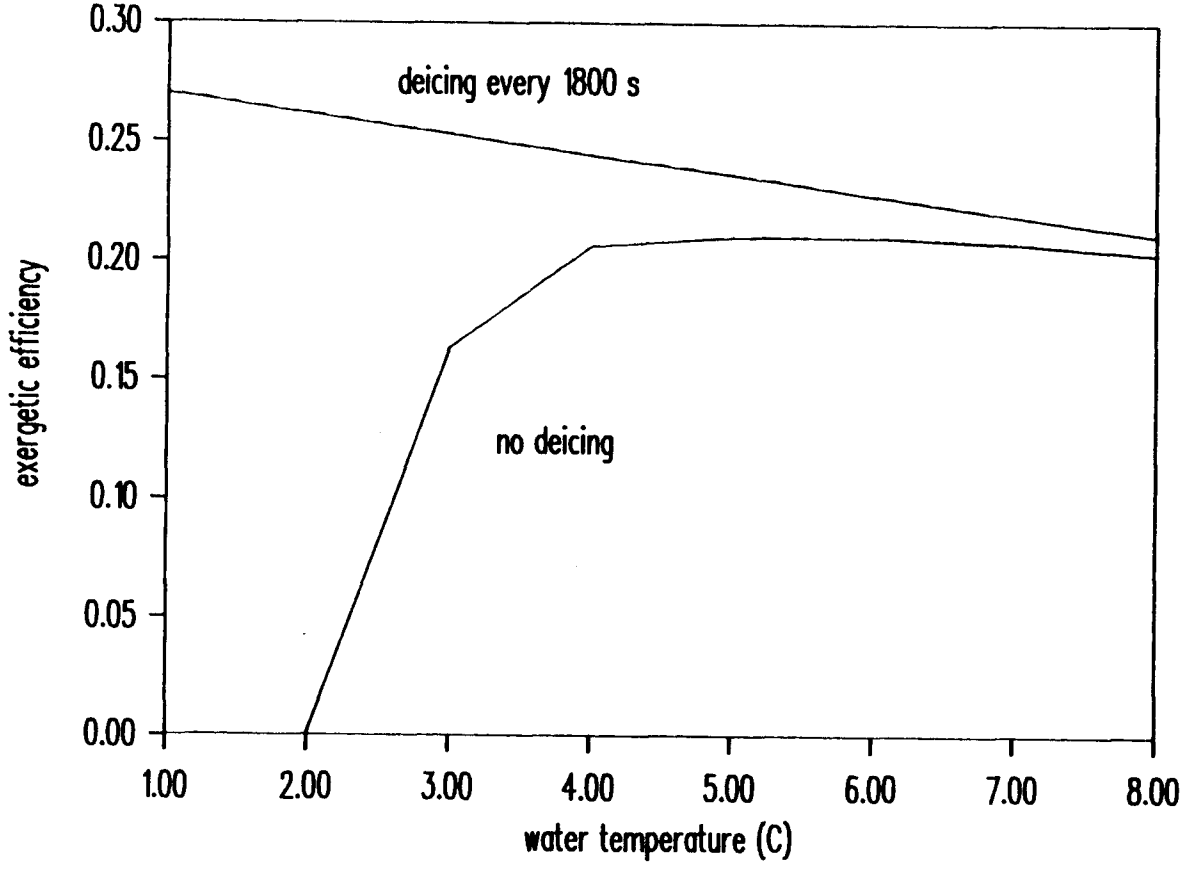

Figure 2.11 Exergetic efficiency for optimum heat pumps as a function of inlet evaporator water temperature for a water-source heat pump (no deicing), and an ice-maker heat pump (deicing every 1800 s).

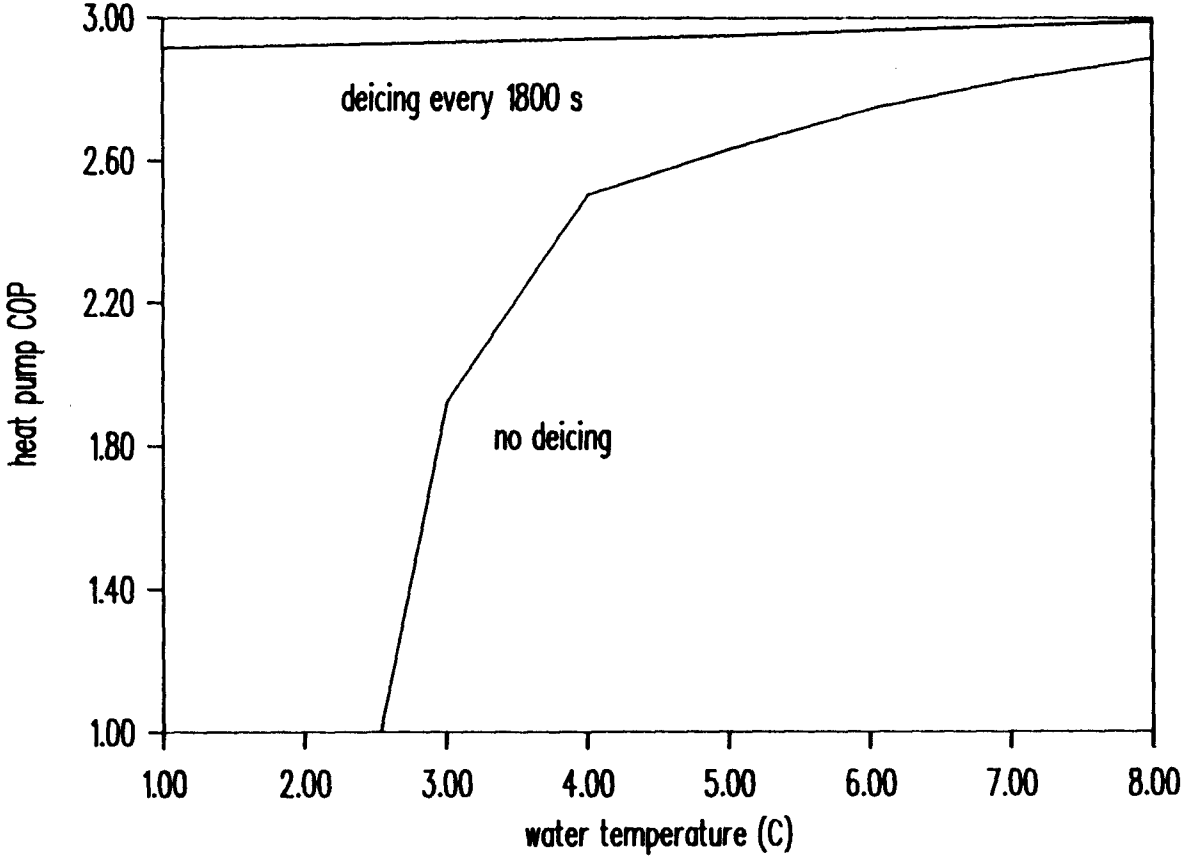

Figure 2.12 Heat pump COP for optimum heat pumps as a function of inlet evaporator water temperature for a water-source heat pump (no deicing), and an ice-maker heat pump (deicing every 1800 s).

every 1800 s (ice-maker heat pumps) and no deicing (water-source heat pump). Both figures show that water temperature has a large influence on performance for water-source heat pumps, and a small effect on ice-maker heat pump performance. COP values are always an increasing function of temperature (although only a slowly-increasing function for ice-maker heat pumps). Exergetic efficiency values decrease as a function of temperature, at least in part of the range, because the dead state temperature is always equal to the inlet water temperature. An increase in dead state temperature causes a decrease in the exergy value of the air flowing out of the condenser. The exergetic efficiency for the water-source heat pump has a maximum value at a temperature of 6°C.

The optimization results presented in Table 2.1 are obtained from a detailed heat pump simulation model. The optimum designs are determined by a trade-off between the cost of pumping the water from a water reservoir to the heat pump, and the cost of pumping the water through an evaporator that is partly blocked with ice (Chapter 5). The theoretical analysis of the evaporator has established an optimum evaporator condition from a trade-off between area cost and deicing cost. Still, even though there are important differences between the two analyses, it can be observed that there is a lot of similarity between an evaporator parameter obtained from the theoretical analysis and a heat pump parameter appearing in this simulation.

The evaporator parameter is s (Equation (2.11)) which is a non-dimensional form of the water temperature in the evaporator. The heat pump parameter is the cycle length. Heat pumps operating with a short operation cycle (1800 s or 3600 s) are mainly ice-maker heat pumps. These heat pumps require frequent deicings, and therefore are similar to the evaporators that operate with a small value of s. Water-source heat pumps never require deicing. This condition makes them similar to the evaporators with a value of s=1. Intermediate operation cycle lengths (7200 s, 14400 s) are similar to the cases with intermediate values of s. The conclusion obtained from the evaporator analysis is that the optimum cycle length and water temperature are closely related, and that intermediate cycle lengths (intermediate values of s) do not yield optimum performance in most cases. The following section introduces a penalty cost in the results presented in Table 2.1 to show the applicability of the conclusions obtained in the theoretical analysis to this detailed heat pump simulation.

2.3.2 Heat Pump Optimization With Deicing Costs: This section shows the effect of a deicing penalty cost on the heat pump designs presented in Table 2.1.

Evaporator deicing in a heat pump is always a very unsteady process, regardless of how the deicing is accomplished. The heat pump model used here is a steady-state model (See Chapter 4), and therefore it cannot be

used to estimate performance losses due to deicing. Deicing losses are also highly dependent on conditions and on the method used for deicing. For this reason, the present analysis does not use a single value for the deicing penalty cost. Rather, it presents a parametric study on how the performance losses due to deicing affect the heat pump performance.

Baxter, 1978, has given data on deicing performance losses for heat pumps. The study included testing of different deicing methods and heat pump models. The results indicate that deicing losses vary from being negligible to being responsible for performance losses of up to 30%, for operation with short time cycles (20 minutes or less), depending on the deicing method used. To take into account these possible variations in penalty costs, several deicing performance loss values are used for this analysis. The performance losses are expressed as a percentage decrease in the heat pump exergetic efficiency. The analysis assumes that each evaporator deicing reduces the heat pump efficiency in the same proportion. In this way, if deicing an evaporator by using some given method causes a decrease in heat pump exergetic efficiency of 10% when the operation cycle length is 1800 s, then the same method applied to a heat pump that requires deicing every 3600 s causes a decrease in efficiency of 5%. The same calculation can be applied to other cycle lengths. There is no performance decrease for water-source heat pumps,

since these do not require deicing.

The results of the analysis are shown in Table 2.2. This table shows the exergetic efficiencies for the optimum designs presented in Table 2.1, as a function of water temperature and operation cycle length. The other heat pump parameters (V, R_o, t_{block}, and COP) are not given in Table 2.2 to avoid repetition. Table 2.1 may be consulted if these values are required. Table 2.2 shows first the exergetic efficiencies obtained in Table 2.1. These values do not take into account any deicing losses and therefore correspond to a no-penalty deicing (ice self-release). Then, the table presents exergy values obtained for different exergy losses due to deicing. The exergy losses are expressed as a percentage, and represent the efficiency drop that they cause to a heat pump operating with a cycle length of 1800 s. Four efficiency drop values are used in this calculation. These are 1%, 5%, 10% and 20% of the efficiency with no deicing for 1800 s cycle length. The efficiency drop for longer operation cycles is a fraction of this percentage, and is calculated as previously discussed.

Table 2.2 shows underlined the optimum performance for each water temperature and performance drop due to deicing. The results follow closely those obtained in the theoretical analysis. If there is no penalty loss, the optimum design is always obtained at the shortest operation cycle length (the smallest value of s). As the deicing

Table 2.2 Exergetic efficiency for the optimum heat pumps presented in Table 2.1, as a function of performance drop due to deicing. The performance drops are expressed as the drop in heat pump exergetic efficiency due to deicing, for a heat pump with an operation cycle of 1800 s. The table shows underlined the optimum design for each water temperature and cycle length.

T_{water} °C	t_{cycle} s	exergetic efficiencies deice penalty cost (%) 0	1	5	10	20
1.0	1800	<u>0.270</u>	<u>0.267</u>	<u>0.256</u>	0.243	0.216
1.0	3600	0.263	0.261	0.256	<u>0.250</u>	<u>0.237</u>
2.0	1800	<u>0.261</u>	<u>0.259</u>	0.248	0.235	0.209
2.0	3600	0.255	0.254	<u>0.249</u>	<u>0.243</u>	<u>0.230</u>
2.0	7200	0.216	0.215	0.213	0.211	0.205
3.0	1800	<u>0.253</u>	<u>0.250</u>	0.240	0.227	0.202
3.0	3600	0.249	0.247	<u>0.242</u>	<u>0.236</u>	<u>0.224</u>
3.0	7200	0.226	0.225	0.223	0.220	0.215
3.0	14400	0.202	0.202	0.201	0.200	0.197
3.0	--	0.163	0.163	0.163	0.163	0.163
4.0	1800	<u>0.244</u>	<u>0.241</u>	0.232	0.220	0.195
4.0	3600	0.241	0.239	<u>0.235</u>	<u>0.228</u>	<u>0.216</u>
4.0	7200	0.227	0.227	0.224	0.221	0.216
4.0	14400	0.210	0.209	0.208	0.207	0.205
4.0	--	0.206	0.206	0.206	0.206	0.206
5.0	1800	<u>0.236</u>	<u>0.234</u>	0.224	0.212	0.189
5.0	3600	0.232	0.231	<u>0.226</u>	<u>0.220</u>	0.209
5.0	7200	0.224	0.223	0.221	0.218	<u>0.213</u>
5.0	14400	0.211	0.211	0.210	0.208	0.206
5.0	--	0.210	0.210	0.210	0.210	0.210

Table 2.2 Cont.

T_{water} °C	tcycle s	exergetic efficiencies deice penalty cost (%) 0	1	5	10	20
6.0	1800	0.227	0.225	0.216	0.205	0.182
6.0	3600	0.224	0.223	0.218	0.213	0.202
6.0	7200	0.218	0.217	0.215	0.212	0.207
6.0	14400	0.211	0.211	0.210	0.208	0.206
6.0	--	0.210	0.210	0.210	0.210	0.210
7.0	1800	0.219	0.217	0.208	0.197	0.175
7.0	3600	0.216	0.215	0.210	0.205	0.194
7.0	7200	0.210	0.210	0.208	0.205	0.200
7.0	14400	0.208	0.208	0.207	0.205	0.203
7.0	--	0.207	0.207	0.207	0.207	0.207
8.0	1800	0.210	0.208	0.200	0.189	0.168
8.0	3600	0.207	0.206	0.202	0.197	0.187
8.0	7200	0.205	0.204	0.202	0.199	0.194
8.0	14400	0.203	0.203	0.202	0.201	0.198
8.0	--	0.202	0.202	0.202	0.202	0.202

penalty increases, the optimum operation cycle length switches to longer operation cycles. However, the cycle length and the water temperature are closely related, so that the optimum cycle length for a given deice penalty is a function of the water temperature. For low water temperatures, the optimum cycle length increases only up to 3600 s, still short enough to be considered an ice-maker heat pump. For high water temperatures, the operation cycle switches almost immediately, from 1800 s at very low penalty, to no deice (water-source heat pump) at higher deice penalties. In addition to this, it can be observed that the change from short cycles (ice-maker heat pumps) to no deicing (water-source heat pumps) occurs very abruptly, usually without going through a range in which intermediate cycle lengths are the optimum. Of all the values given in the table, only once does the optimum correspond to an intermediate cycle length (7200 s, at 5°C). This agrees with the conclusion reached in the theoretical analysis, that the heat pump should operate either as an ice-maker heat pump with short operation cycles, or as a water-source heat pump, with no deicing, but not with intermediate cycle lengths.

Figures 2.13 and 2.14 illustrate part of the information presented in Table 2.2. These figures present the heat pump exergetic efficiency as a function of the deice penalty. The deice penalty is again expressed as the fractional loss in exergetic efficiency that deicing causes

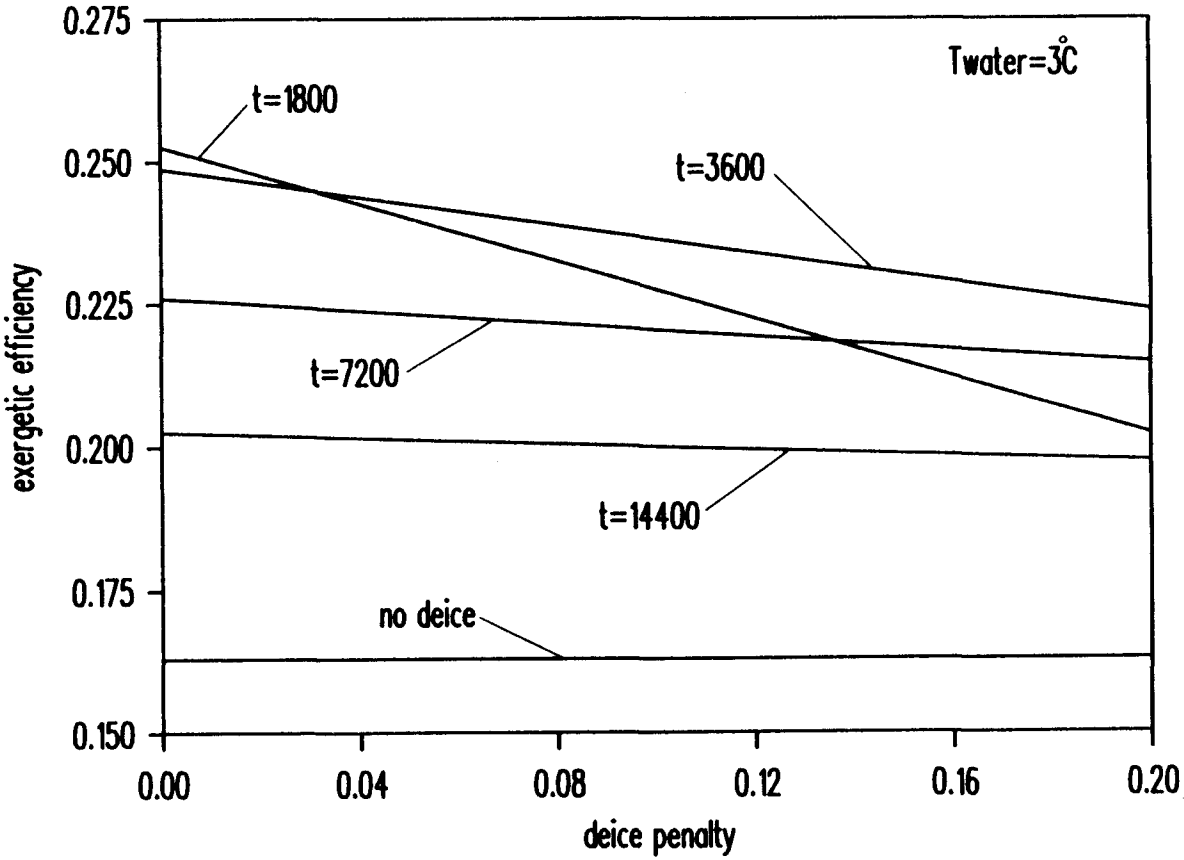

Figure 2.13 Exergetic efficiency as a function of the deice penalty for a water inlet temperature of 3°C.

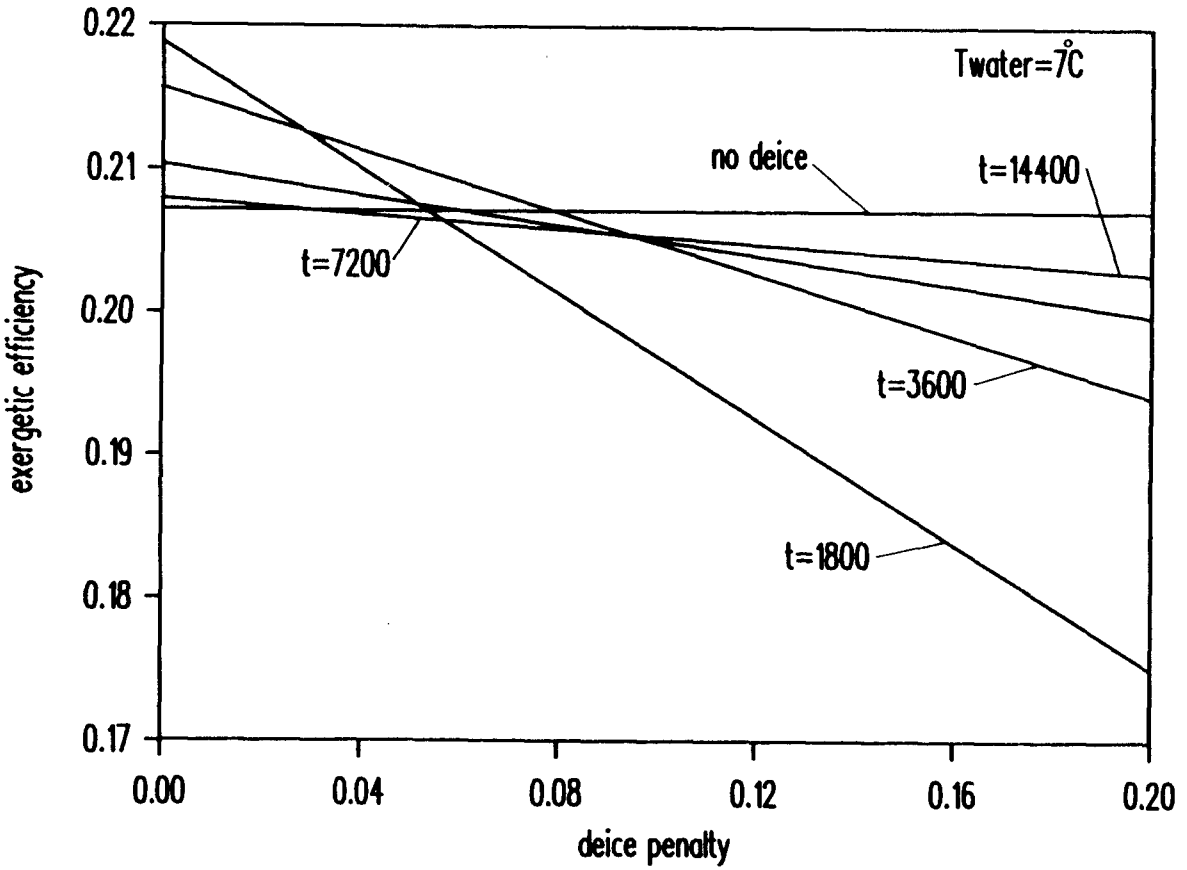

Figure 2.14 Exergetic efficiency as a function of the deice penalty for a water inlet temperature of 7°C.

on a heat pump operating with a 1800 s length of cycle. Figure 2.13 shows the exergetic efficiencies for a water inlet temperature of 3°C. This figure shows that ice-maker heat pumps (1800 s and 3600 s) are the optimum heat pumps for any deice penalty in the range being considered. Figure 2.14 shows the same curves for a water temperature of 7°C. The figure shows that the optimum heat pump is an ice-maker heat pump for small deice penalties. At an intermediate point (about 8% in penalty) the water-source heat pump suddenly becomes the best choice. Intermediate cycle lengths are not the optimum choice for any value of the deicing penalty.

2.4 Conclusions

This chapter has presented a theoretical analysis of a water-source evaporator, and a numerical simulation of a water-source heat pump. The theoretical analysis is first used to calculate optimum evaporator area and water temperature for a case in which there is no penalty for deicing (ice self-releases from the evaporator once a critical thickness is reached). The results indicate that, if there is no deicing penalty, the optimum water temperature is always equal to the freezing point, and the optimum heat pump is an ice-maker heat pump.

The results obtained for the evaporator with ice self-release are then used to compare the performance of an ice-maker evaporator operating with water at 0°C to the

performance of an air-source evaporator operating with air at a temperature $T_{air}>0°C$. The results show that the ice-maker evaporator is capable of operating with higher performance than the air-source evaporator, especially if the deicing occurs at small ice thicknesses.

Introducing deicing costs into the analysis changes the results from those obtained with no deice penalty. The optimum water temperature for an evaporator with low deice costs is equal to 0°C (same as for the no deice case), but then the optimum water temperature increases rapidly as the deice costs increase, until reaching a point at which deicing is so expensive that the heat pump should never be deiced, but rather it should operate as a water-chiller (water-source heat pump). The change between ice-maker heat pump and water-source heat pump is very abrupt, and intermediate values of the water temperature are convenient only for a narrow range of deice penalty costs. Therefore, the evaporator should operate as an ice-maker evaporator, with a water temperature of 0°C; or as a water chiller, without ever deicing. The smallness of the range of values of the deice cost for which intermediate temperatures are optimum (intermediate temperatures are water temperatures above 0°C for which deicing is still required), makes these temperatures undesirable for most applications.

The numerical simulation code is also used to perform a calculation of heat pump efficiencies with deicing penalties for a water-source/ice-maker heat pump. First,

the heat pump is optimized for different values of the temperature and the heat pump operation cycle length (time between consecutive evaporator deicings). Then, the analysis introduces performance drops due to deicing. The simulation code cannot be used to estimate deicing performance losses. Therefore, the analysis uses different performance loss values within a wide range, to observe the effect of performance loss in the optimum designs. The purpose of these calculations is to test the generality of the conclusions obtained from the evaporator analysis.

The calculations used to optimize the heat pump from the simulation code, and the theoretical calculations used to optimize the evaporator do not have much in common. However, the results from the heat pump simulation including deice losses are very similar to the results obtained from the evaporator analysis in three important aspects. First, the heat pump simulation results indicate that heat pumps operating with no penalty for deicing should have a short operation cycle (operate as an ice-maker heat pump), in agreement with the results obtained from the evaporator analysis. Second, the heat pump simulation results and the evaporator results show a close relationship between water temperature and optimum operation cycle length. Third, the results obtained from both analyses indicate that the optimum heat pump corresponds in almost every case to either an ice-maker

heat pump or to a water-source heat pump. Intermediate conditions (heat pumps with a long operation cycle that require deicing) should be avoided, because they only rarely correspond to the optimum.

In this way, all the main conclusions obtained from the theoretical analysis are true also for a detailed heat pump simulation, and therefore they are expected to have a very extended validity.

III. THE EVAPORATOR MODEL

3.1 Introduction

This chapter describes the model used to simulate the heat pump evaporator. The evaporator under consideration is made of copper, and it has a specified number of ducts in parallel, N, each acting as a water-to-refrigerant heat exchanger. Each individual duct is a tube-in-tube heat exchanger with the refrigerant flowing in the inner tube and the water flowing in the annulus. The analysis assumes the ducts to be straight, or at least having a radius of curvature large enough so that centrifugal effects are negligible. A fully-distributed model is used for the water side, while the refrigerant side model lumps all variables in the radial direction. Water temperatures are low enough for some freezing to occur inside the heat exchanger.

Two different geometries are considered for the water side of the evaporator. In one, the annulus has four fins distributed at equal (90°) angles. In the other, the annulus has no fins. Although the results indicate that the finned duct performs better, the non-finned duct is the model used for the heat pump simulation, due to limitations in the simulation model for the finned duct. The chapter presents some preliminary results for the finned duct evaluation, and a discussion on the limitations that

restrict the application of the finned duct to the overall heat pump simulation.

Later sections of the chapter describe the model used for the refrigerant side of the heat exchanger, as well as the solution procedure used for the evaporator.

3.2 Finned Duct Model for the Water Side

This section deals with the development of a numerical model that can solve for ice formation in a finned annular sector and allows for periodic water flow reversals.

The geometry of the finned annular duct is shown in Figure 3.1. The primary and transversal fins are included to improve the performance of the evaporator. The surfaces along the fins enhance the heat transfer between the water and refrigerant. In addition to this, reversing the water flow direction in the finned duct causes some ice detachment from the fin surfaces. This ice detachment helps to partially deice the evaporator and improves its performance.

Ice detachment in the finned duct occurs after every water flow reversal. After a reversal, the warm water entering the duct comes in contact with a thick layer of ice (that existed at the end of the duct immediately before the reversal). This flow of warm water causes some of the ice to melt, starting with the ice in contact with the fin. When the ice at the fin melts down to the transversal fins, the remaining ice between the transversal fin and the

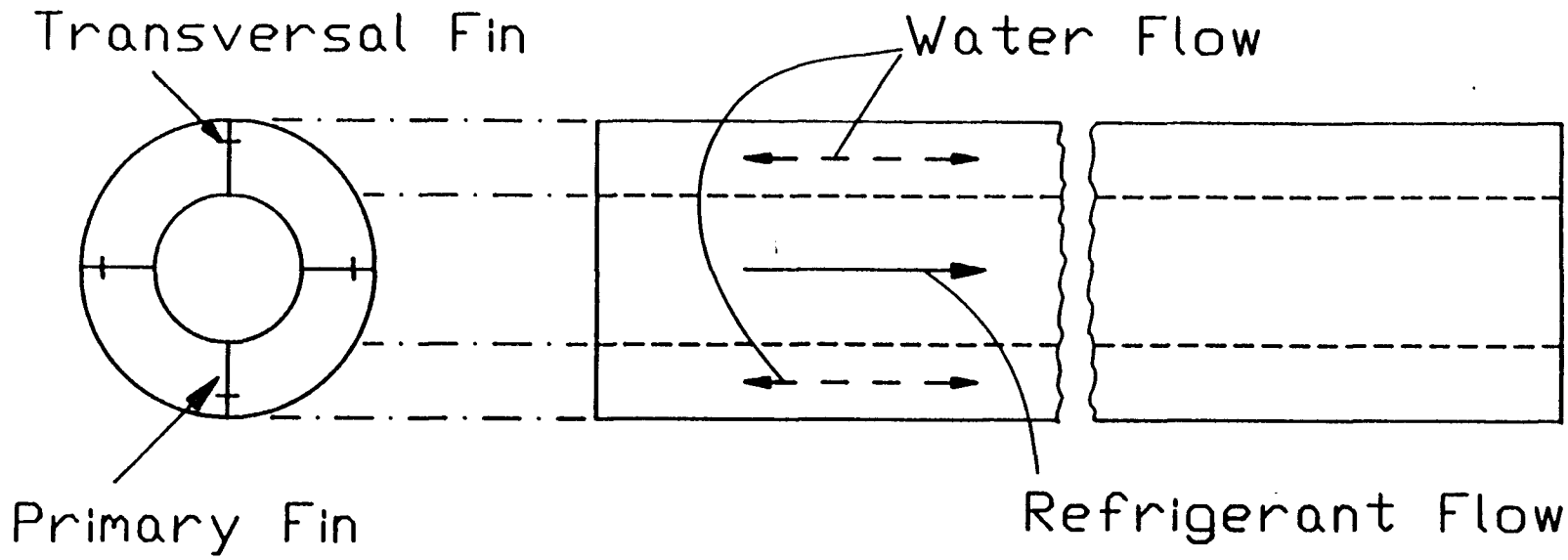

Figure 3.1 Finned evaporator configuration. Water flows in annulus formed by inner and outer tubes, and refrigerant flows inside inner tube. The positions of the primary longitudinal and transversal fins are shown (end view only). Water and refrigerant flow directions are longitudinal to the evaporator and fins. The dotted arrows indicate the two possible water flow directions. The refrigerant flow direction is indicated by an arrow.

external duct wall loses support and is free to flow out with the water. In this way, the transversal fins help in deicing the evaporator.

This section covers the development of the governing equations, the substitutions employed, the procedure for solving for temperatures and velocities for the three domains existing in the water side (water in solid and liquid phases, and the metallic wall), the assumptions made along the analysis, some evaporator evaluation results, and finally, a discussion on the application of this model to an overall heat pump simulation.

3.2.1 Governing Equations: The equations governing the flow and heat transfer in the water side of the evaporator are developed in this section. These equations include the energy equation for the solid and liquid phases, as well as the momentum and continuity equation for the liquid phase. Cylindrical coordinates are used throughout the analysis. By symmetry, it is necessary to solve for only half of the distance between consecutive fins. Figure 3.2 shows the solution domain, with all the cross sectional dimensions for the finned duct.

The assumptions used in the process are indicated along the way, and all the assumptions used are summarized in a later section.

The water flow rate through the evaporator is assumed to be constant. Therefore, the continuity equation can be written in integral form, as shown by Equation (3.1). This

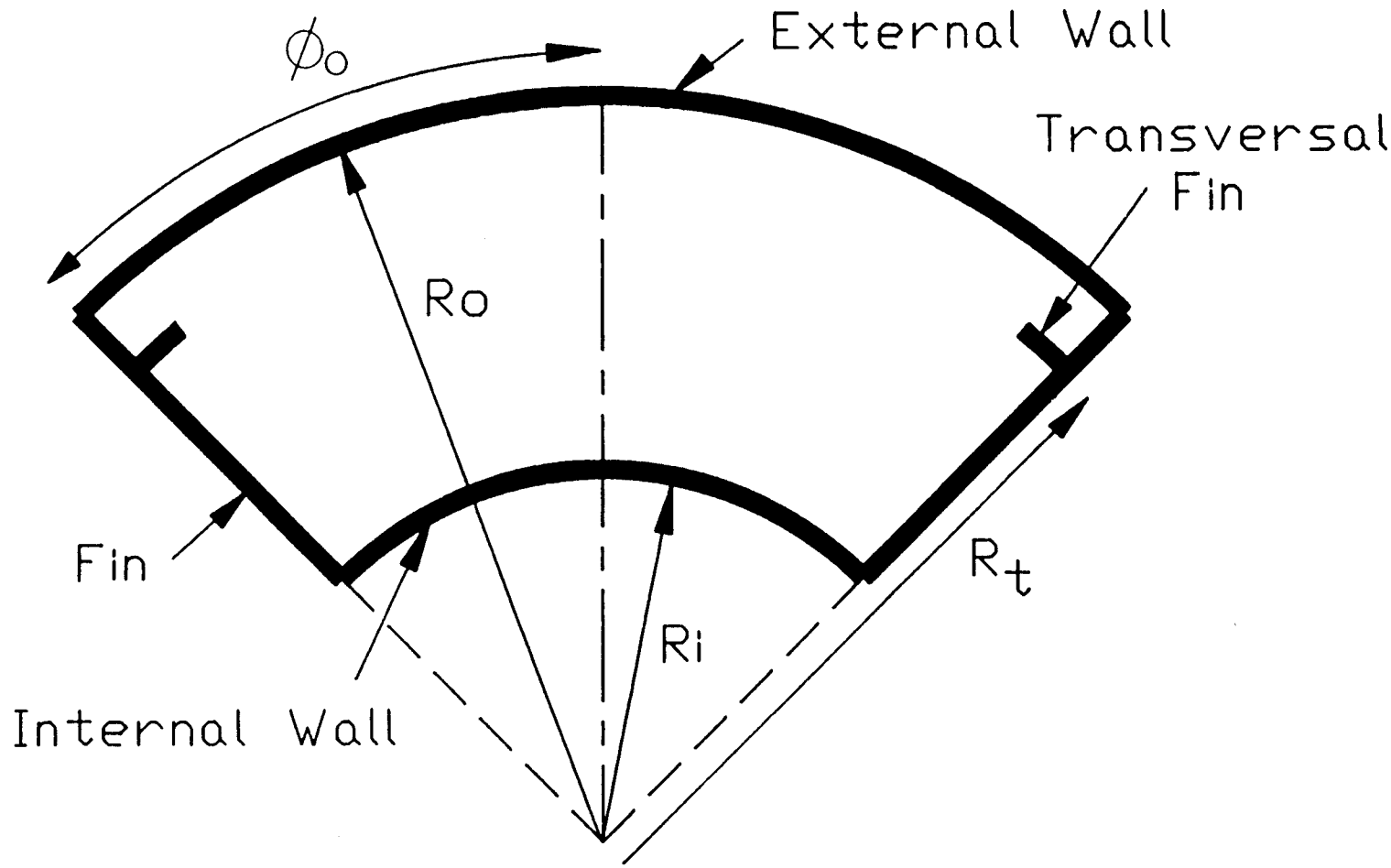

Figure 3.2 Solution domain. The dimensions indicated are: R_i, internal radius; R_o, external radius; R_t, radius to the transversal fin; ϕ_o, half the angle between two consecutive fins.

equation expresses the requirement that the flow rate is the same at all sections all the time.

$$V = \text{constant} = \int UdA = \int U\, r\, dr\, d\phi \tag{3.1}$$

The momentum equation for the liquid phase is,

$$\nabla^2 U = \frac{1}{\mu}\frac{dp}{dz} \tag{3.2}$$

this equation assumes a laminar, fully developed and steady-state flow.

The energy equation for the liquid and solid phases are respectively:

$$\frac{\partial T}{\partial t} + U\frac{\partial T}{\partial z} = \alpha_f \nabla^2 T \tag{3.3}$$

$$\frac{\partial T}{\partial t} = \alpha_i \nabla^2 T \tag{3.4}$$

Both equations neglect axial heat conduction.

The small thickness of the metallic wall makes it possible to reduce the energy equation for the metal to the one-dimensional heat transfer equation. This is expressed as,

$$k_s A \frac{\partial^2 T}{\partial x^2} - h P_h (T-T_r) = A Cp_s \rho_s \frac{\partial T}{\partial t} \tag{3.5}$$

where A represents the heat conduction area and P_h is the heat transfer perimeter of the metallic wall.

3.2.2 Initial And Boundary Conditions: Initially, the water inside the evaporator is assumed to have a constant temperature T_o. This condition is expressed as,

$$T_f = T_o \quad \text{at } t=0 \tag{3.6}$$

where T_f represents the fluid temperature.

The fluid entering the evaporator has a uniform temperature T_o, equal to the initial temperature. This condition is expressed as,

$$T_f = T_o \quad \text{at } z=0 \tag{3.7}$$

The boundary conditions for the momentum equation are:

$$U = 0 \quad \text{at the walls and solid interface} \tag{3.8}$$

$$\frac{\partial U}{\partial \phi} = 0 \text{ at the symmetry line} \tag{3.9}$$

The boundary conditions for the energy equation for both the liquid and solid phases are,

$$\frac{\partial T}{\partial r} = 0 \qquad \text{at the external radius} \tag{3.10}$$

$$T = T_c \qquad \text{at the ice-water interface} \tag{3.11}$$

$$T = T_s \qquad \text{at the walls} \tag{3.12}$$

$$\frac{\partial T}{\partial \phi} = 0 \qquad \text{at the symmetry line} \tag{3.13}$$

The energy balance at the interface is,

$$k_i \frac{\partial T_i}{\partial n} = k_f \frac{\partial T_f}{\partial n} + L \rho \frac{dFn}{dt} \tag{3.14}$$

where Fn represents the radius of the ice-water interface, and n is a coordinate in the direction normal to the interface.

3.2.3 Solution Procedure: Several methods have been developed to discretize the equations in moving boundary problems. The methods are divided into two major categories. Some methods use a fixed grid, while others use a grid that moves as the interface moves. See Crank, 1981, for a review of existing methods.

The solution method used here is a moving-grid solution based on the Landau transformation (Landau, 1950). In this method, a coordinate transformation is used to fix the position of the interface. The coordinate transformations used here are,

for the liquid phase,

$$r^* = \frac{R_o - r}{R_o - F(\phi,z,t)}$$
$$\phi^* = \frac{\phi}{\phi_o} \qquad (3.15)$$

for the solid phase,

$$r^* = \frac{r - R_i}{F(\phi,z,t) - R_i}$$
$$\phi^* = \frac{\phi}{\phi_o} \qquad (3.16)$$

where R_i is the radius of inner tube and R_o is the radius of the external tube.

The partial derivatives appearing in the governing equations are transformed to derivatives in the new system of coordinates by using the chain rule and Equations (3.15) and (3.16).

The solution domain is divided into 16 subintervals in the ϕ-direction, 10 subintervals in the radial direction for the liquid phase, and 10 subintervals in the radial direction for the solid phase. The program allows an irregular partition in the ϕ-direction to improve the accuracy, because the ice profiles present a steep slope near the fin. This situation requires the use of a small step size in the ϕ-direction near the fin, while a larger value can be used in other points.

The resulting discretized equations for the liquid and solid phases are solved by using the successive overrelaxation method (SOR). The derivative in the axial direction appearing in the liquid energy equation is discretized by using an upwind finite difference formula, as given by Patankar, 1980. The matrix resulting from the equation for the metallic wall is tridiagonal, and is solved by using an L-U decomposition method (Atkinson, 1978). See Aceves-Saborio, 1987, for more details on the iteration process and the non-dimensionalization of the variables.

3.2.4 Model Assumptions:

The assumptions made in the process of writing the model deal mostly with the neglect of second order factors. These assumptions were indicated in the development of the method and are summarized here.

1. The liquid flow is laminar everywhere and has a fully

developed, steady-state velocity profile and a uniform temperature at the entrance.

2. The liquid is newtonian, incompressible and a pure substance.

3. The physical properties of each phase are independent of temperature.

4. Axial heat conduction, viscous energy dissipation, radiant heat transfer and free convection are negligible.

5. The temperature at the liquid-solid interface is constant and equal to the freezing temperature.

6. The metallic walls are thin and the temperature profile in them can be described accurately as one-dimensional.

7. The water flow rate is always constant, regardless of the total head required to circulate it through the evaporator.

8. The external tube wall is perfectly insulated.

9. The ice layer that forms on the external tube wall is very thin and grows very slowly.

10. The transversal fin is sufficiently small so that it does not alter the flow or thermal conditions.

3.2.5 Testing of the Finned Duct Model: The evaporator model described in this section was written with the intention of using it in conjunction with a heat pump model, therefore permitting an evaluation of an overall heat pump system. However, this model was first tested as an individual unit. The intention of this is to get an early estimate of performance parameters, and evaluate the

improvements obtained by using the flow reversal method. To carry out this testing, the refrigerant side was modelled by assuming that the refrigerant temperature and refrigerant-side heat transfer coefficient are constant all along the evaporator. The evaporator parameters used for this testing are given in Table 3.1.

Figures 3.3, 3.4 and 3.5 show the results obtained from the finned duct model. Figure 3.3 shows steady-state ice profiles in the annular segment between two consecutive fins for a refrigerant-side heat transfer coefficient equal to 1500 $W/m^2 \cdot C$. The profiles are shown as a function of the axial position for the non-reversal case (water flow direction is never reversed). The figure does not show the transversal fins. Figure 3.4 shows energy transfer values between the water and refrigerant for the reversal case with a heat transfer coefficient of 1500 $W/m^2 \cdot C$ in the refrigerant side. The figure shows a curve with the overall heat transfer as a function of time. The other curves show the parts of the total energy transfer that corresponds to sensible energy (obtained by cooling down the water), latent energy (obtained by freezing the water), and energy obtained by ice that forms and then detaches from the wall in a reversal cycle. It can be seen that only a small portion of the ice detaches from the wall. However, this energy is significant, because it represents a net improvement compared with the water flow with no reversal, where no deicing ever occurs.

Table 3.1 Evaporator dimensions and physical conditions used during the testing of the finned annulus model. Several values were taken for the heat transfer coefficient in the range indicated.

Dimension	Value
external duct radius	0.02 m
internal duct radius	0.01 m
number of fins in annulus	4
duct wall thickness	0.001 m
fin thickness	0.001 m
inlet water temperature	5 °C
refrigerant temperature	-5 °C
refrigerant-side heat transfer coeff.	1500-2250 $W/m^2 °C$
water flow rate	0.0001 m^3/s
reversal time	200 s

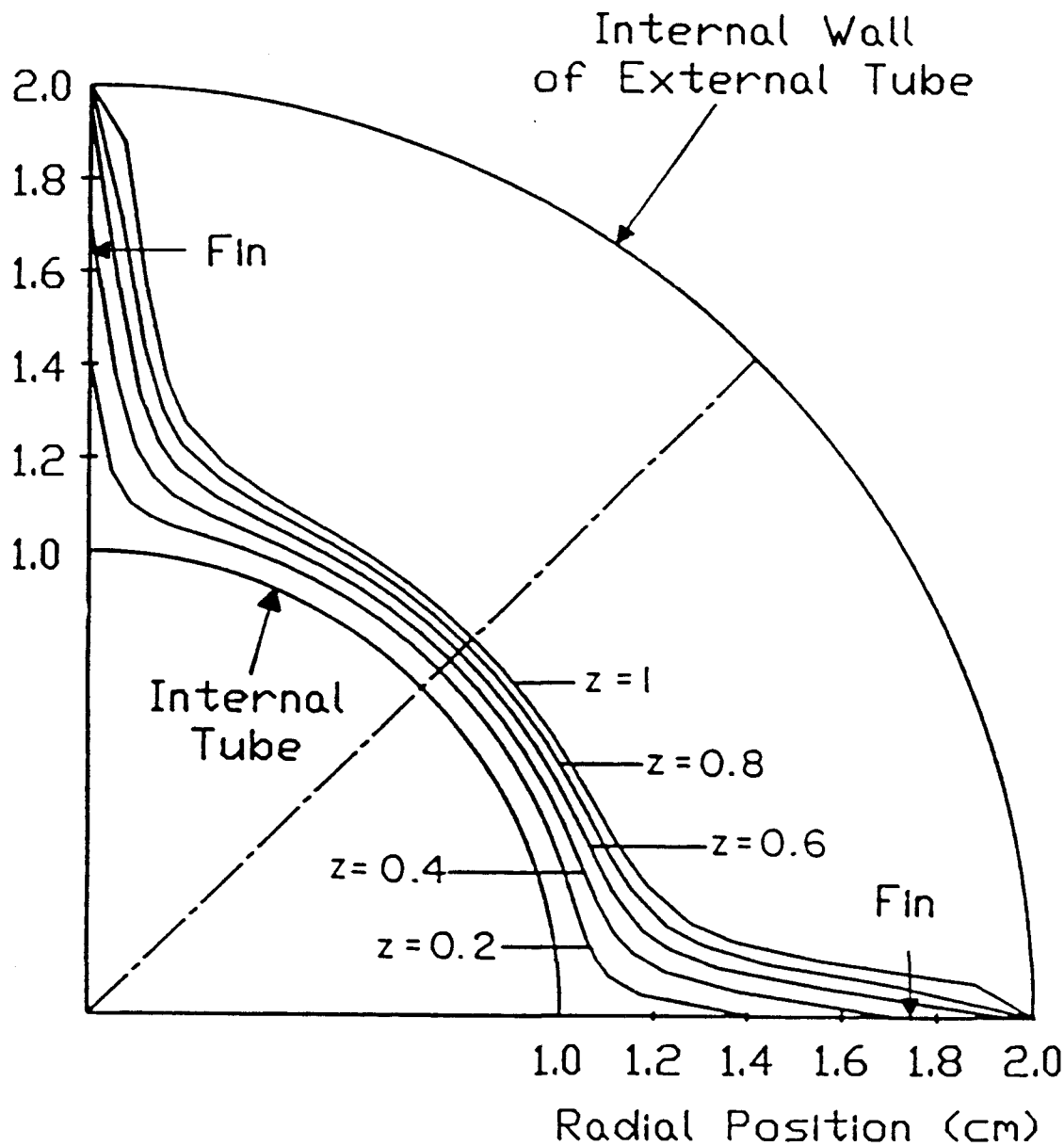

Figure 3.3 Steady-state ice profiles for h=1500 W/m^2°C and no water flow reversal as a function of the axial position z. Transversal fins not shown

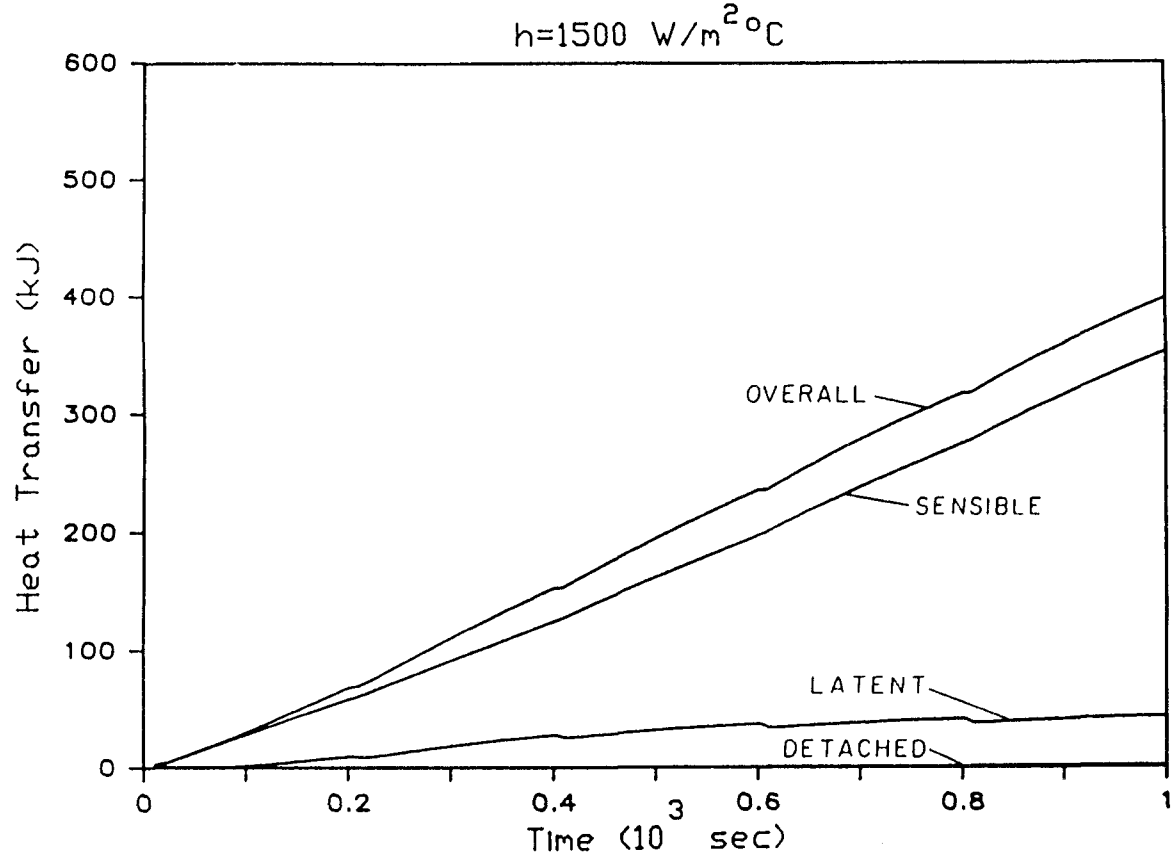

Figure 3.4 Energy transfer results for the reversal case with no refrigerant flow interruption. The refrigerant-side heat transfer coefficient is h=1500 W/m^2°C.

The overall average heat transfer power (total heat transfer divided by time elapsed) is an important evaporator parameter. Heat transfer power is useful to compare different evaporators with the same water mass flow rate. Under constant mass flow rate, the best evaporator is the one that has the highest heat transfer power, because an evaporator with the highest heat transfer power requires the least amount of water to satisfy a heating demand. Figure 3.5 shows the average heat transfer power for h = 2250 $W/m^2 \cdot C$ and for three cases being analyzed (no water flow reversal, water flow reversal every 200 s, and water flow reversal every 200 s followed by a 4-second refrigerant flow interruption). The heat transfer power starts at zero at time t=0, and increases until reaching its steady-state value. The curves in the figure are identical up to 200 s, when the first reversal occurs. From that point, the curves diverge. In steady-state, the curves go parallel to one another, with the reversal curve above the non-reversal curve by about 20% of the overall reversal power. This power increase is due mainly to an increase in sensible heat transfer (reversing the flow results in colder water exiting the evaporator). No gain in heat transfer power is obtained by interrupting the refrigerant flow immediately after a reversal.

3.2.6 Integration of The Finned Duct Model and the Heat Pump Model: The next step in the evaluation of the model for ice formation in the finned duct was to integrate it

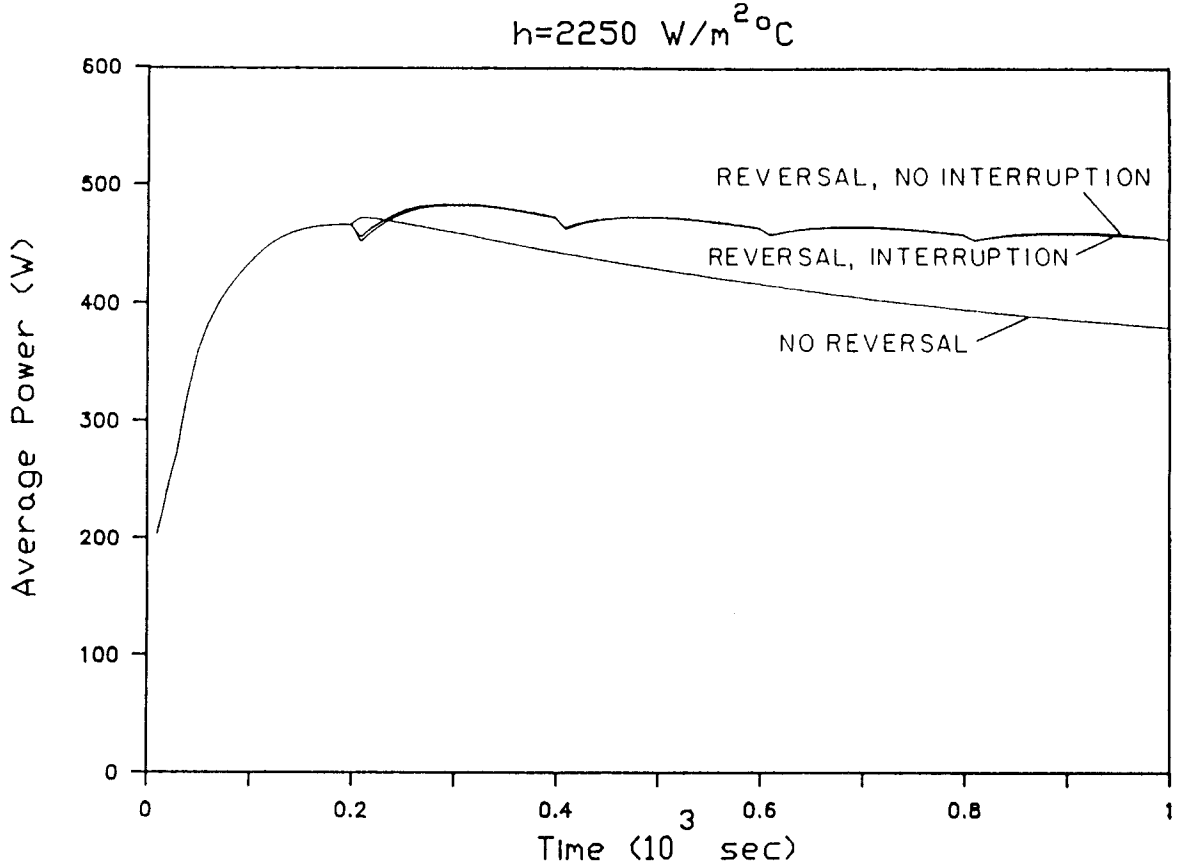

Figure 3.5 Comparison of the overall average power between the three cases being considered. The refrigerant-side heat transfer coefficient is h=2250 W/m²°C.

into the heat pump model, allowing then an overall heat pump evaluation. The results given in the previous section indicate that the use of the flow reversal method in the finned duct yielded a high evaporator performance. The fins have a double effect in producing this enhanced performance. They improve the heat transfer between the liquid and the refrigerant, and also allow a partial evaporator deicing.

Integrating the finned duct evaporator with the overall heat pump model (described in Chapter 4) does not present any major difficulties. The heat pumps operating with the finned duct evaporator have a good efficiency. However, the applicability of this model to overall heat pump simulations is limited. This is because the model cannot be applied to cases in which there is a thick layer of ice on the external tube wall (assumption 9, Section 3.2.4). This limitation takes special importance because the optimum heat pumps always have a high ice blockage rate (see Chapter 5). Therefore, this assumption makes it impossible to use this model for a heat pump optimization, which is the desired application in this thesis. Modifying the simulation code to lift this restriction requires adding the upper layer of ice as a different part of the solution domain. Adding another domain into the existing code would require substantial changes, and these modifications are considered to be beyond the scope of this thesis. For this reason, the finned duct model was

replaced by a duct with no fins, which can be modelled with relative facility without using any assumptions that require limiting the amount of ice in the evaporator. This model is described in the following section.

Although it was not possible to use the finned duct model for the heat pump optimization, the evaluation of the finned duct evaporator is still considered to be worthwile, and should be pursued in the future. The possibility of obtaining ice detachment in the evaporator is beneficial for the heat pump performance, and this possibility does not exist for the non-finned duct.

3.3 Non-Finned Duct Model for the Water Side

This section deals with the development of a numerical model that can solve for ice formation in an annular sector and allows for periodic water flow reversals. The annular sector has no fins. The model presented in this section is used to simulate the water side of the evaporator in the overall heat pump optimization (Chapter 5).

The development of this model follows closely the steps used to simulate the finned duct in the previous section. Still, the whole procedure is indicated here, to make both sections independent from each other, even if this implies some repetition. This section covers the development of the governing equations, the substitutions employed, the procedure for solving for temperatures and velocities for the two domains existing in the water side

(solid and liquid phases), and a summary of the assumptions used during the analysis.

3.3.1 Governing Equations: The equations governing the flow and heat transfer in the water side of the evaporator are developed in this section. These equations include the energy equation for the solid and liquid phases, as well as the momentum and continuity equation for the liquid phase. Cylindrical coordinates are used throughout the analysis. Due to symmetry, there is no ϕ-dependence in any variable. This condition simplifies the analysis. Assumptions used in the process are indicated along the way, and all the assumptions used are summarized in a later section.

The water flow rate through the evaporator is assumed to be constant. Therefore, the continuity equation can be written in integral form, as shown by Equation (3.1). This equation expresses the requirement that the flow rate is the same at all sections all the time.

$$V = \text{constant} = \int UdA = 2\,\pi \int U\,r\,dr \tag{3.17}$$

The momentum equation for the liquid phase is,

$$\frac{d^2U}{dr^2} + \frac{1}{r}\frac{dU}{dr} = \frac{1}{\mu}\frac{dp}{dz} \tag{3.18}$$

this equation assumes a laminar, fully developed and steady-state flow.

The energy equation for the liquid and solid phases are respectively:

$$\frac{\partial T}{\partial t} + U \frac{\partial T}{\partial z} = \alpha_f \nabla^2 T \qquad (3.19)$$

$$\frac{\partial T}{\partial t} = \alpha_i \nabla^2 T \qquad (3.20)$$

Both equations neglect axial heat conduction.

3.3.2 Initial And Boundary Conditions: Initially, the water inside the evaporator is assumed to have a constant temperature T_o. This condition is expressed as,

$$T_f = T_o \quad \text{at } t=0 \qquad (3.21)$$

where T_f represents the fluid temperature.

The fluid entering the evaporator has a uniform temperature T_o, equal to the initial temperature. This condition is expressed as,

$$T_f = T_o \quad \text{at } z=0 \qquad (3.22)$$

The boundary conditions for the momentum equation are:

$$U = 0 \quad \text{at the walls and solid interface} \qquad (3.23)$$

The boundary conditions for the energy equation in the liquid phase are,

$$\frac{\partial T}{\partial r} = 0 \qquad \text{at the external radius}$$
$$T = T_c \qquad \text{at the ice-water interface} \qquad (3.24)$$

and for the solid phase,

$$T = T_c \qquad \text{at the ice-water interface} \tag{3.25}$$

$$h_r\,(T_i - T_r) = k_i \frac{\partial T}{\partial r} \qquad \text{at the inner tube wall}$$

where h_r and T_r are the refrigerant-side heat transfer coefficient and temperature respectively.

The energy balance at the interface is,

$$k_i \frac{\partial T}{\partial r} = k_f \frac{\partial T}{\partial r} + L\,\rho\,\frac{dF}{dt} \tag{3.26}$$

where F represents the radius of the ice-water interface.

3.3.3 Solution Procedure: The solution method is based on the Landau transformation (Landau, 1950). In this method, a coordinate transformation is used to fix the position of the interface. The coordinate transformations used here are,

for the liquid phase,

$$r^* = \frac{R_o - r}{R_o - F(z,t)} \tag{3.27}$$

for the solid phase,

$$r^* = \frac{r - R_i}{F(z,t) - R_i} \tag{3.28}$$

where R_i is the radius of inner tube and R_o is the radius of the external tube.

The partial derivatives appearing in the governing equations are transformed to derivatives in the new system of coordinates by using the chain rule and Equations (3.27) and (3.28).

The first step in the solution procedure is to solve for the pressure drop and the velocity profile. The pressure drop and velocity profile in an annulus have a well-known closed form solution that can be obtained from Equations (3.17) and (3.18).

The energy equations for the liquid and solid phases do not accept closed-form solutions and therefore they are solved numerically. Both partial differential equations are parabolic, and therefore a marching solution in the axial direction is required. The matrices resulting for each axial step are tridiagonal and are solved by the L-U decomposition method (Atkinson, 1978). The derivative in the axial direction appearing in the liquid energy equation is discretized by using an upwind finite difference formula, as given by Patankar, 1980.

Once the temperatures of both the water and ice sides are known, Equation (3.26) is used to calculate the position of the ice-water interface. The process requires iteration, assuming an initial value of the radius of the interface and iterating until convergence.

3.3.4 Model Assumptions: The assumptions made in the process of writing the model deal mostly with the neglect of second order factors. These assumptions were indicated in the development of the method and are summarized here.
1. The liquid flow is laminar everywhere and has a fully developed, steady-state velocity profile and a uniform temperature at the entrance.

2. The liquid is newtonian, incompressible and a pure substance.
3. The physical properties of each phase are independent of temperature.
4. Axial heat conduction, viscous energy dissipation, radiant heat transfer and free convection are negligible.
5. The temperature at the liquid-solid interface is constant and equal to the freezing temperature.
6. The water flow rate is always constant, regardless of the total head required to circulate it through the evaporator.
7. The metallic walls are thin so that their thermal resistance is negligible.
8. The external tube wall is perfectly insulated.

3.4 The Refrigerant Side

It is difficult to obtain a distributed model that accurately predicts temperatures and velocities of a boiling refrigerant flowing in a cylindrical tube. Therefore, the analysis used here lumps the refrigerant properties in the radial direction, leaving pressure and temperature as a function of axial position only. Lumped analyses require previous knowledge of expressions for heat transfer coefficient and pressure drop. This section describes the heat transfer coefficient and pressure drop models used. The analysis that equilibrium exists between the two refrigerant phases.

3.4.1 The Heat Transfer Expression: A considerable number of correlations have been proposed for the calculation of heat transfer coefficients for boiling fluids flowing along a duct. However, most are not reliable beyond the range of data in which they are based. Even the Chen correlation (Chen, 1966), one of the most widely used and recommended expressions, is limited in application to vertical flows with a quality of less than 70%.

The most general expression for a heat transfer coefficient that can be applied to this problem is the one presented by Shah, 1976. Shah's method has been compared with about 800 data points from 18 independent experimental studies. These data include most of the common refrigerants in their entire range of application, as well as many different tube materials and orientations respect to the vertical.

To determine a heat transfer coefficient by using Shah's method, the following non-dimensional parameters are first calculated,

$$Bo = \frac{q}{G\, i_{fg}} \qquad \text{(boiling number)} \qquad (3.29)$$

$$Co = \left[\frac{1-x_r}{x_r} \right]^{0.8} \left[\frac{\rho_g}{\rho_f} \right]^{0.5} \qquad \text{(convection number)} \qquad (3.30)$$

$$Fr_f = \frac{G^2}{\rho_f^2\, g\, D} \qquad \text{(Froude number)} \qquad (3.31)$$

Then, these numbers are used to obtain a new parameter, σ, from a chart (Shah's chart). The parameter σ

is defined as,

$$\sigma = h_{tp}/h_f \tag{3.32}$$

where h_{tp} is the two-phase heat transfer coefficent and h_f is a single-phase, liquid-only, heat transfer coefficient, calculated from a Dittus-Boelter correlation,

$$h_f = 0.023 \left[\frac{D_{eq}\ G\ (1-x_r)}{\mu_f} \right]^{0.8} Pr_f^{0.4}\ k_f/D_{eq} \tag{3.33}$$

The need to obtain σ from a graph makes Shah's method difficult to use in a computer simulation. The task of programming Shah's chart into the computer is accomplished here by reading a number of points from the graph and interpolating between them with a Lagrangian interpolation subroutine.

A short segment at the end of the evaporator is likely to have superheated refrigerant vapor. For this segment, the simulation model uses a Dittus-Boelter correlation, similar to Equation (3.33).

3.4.2 The Pressure Drop Expression: The pressure drop in a flowing fluid can be written as a sum of three contributions, as follows (Collier, 1981),

$$-\frac{dp}{dz} = \left[-\frac{dp}{dz}\right]_F + \left[-\frac{dp}{dz}\right]_a + \left[-\frac{dp}{dz}\right]_g \tag{3.34}$$

the first term represents the friction contribution, the second term the acceleration contribution and the third term the gravity contribution.

Differences in level between inlet and outlet of heat pump evaporators are in general very small, so that the gravity contribution to the pressure drop can be safely neglected. The friction and acceleration contributions are estimated here by using the Thom-Goldstein method (Thom, 1964; Goldstein, 1979). The procedure is indicated next.

a) The Friction Term: The friction term for a boiling fluid is usually calculated by first finding the pressure drop that would exist if all the fluid were in the liquid state. This value is then multiplied by a correcting factor, as follows,

$$\left[- \frac{dp}{dz} \right]_F = \frac{2 f_{fo} G^2}{\rho_f D} \phi_{fo}^2 \qquad (3.35)$$

in this equation, ϕ_{fo}^2 is the correction factor and f_{fo} is the liquid-only friction factor.

Thom, 1964, calculated values of ϕ_{fo}^2 and of the integral of ϕ_{fo}^2 dz, necessary to obtain average friction factors along a finite length of the evaporator. The data was obtained for water-steam systems only, but later proved applicable to other fluids less viscous than water. However, the method can be applied only when the fluid is initially a saturated liquid (quality equal to zero). Goldstein, 1979, generalized the method to cases where the inlet quality is different to zero. The method consists of defining a pseudo-tube length. This pseudo length is the length that would be necessary to increase the quality of the fluid from a saturated liquid condition to the inlet

condition. Once this length is known, Thom's method can be applied to calculate pressure drops from a fictitious saturated liquid state to the actual inlet and outlet conditions. The pressure drop is the difference between these two pressure drops.

b) The Acceleration Term: A boiling fluid flowing inside a tube has a density that decreases as the fluid evaporates. This causes an increase in flow velocity. The resulting acceleration on the fluid originates a pressure drop.

Again, Thom integrated the expression for the accelerational pressure drop when the initial condition is a saturated liquid. The pressure drop was written in the form,

$$\Delta p_a = \frac{G^2}{\rho_f g} v_2 \qquad (3.36)$$

where v_2 is a factor that depends on the pressure and outlet quality of the fluid.

Goldstein applied the same concept of a fictitious length to calculate acceleration pressure drops. The pressure drop is calculated as the difference between two terms identical to the right hand side of Equation (3.36), as shown in the following equation,

$$\Delta p_a = \frac{G^2}{\rho_f g} v_{2out} - \frac{G^2}{\rho_f g} v_{2in} \qquad (3.37)$$

where the factors v_{2out} and v_{2in} are evaluated at the outlet and inlet conditions respectively.

3.5 Solution Procedure

This section presents a global view of the solution for the evaporator and the order in which all the operations are done. The presentation is based on the flow chart of the program (Figure 3.6). Many blocks in this figure indicate solutions for velocities, temperatures, heat transfer coefficients and pressure drops. These solutions are obtained by following the procedures described in earlier sections of this chapter.

The program starts by obtaining the appropriate values of the inlet conditions. For the water, the inlet temperature is a given value. For the refrigerant, the inlet temperature, pressure and quality have to be obtained from the global heat pump simulation. The next step is to calculate the heat transfer coefficient in the refrigerant side. However, the heat transfer coefficient is a function of the heat transfer rate (Equation (3.29)), and therefore it is necessary to guess an initial value of the heat transfer rate.

Once the conditions in the refrigerant side have been evaluated, the program solves for the water side. Velocities, temperatures and ice profiles are calculated. At this point, everything is known and the heat transfer rate can be calculated and compared to the initial assumption. The program iterates until reaching convergence.

When convergence is obtained, the program updates both

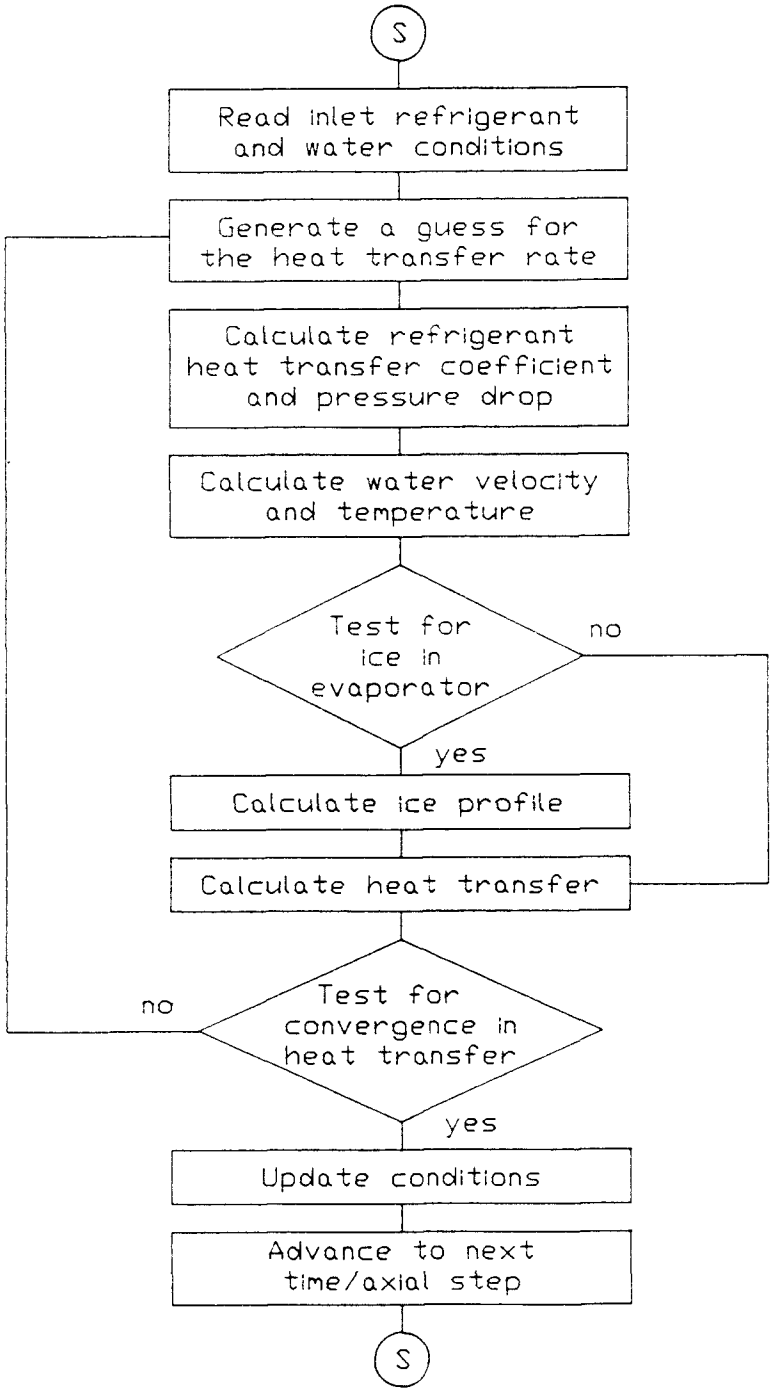

Figure 3.6 Flow chart of the solution procedure for the evaporator

water and refrigerant-side conditions. For the water side, these include temperatures and radius of the interface. For the refrigerant side, pressure, temperature, enthalpy and quality need to be updated. Updating completes the calculations for the segment of the evaporator, and leaves the program ready to move to the next axial or time step.

IV. THE HEAT PUMP MODEL

4.1 Introduction

Heat pump performance is estimated here by using the Oak Ridge National Laboratory (ORNL) heat pump model (Fischer et al., 1988). The ORNL model was written to simulate air-source heat pumps in steady-state. To make this model applicable to water-source heat pumps, the evaporator model used in the ORNL model was replaced by the evaporator model described in the previous chapter.

This chapter describes the ORNL model as modified to simulate the water-source heat pump. First, the major characteristics of the ORNL model are indicated, followed by a description of the modules used to simulate the compressor, condenser and expansion device. Later sections of the chapter summarize the data used during the heat pump simulation, and the assumptions and limitations involved with using a steady-state heat pump model in conjunction with a time-dependent evaporator to calculate time-dependent heat pump performance. The last section shows the solution procedure for the heat pump. The descriptions included in this chapter only highlight the major characteristics of the model. For more details, consult Fischer et al., 1988.

4.2 The ORNL Heat Pump Model

The ORNL model is used to simulate the performance of the high-pressure side of the heat pump (condenser, compressor, expansion device). The model is a steady-state simulation, and is based on lumped analyses for the heat pump components. The necessary data input includes the following:

1. The level of evaporator exit superheat (or quality).
2. Design parameters for a flow control device or the level of condenser exit subcooling.
3. Condenser inlet air temperature.
4. Dimensions of components and interconnecting pipes.
5. Heat losses from interconnecting pipes.

From this input, the original ORNL model predicts heat pump performance data, such as COP, capacity, power consumptions and refrigerant conditions at different points in the heat pump. In addition to these, the modified model used here was extended to allow calculation of irreversibility generation rates in heat pump components, as well as exergetic efficiency values.

The heat pump system is simulated by modeling the individual components and then performing an iteration to establish a balance point among these components. The following section presents the heat pump component models. The solution procedure is given in a later section.

4.3 Models Used For Heat Pump Component Simulation

This section describes briefly the three high-pressure side components.

4.3.1 Compressor: The ORNL model gives two different alternatives to simulate compressor performances. One is based on the use of compressor manufacturer's data (compressor maps), and the other is to use a loss-and-efficiency-based compressor model. The map model can predict more accurately the performance of existing compressors and therefore is used in this analysis. The map model calculates compressor power and mass flow rate as a function of the inlet and outlet compressor saturated temperatures. The model includes corrections to adjust for levels of refrigerant superheat that are different to those for which the maps were generated.

4.3.2 Condenser: The ORNL heat pump model calculates the condenser performance by using effectiveness vs. number of heat transfer units (NTU) correlations. The evaporator is divided in three sections, the desuperheating section, the two phase section and the subcooling section. Different correlations are used for heat transfer coefficient and pressure drop in each one of the three sections of the evaporator. The two phase section calculations use the Chaddock and Noerager (Chaddock and Noerager, 1966) correlation for the heat transfer coefficient and the Thom-Goldstein (Thom, 1964; Goldstein, 1979) correlation for

pressure drop. For details see Fischer et al., 1988.

In the air side, the model calculates exit temperature, pressure drop and required fan power.

4.3.3 Flow Control Device: There are also two different alternatives to specify the flow control device in the ORNL model. The first one consists of fixing a condenser outlet supercool. The second alternative is to specify a flow control device and a set of characteristic parameters for the device. The following flow control devices can be specified,

1. Capillary tube
2. Thermostatic expansion valve
3. Short tube orifice

A fixed condenser outlet supercool is specified for the present work. The computer program then calculates expansion device parameters that would yield the desired supercool for the three possible flow control devices listed above.

4.4 Heat Pump Parameters

This work is focused on improving evaporator performance. Therefore, the high-pressure side parameters were not changed during program execution. The values of all the parameters were obtained from ORNL model files (the data files used from the ORNL model are EXAMPLE1.HET and BLOCK.FOR), and represent typical values for a good-efficiency heat pump. The present section shows the values

for some of the main parameters. The original files should be consulted if more information is required.

Refrigerant - R22

Water temperature entering evaporator - 5°C

Air temperature entering condenser - 21.7°C

Air relative humidity entering condenser - 54%

Air flow rate into condenser - 0.59 m^3/s

Compressor displacement - 59.6 cm^3

Compressor synchronous motor speed - 3450 rpm.

Refrigerant superheat at compressor inlet - 10.2°C

Refrigerant subcool at condenser outlet - 12.2°C

Tolerance in superheat at compressor inlet - 0.05°C

Tolerance in subcool at condenser outlet - 0.11°C

4.5 The Quasi-Steady-State Assumption

The present work uses a steady-state heat pump model to estimate time-dependent performance. Simulating time-dependent behavior with a steady-state model is likely to yield inaccurate results, with the inaccuracy increasing rapidly as the situation being studied becomes more time-dependent.

However, a steady-state model yields good results if the process being simulated is slow relative to other time scales involved in the problem. In the heat pump studied here, all time dependence comes from the evaporator. The evaporator conditions vary with time as ice builds on the surfaces and water temperature drops. The two time scales

present in the problem are the time for the ice to grow in the evaporator and the time that it takes for the heat pump to react to the changes in evaporator conditions. Using a steady-state assumption is equivalent to assuming that the heat pump can react to the changes in conditions much faster than it takes for the ice to form in the evaporator. If this assumption holds, the heat pump adjusts rapidly to any change and remains basically at steady-state all the time, with some time-dependence introduced by changes occurring in the evaporator. This condition of slow time dependence in a nearly steady-state process is commonly called quasi-steady-state.

Therefore, the use of the steady-state model is justified if the time of response of the heat pump is much shorter than the time scale associated with ice formation. The time of response for a typical heat pump can be estimated from the work of MacArthur and Grald, 1987. They predict a time of the order of 100 s for a heat pump to reach steady state from start-up. On the other hand, the transient period for ice formation in the evaporator was estimated by Aceves-Saborio as being in the order of 1200 s (Aceves-Saborio et al., 1989a). Therefore, the heat pump can be assumed to operate in quasi-steady-state all the time, with the only time dependence coming from the evaporator time evolution. In this way, the model can calculate unsteady-state performance during ice buildup and flow reversals.

Although the quasi-steady-state assumption justifies the use of the steady-state model to calculate time dependent performance, it does not allow the use of the model for more highly time-dependent situations, such as the reversal cycles commonly used to deice the evaporator. Therefore, the use of the steady-state model makes it impossible to calculate the energy required for evaporator deicing.

4.6 Solution Method

The solution method used in the present work for the high pressure side of the heat pump is exactly the same as that used in the original ORNL model. Since this method is presented with great detail by Fisher et al., 1988, only its major characteristics are described here. The solution for the low pressure side has been changed from that used in the ORNL model and is discussed with more detail.

Figure 4.1 is a flow chart of the method, and indicates the major calculational steps. The procedure starts by reading the program data. In addition to the data input, the procedure requires initial guesses for the refrigerant saturation temperature at compressor inlet, TSICMP, and refrigerant saturation temperature at compressor outlet, TSOCMP. With these guesses, the program can solve for all the high pressure side conditions, including the refrigerant subcool at the condenser outlet. This refrigerant subcool must be equal to a specified

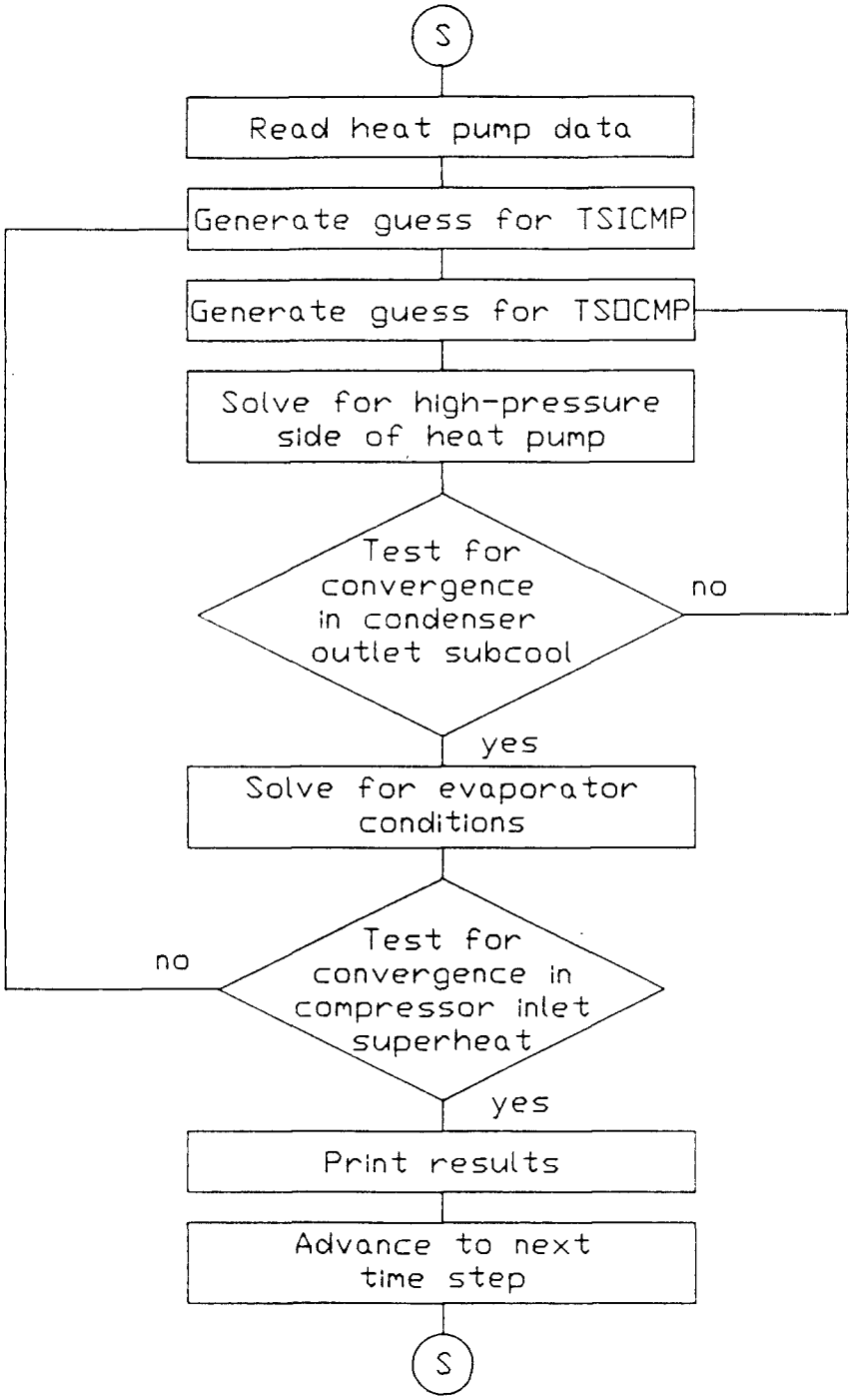

Figure 4.1 Flow chart of the heat pump simulation method

value. If the calculated value and required value do not agree within the given tolerance, the program generates an improved guess for TSOCMP and iterates until convergence.

Once convergence is obtained in the high pressure side, the program solves for the evaporator conditions. The procedure to solve for the evaporator is given in Section 3.4 and Figure 3.1. The compressor inlet superheat is also calculated, and its value is compared to a required value. If both values do not agree within a given tolerance, the program makes a new guess for TSICMP and iterates until convergence. The new guess is generated by using the Newton-Raphson method until the solution is bound (until the correct value of TSICMP is known to be within some temperature interval). Once the solution is bound, the program generates improved solutions by interpolation. When the program reaches convergence, the results are written in the data files and the program proceeds to solve for the next time step.

V. RESULTS. HEAT PUMP OPTIMIZATION

5.1 Introduction

This chapter presents the optimization of the water-source heat pump described in the previous chapters. The chapter shows the results of five different optimizations. The first optimization is for the heat pump operating as a water-source heat pump (with no evaporator deicing). The other four optimizations are done for the heat pump operating as an ice-maker heat pump. Each of these four optimizations takes into account a different time length of heat pump operation cycle (time between consecutive deicings), because the efficiency of an ice-maker heat pump depends on the frequency of the deicings. In addition, to illustrate the influence of reversing the water flow direction, three different cases are considered within each optimization: no water flow reversal (continuous water flow in one direction), water flow reversal every 300 s and water flow reversal every 600 s.

The main purpose of this analysis is to find evaporator characteristics that improve the heat pump performance. Therefore, the optimization is done only with respect to evaporator parameters. The high-pressure-side parameters are kept fixed, at values given in Section 4.4.

There are two usual means of optimizing a heat pump. The first is an economic optimization and the second is a

maximization of a performance parameter. From the point of view of heat pump ownership, an economic optimization is the preferred method. However, there is always some uncertainty in the parameters involved in an economic optimization. Therefore, the present optimization is done in terms of performance parameters.

Some authors (Rice et al., 1981; Elger, 1983; Lee, 1989) have done performance optimizations for heat pumps. These analyses use the heat pump COP as the objective function. The present study uses the exergetic efficiency as the figure of merit to be maximized, due to its more fundamental character. However, COP values are also reported, and the designs that maximize the exergetic efficiency are found to correspond closely with those that maximize the COP.

The following sections present a description of the objective functions, the decision variables, the design constraints, the optimization results, a discussion section that looks in detail at how the different evaporator parameters affect the performance, and finally a section that summarizes the conclusions developed in the chapter.

5.2 Objective Function

The objective function to be maximized in this optimization is the exergetic efficiency. The exergetic efficiency is defined as,

$$\Phi \equiv \frac{EX_{out}}{EX_{in}} \tag{5.1}$$

The exergetic efficiency of a water-source heat pump with freezing depends on the length of the operation cycle (period of time between consecutive deicings). A water-source heat pump can operate in steady-state, without ever requiring deicing. A heat pump may also require periodic deicings. If periodic deicing is required, the heat pump operates as an ice-maker heat pump. Different efficiencies exist also for an ice-maker heat pump as the operation period varies. Therefore, the optimization is done for ice-maker heat pumps requiring deicing at four different times (30 min, 1 hour, 2 hours, and 4 hours), as well as for water-source heat pumps operating in steady-state, with no deicing. Then, five different optimizations are done. The objective function for the ice-maker heat pumps is the average exergetic efficiency along the time period of operation. The objective function for the water-source heat pump is the steady-state exergetic efficiency. The exergetic efficiencies for the ice-maker heat pump do not include the energy required for deicing the evaporator, since, as discussed in Section 4.5, the steady-state model used for the heat pump simulation cannot be used to predict this value. Therefore, the calculated values for the exergetic efficiencies of the ice-maker heat pumps are overestimations. See Section 5.5.1 for a more complete discussion.

It is possible to argue that ice-maker heat pumps with a long operation time (like 2 hours, but especially 4 hours) should be called water-source heat pumps, since they obtain most of their energy by cooling down the water, rather than by freezing the water. However, these heat pumps are still called ice-maker heat pumps here because they require a periodic deicing and reduce water consumption by producing ice. Ice-maker heat pumps with a short operation time can be considered to be closer to a pure ice-maker heat pump, since most of their energy comes from freezing the water.

Exergy values are always referred to a dead state. For a water-source heat pump, it is natural to choose the inlet water temperature (5°C, see Section 4.4) and atmospheric pressure as the dead state conditions. No chemical changes occur in either the water or the air circulating through the heat exchangers and therefore no chemical exergy components have to be considered.

The value of EX_{out} is given as a sum of two components. The air circulating by the condenser gains exergy as its temperature increases, and also the water circulating through the evaporator gains exergy as it cools down or freezes. The exergy of the air is used to satisfy the heating demand. The exergy of the water could be used for seasonal cool storage applications, where cold water and/or ice generated during the heating season are stored and later used to provide air conditioning (Fischer and

Nephew, 1976). However, seasonal cold storage requires the use of substantial extra hardware, like a big storage tank and control instruments, and therefore this option is not considered here. Therefore, the only useful exergy stream is the air exergy, and only this value is used to calculate EX_{out}.

The exergy inlet includes the energy provided to the compressor, air fan and water pump. The water used for the heat pump operation has to be pumped from a water reservoir that can be either at the surface or underground. In any case, some power is necessary to pump the water to the heat pump. In this analysis, this power is taken into account by considering that it is necessary to overcome a total head of 50 m to pump the water from the reservoir to the heat pump. This head is added to the pressure drop inside the evaporator to obtain the total required pumping power. The value of 50 m was chosen as a typical value, in close agreement with the value used by Mei, 1983. Although the optimization was carried out with the pumping head fixed at this value, Section 5.5.7 studies the effect of changing the pumping head on the optimum design.

Writing EX_{in} and EX_{out} in terms of their components as previously discussed, Equation (5.1) becomes,

$$\Phi = \frac{EX_{air}}{W_{comp} + W_{fan} + W_{pump}} \qquad (5.2)$$

where W is the power consumption. The exergy gained by the air can be calculated as (Moran, 1982),

$$EX_{air} = m_{air}\, Cp_{air} \left[T_{out,air} - T_{in,air} - \ln \frac{T_{out,air}}{T_{in,air}} \right] \quad (5.3)$$

5.3 Decision Variables and Constraints

As previously discussed, all decision variables in the optimization problem are evaporator parameters. The decision variables used and the allowable range of values for each one are as follows,

water volumetric flow rate, V, m^3/s	$V \geq 2x10^{-4}$
number of evaporator circuits in parallel, N	$4 \leq N \leq 8$
evaporator circuit length, l, m	$1 \leq 20$
evaporator circuit external radius, R_o, cm	$1 \leq R_o \leq 2$

The internal radius of the evaporator circuit, R_i, is kept at a value equal to half of the external radius. The volumetric flow rate is constrained to guarantee that natural convection and axial conduction effects are negligible. The dimensions of the evaporator need to be kept under a certain maximum value because the objective function used is a performance figure. Performance figures do not take into account the cost of area and therefore their use in heat exchanger optimizations with no area constraints result in optimum heat exchangers with unreasonably large or even infinite area. The present analysis can be combined with an economic analysis or with a material exergy analysis (Aceves-Saborio et al., 1989b) to yield optimum heat exchangers with finite area. However, neither of these are used for this optimization.

For further discussion on material exergy analysis, consult Section 5.5.5. This section includes an analysis based on the material exergy method where optimum finite areas are calculated as a function of area costs.

5.4 Optimization Results

Tables 5.1 through 5.5 show the optimum designs from the optimization for each one of the 5 objective functions being optimized (average exergetic efficiencies for ice-maker heat pumps with operation periods lasting 1800 s, 3600 s, 7200 s, and 14400 s; as well as the exergetic efficiency for a water-source heat pump operating in steady-state). All the optimum designs have the maximum allowable number of circuits in parallel (8). This is a consequence of using an objective function that does not take area costs into account.

Each table shows the optimum designs for the three cases studied, water flow direction reversal every 300 s, reversal every 600 s, and no reversal. For the no reversal case the water and refrigerant flow in opposite directions (counterflow) because this configuration gives a higher performance (see Section 5.5.2).

Tables 5.1 to 5.5 show nine selected combinations of external duct radius and length, followed by the water volumetric flow rate that maximizes the efficiency at the given radius and length. The tables also show the efficiencies, COP values, and times of duct freeze-up for

Table 5.1 Optimum evaporator conditions. The objective function is the average exergetic efficiency for an ice-maker heat pump with an operation period of 1800 s. The table shows flow rates, average performance values during the operation time, and times of duct blockage. No indication of blockage time means that blockage never occurs. The results are shown for selected values of the evaporator duct radius and length, and for the three cases being studied (no water flow reversal, reversal every 300 s, and reversal every 600 s). The number of evaporator ducts is equal to 8. The optimum efficiency and COP for each set are underlined.

(a) Reversal Period of 300 s

radius R_o, cm	length l, m	flow rate $Vx10^4$, m^3/s	ex effncy Φ	COP	time block t_{block}, s
1.0	10	2.6	0.211	2.706	2150
1.0	15	2.1	0.227	2.801	2000
1.0	20	2.0	<u>0.235</u>	<u>2.950</u>	2300
1.5	10	2.0	0.214	2.768	3400
1.5	15	2.0	0.227	2.883	4300
1.5	20	2.0	0.235	2.945	5100
2.0	10	2.0	0.212	2.750	5800
2.0	15	2.0	0.223	2.844	7150
2.0	20	2.0	0.230	2.909	8600

(b) Reversal Period of 600 s

radius R_o, cm	length l, m	flow rate $Vx10^4$, m^3/s	ex effncy Φ	COP	time block t_{block}, s
1.0	10	2.7	0.210	2.696	2250
1.0	15	2.0	0.227	2.880	1950
1.0	20	2.0	<u>0.235</u>	<u>2.950</u>	2350
1.5	10	2.0	0.215	2.769	3500
1.5	15	2.0	0.228	2.885	4450
1.5	20	2.0	0.235	2.946	5350
2.0	10	2.0	0.212	2.751	6150
2.0	15	2.0	0.223	2.846	7700
2.0	20	2.0	0.231	2.910	9300

(c) No Reversal

radius R_o, cm	length l, m	flow rate $Vx10^4$, m^3/s	ex effncy Φ	COP	time block t_{block}, s
1.0	10	3.2	0.206	2.639	2100
1.0	15	2.2	0.226	2.851	2000
1.0	20	2.0	<u>0.236</u>	<u>2.951</u>	2450
1.5	10	2.0	0.215	2.771	2650
1.5	15	2.0	0.228	2.887	3750
1.5	20	2.0	0.235	2.950	4900
2.0	10	2.0	0.212	2.753	4450
2.0	15	2.0	0.223	2.849	5850
2.0	20	2.0	0.231	2.914	7300

Table 5.2 Optimum evaporator conditions. The objective function is the average exergetic efficiency for an ice-maker heat pump with an operation period of 3600 s. The table shows flow rates, average performance values during the operation time, and times of duct blockage. No indication of blockage time means that blockage never occurs. The results are shown for selected values of the evaporator duct radius and length, and for the three cases being studied (no water flow reversal, reversal every 300 s, and reversal every 600 s). The number of evaporator ducts is equal to 8. The optimum efficiency and COP for each set are underlined.

(a) Reversal Period of 300 s

radius R_o, cm	length l, m	flow rate $Vx10^4$, m^3/s	ex effncy Φ	COP	time block t_{block}, s
1.0	10	3.3	0.202	2.598	--
1.0	15	3.2	0.214	2.713	4800
1.0	20	3.0	0.222	2.786	4150
1.5	10	2.2	0.207	2.694	3800
1.5	15	2.0	0.223	2.848	4300
1.5	20	2.0	<u>0.231</u>	<u>2.918</u>	5100
2.0	10	2.0	0.208	2.710	5800
2.0	15	2.0	0.221	2.822	7150
2.0	20	2.0	0.228	2.887	8600

(b) Reversal Period of 600 s

radius R_o, cm	length l, m	flow rate $Vx10^4$, m^3/s	ex effncy Φ	COP	time block t_{block}, s
1.0	10	3.4	0.201	2.586	--
1.0	15	3.2	0.214	2.710	4800
1.0	20	3.0	0.222	2.790	4300
1.5	10	2.2	0.208	2.697	3950
1.5	15	2.0	0.224	2.850	4450
1.5	20	2.0	<u>0.232</u>	<u>2.920</u>	5350
2.0	10	2.0	0.208	2.711	6150
2.0	15	2.0	0.221	2.822	7700
2.0	20	2.0	0.228	2.889	9300

(c) No Reversal

radius R_o, cm	length l, m	flow rate $Vx10^4$, m^3/s	ex effncy Φ	COP	time block t_{block}, s
1.0	10	3.8	0.198	2.530	--
1.0	15	3.7	0.211	2.659	5550
1.0	20	3.3	0.219	2.756	4000
1.5	10	2.9	0.202	2.615	3800
1.5	15	2.0	0.222	2.837	3750
1.5	20	2.0	<u>0.232</u>	<u>2.924</u>	4900
2.0	10	2.0	0.209	2.715	4450
2.0	15	2.0	0.221	2.828	5850
2.0	20	2.0	0.229	2.894	7300

Table 5.3 Optimum evaporator conditions. The objective function is the average exergetic efficiency for an ice-maker heat pump with an operation period of 7200 s. The table shows flow rates, average performance values during the operation time, and times of duct blockage. No indication of blockage time means that blockage never occurs. The results are shown for selected values of the evaporator duct radius and length, and for the three cases being studied (no water flow reversal, reversal every 300 s, and reversal every 600 s). The number of evaporator ducts is equal to 8. The optimum efficiency and COP for each set are underlined.

(a) Reversal Period of 300 s

radius R_o, cm	length l, m	flow rate $Vx10^4$, m^3/s	ex effncy Φ	COP	time block t_{block}, s
1.0	10	3.5	0.199	2.558	--
1.0	15	3.6	0.209	2.651	--
1.0	20	3.7	0.215	2.702	--
1.5	10	2.9	0.198	2.578	8200
1.5	15	3.0	0.211	2.700	8200
1.5	20	2.9	0.219	2.779	7800
2.0	10	2.4	0.200	2.619	7500
2.0	15	2.1	0.216	2.776	7400
2.0	20	2.0	<u>0.225</u>	<u>2.861</u>	8600

(b) Reversal Period of 600 s

radius R_o, cm	length l, m	flow rate $Vx10^4$, m^3/s	ex effncy Φ	COP	time block t_{block}, s
1.0	10	3.6	0.198	2.551	--
1.0	15	3.6	0.209	2.653	--
1.0	20	3.6	0.215	2.709	--
1.5	10	2.9	0.198	2.582	8950
1.5	15	2.9	0.212	2.711	8000
1.5	20	2.7	0.221	2.798	7500
2.0	10	2.3	0.201	2.631	7500
2.0	15	2.0	0.217	2.792	7700
2.0	20	2.0	<u>0.225</u>	<u>2.862</u>	9300

(c) No Reversal

radius R_o, cm	length l, m	flow rate $Vx10^4$, m^3/s	ex effncy Φ	COP	time block t_{block}, s
1.0	10	4.0	0.195	2.508	--
1.0	15	4.1	0.206	2.607	--
1.0	20	4.1	0.212	2.668	--
1.5	10	3.5	0.194	2.528	--
1.5	15	3.6	0.207	2.644	--
1.5	20	3.4	0.217	2.735	7900
2.0	10	3.1	0.195	2.553	9100
2.0	15	2.8	0.211	2.706	7650
2.0	20	2.1	<u>0.224</u>	<u>2.853</u>	7500

Table 5.4 Optimum evaporator conditions. The objective function is the average exergetic efficiency for an ice-maker heat pump with an operation period of 14400 s. The table shows flow rates, average performance values during the operation time, and times of duct blockage. No indication of blockage time means that blockage never occurs. The results are shown for selected values of the evaporator duct radius and length, and for the three cases being studied (no water flow reversal, reversal every 300 s, and reversal every 600 s). The number of evaporator ducts is equal to 8. The optimum efficiency and COP for each set are underlined.

(a) Reversal Period of 300 s

radius R_o, cm	length l, m	flow rate $Vx10^4$, m^3/s	ex effncy Φ	COP	time block t_{block}, s
1.0	10	3.6	0.197	2.542	--
1.0	15	3.7	0.207	2.629	--
1.0	20	3.9	<u>0.213</u>	2.673	--
1.5	10	3.2	0.194	2.536	--
1.5	15	3.4	0.206	2.635	--
1.5	20	3.6	0.212	2.687	21100
2.0	10	3.0	0.193	2.528	20500
2.0	15	3.1	0.205	2.636	15050
2.0	20	3.1	0.212	<u>2.701</u>	14800

(b) Reversal Period of 600 s

radius R_o, cm	length l, m	flow rate $Vx10^4$, m^3/s	ex effncy Φ	COP	time block t_{block}, s
1.0	10	3.6	0.197	2.537	--
1.0	15	3.8	0.207	2.629	--
1.0	20	3.8	0.213	2.681	--
1.5	10	3.1	0.194	2.539	--
1.5	15	3.3	0.207	2.643	18950
1.5	20	3.4	0.214	2.707	16850
2.0	10	2.9	0.193	2.538	18650
2.0	15	3.0	0.206	2.654	16450
2.0	20	2.9	<u>0.214</u>	<u>2.732</u>	15500

(c) No Reversal

radius R_o, cm	length l, m	flow rate $Vx10^4$, m^3/s	ex effncy Φ	COP	time block t_{block}, s
1.0	10	4.1	0.194	2.495	--
1.0	15	4.2	0.204	2.591	--
1.0	20	4.2	0.211	2.649	--
1.5	10	3.6	0.192	2.503	--
1.5	15	3.8	0.204	2.606	--
1.5	20	3.9	<u>0.211</u>	2.669	--
2.0	10	3.3	0.191	2.503	--
2.0	15	3.5	0.203	2.604	--
2.0	20	3.5	0.210	<u>2.677</u>	16300

Table 5.5 Optimum evaporator conditions. The objective function is the steady-state exergetic efficiency for a water-source heat pump. The table shows flow rates, average performance values during the operation time, and times of duct blockage. No indication of blockage time means that blockage never occurs. The results are shown for selected values of the evaporator duct radius and length, and for the three cases being studied (no water flow reversal, reversal every 300 s, and reversal every 600 s). The number of evaporator ducts is equal to 8. The optimum efficiency and COP for each set are underlined.

(a) Reversal Period of 300 s

radius R_o, cm	length l, m	flow rate $Vx10^4$, m^3/s	ex effncy Φ	COP	time block t_{block}, s
1.0	10	3.6	0.196	2.531	--
1.0	15	3.9	0.206	2.613	--
1.0	20	3.9	<u>0.211</u>	<u>2.658</u>	--
1.5	10	3.3	0.191	2.502	--
1.5	15	3.7	0.201	2.588	--
1.5	20	3.9	0.208	2.635	--
2.0	10	3.2	0.187	2.468	--
2.0	15	3.5	0.198	2.555	--
2.0	20	3.7	0.203	2.602	--

(b) Reversal Period of 600 s

radius R_o, cm	length l, m	flow rate $Vx10^4$, m^3/s	ex effncy Φ	COP	time block t_{block}, s
1.0	10	3.7	0.195	2.519	--
1.0	15	3.8	0.206	2.611	--
1.0	20	4.1	<u>0.212</u>	<u>2.659</u>	--
1.5	10	3.2	0.192	2.510	--
1.5	15	3.5	0.202	2.599	--
1.5	20	3.7	0.208	2.648	--
2.0	10	3.1	0.188	2.481	--
2.0	15	3.3	0.199	2.579	--
2.0	20	3.4	0.205	2.627	--

(c) No Reversal

radius R_o, cm	length l, m	flow rate $Vx10^4$, m^3/s	ex effncy Φ	COP	time block t_{block}, s
1.0	10	4.1	0.193	2.484	--
1.0	15	4.2	0.204	2.578	--
1.0	20	4.2	<u>0.210</u>	2.633	--
1.5	10	3.6	0.190	2.485	--
1.5	15	3.9	0.202	2.584	--
1.5	20	4.0	0.209	<u>2.644</u>	--
2.0	10	3.4	0.188	2.474	--
2.0	15	3.7	0.200	2.573	--
2.0	20	3.8	0.206	2.641	--

each one of the sets of conditions. Times of duct freeze-up for ice-maker heat pumps indicate the time that it takes for the ice to cause duct blockage if no deicing takes place before that. Water-source heat pumps operate at steady-state and therefore they are not subjected to blockage (see Section 5.5.6). The tables include results for all these combinations of external duct radius and length values to illustrate their effect on performance. The global optimum always corresponds to the longest heat exchanger, because the objective function does not take into account the cost of area.

5.5 Discussion

This section presents a study of the different factors that affect the heat pump performance. The following effects are studied in the given order:

1. Effect of the length of the operation cycle.
2. Effect of water flow direction.
3. Time evolution.
4. Effect of evaporator dimensions.
5. Effect of area cost.
6. Effect of water flow rate. Blockage.
7. Effect of pumping head.
8. Effect of the frequency of water flow reversals.

The study focuses mainly on discussing how the optimum performances shown in Tables 5.1 through 5.5 vary as a function of evaporator parameters. However, the following

analysis is not limited to the cases presented in the tables, as shown in the next sections.

5.5.1 Effect of the Length of the Operation Cycle: The results in Tables 5.1-5.5 show optimum designs for different durations of the operation cycle. Table 5.1 shows results for the shortest operation time (1800 s). These designs have the highest ratio of latent energy to sensible energy obtained from the water, and therefore operate mainly as ice-maker heat pumps. From the results presented in the table, it can be observed that ice-maker heat pumps operate best with low water flow rates. Table 5.1 also indicates that ice-maker heat pumps should operate with large duct radii, because this extends the time for duct blockage, even though the performance is slightly better for ducts with a small radius.

Heat pump designs from Table 5.5 operate as water-source heat pumps, because there is no ice formation once steady-state is reached, there is no need for deicing, no duct blockage regardless of the length of the operation cycle, and all the energy obtained from the water is sensible energy. From the table it can be seen that water-source heat pumps require a high water flow rate and a small duct radius.

The tables show that both the exergetic efficiency and the COP decrease as the operation cycle becomes longer. While this seems to indicate that ice-maker heat pumps operate better than water-source heat pumps, it must be

remembered that the results in the tables do not take into account the energy required to deice the evaporator after each operation cycle. This energy expense reduces the performance parameters from the values presented in Tables 5.1-5.4. Ice-maker heat pumps may also present problems with duct blockage, if there is the possibility that operation cycles may last longer than expected. This is illustrated by the blockage times included in the tables. Compressor damage may also result from the heat pump cycling required for deicing. Determining whether an ice-maker or a water-source heat pump operate better requires the evaluation of the costs of energy spent in deicing the evaporator and the possible cost of a damage to the compressor (a situation similar to that studied in Section 2.3). However, this calculation cannot be done here, since the heat pump model used here is a steady-state model and all the deicing methods for a heat pump involve highly time-dependent processes.

Therefore, the present study does not evaluate which mode of operation has a higher efficiency. Instead, it tries to find conditions that help in solving the major problems for the two types of heat pumps, namely, the need for frequent deice cycles in ice-maker heat pumps and the high water consumption required to operate water-source heat pumps.

5.5.2 Effect of water flow direction: It is usually assumed that the performance of an evaporator does not

depend on the relative flow direction of the fluids, because the temperature of one of the fluids has a nearly constant value along the evaporator. However, in this case, the heat transfer coefficent along the evaporator varies within a wide range of values. This variation is responsible for a difference in efficency between the two relative flow directions.

The water flow direction is a factor only in the no reversal case. In the reversal case, the direction is changed often, so that the initial direction does not have much effect in the long-term performance.

This analysis is based on the optimum design for a water-source heat pump with no reversal (l=20 m, R_O=0.01 m, N=8, and V=4.2x10^{-4}m^3/s). For this case, the steady-state heat pump parameters are evaluated for the two water directions relative to the refrigerant direction, counterflow and parallel flow.

The steady-state exergetic efficiencies for the two relative directions have values of 0.210 for counterflow, and 0.206 for parallel flow. This is a substantial difference, considering the closeness of the values obtained in Tables 5.1-5.5 for widely different design conditions.

Figures 5.1, 5.2 and 5.3 are included to illustrate the differences between the two possible orientations. Figures 5.1 and 5.2 show water and refrigerant temperatures, as well as refrigerant-side heat transfer

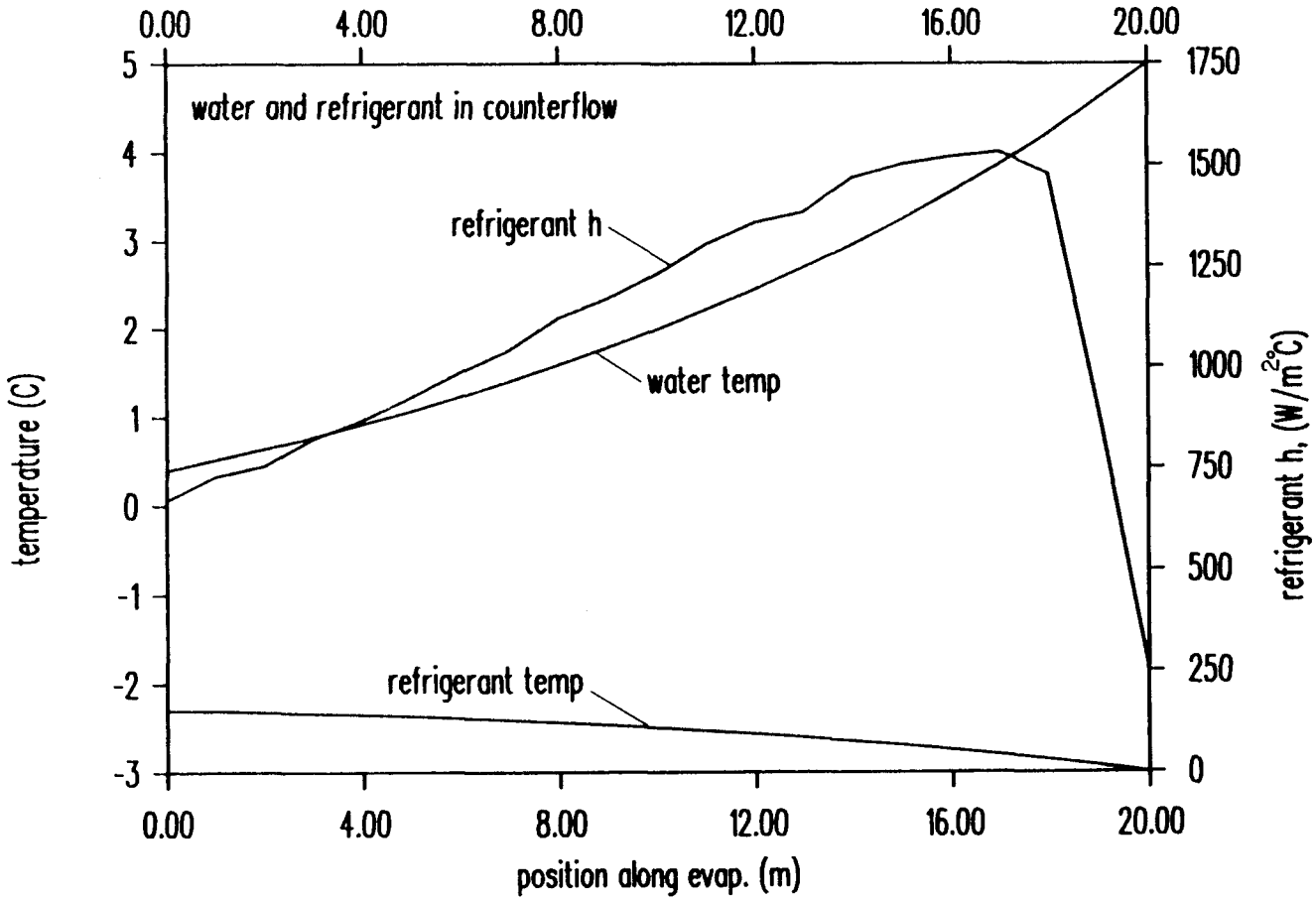

Figure 5.1 Water temperature, refrigerant temperature and refrigerant-side heat transfer coefficient as a function of position along the evaporator for water and refrigerant in counterflow. The results are shown for a water-source heat pump in steady-state with no water flow reversal and l=20 m, R_o=0.01 m, N=8 and V=4.2x10^{-4} m^3/s.

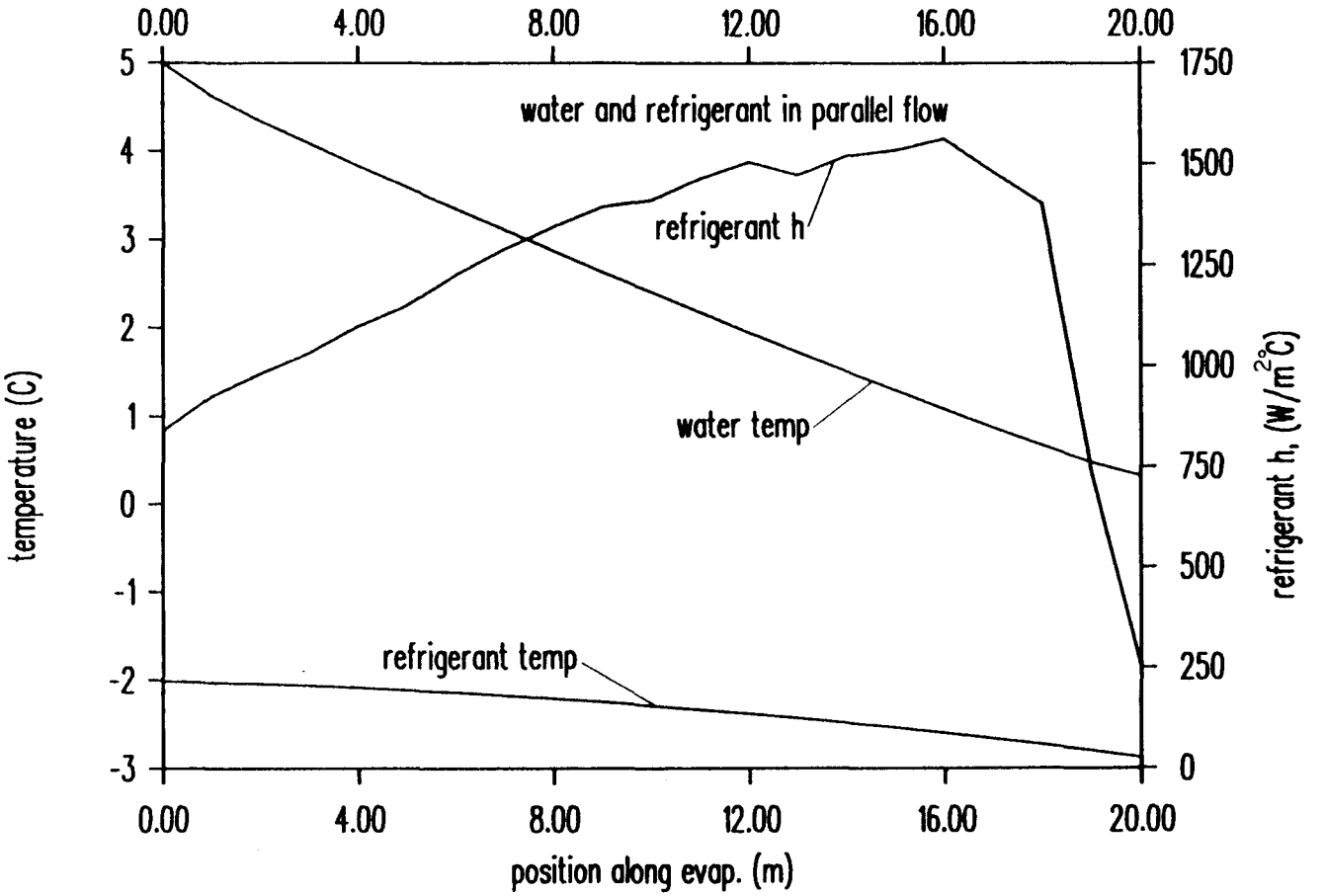

Figure 5.2 Water temperature, refrigerant temperature and refrigerant-side heat transfer coefficient as a function of position along evaporator for water and refrigerant in parallel flow. The results are shown for a water-source heat pump in steady-state with no water flow reversal and l=20 m, R_o=0.01 m, N=8 and V=4.2x10^{-4} m^3/s.

coefficents, for counterflow and parallel flow respectively. The heat transfer coefficent curve has about the same shape in both cases, starting at a low value at the entrance of the duct, and then increasing until reaching a maximum. From this point, the heat transfer coefficient decreases abruptly, as most of the liquid boils and only vapor remains. While the heat transfer coefficient has nearly the same value for both cases, what makes the difference is the position of the maximum heat transfer coefficient relative to the temperature difference between the two fluids. For the counterflow case, the maximum heat transfer coefficient and the maximum temperature difference are located in the same side of the evaporator, while in the parallel flow case they are located in opposite ends of the evaporator. This gives an advantage in heat transfer performance to the counterflow case relative to the parallel flow case.

Figure 5.3 shows still another reason for the higher value of the counterflow performance. Figure 5.3 shows the quality as a function of position for the two cases. It is seen that the quality for parallel flow is always higher than the counterflow quality. Therefore, there is more vapor in the duct in the case of parallel flow. The presence of additional vapor causes an increase in pressure drop and a decrease in performance.

5.5.3 Time evolution: The variation of efficiency with time can be immediately seen from Tables 5.1-5.5. These

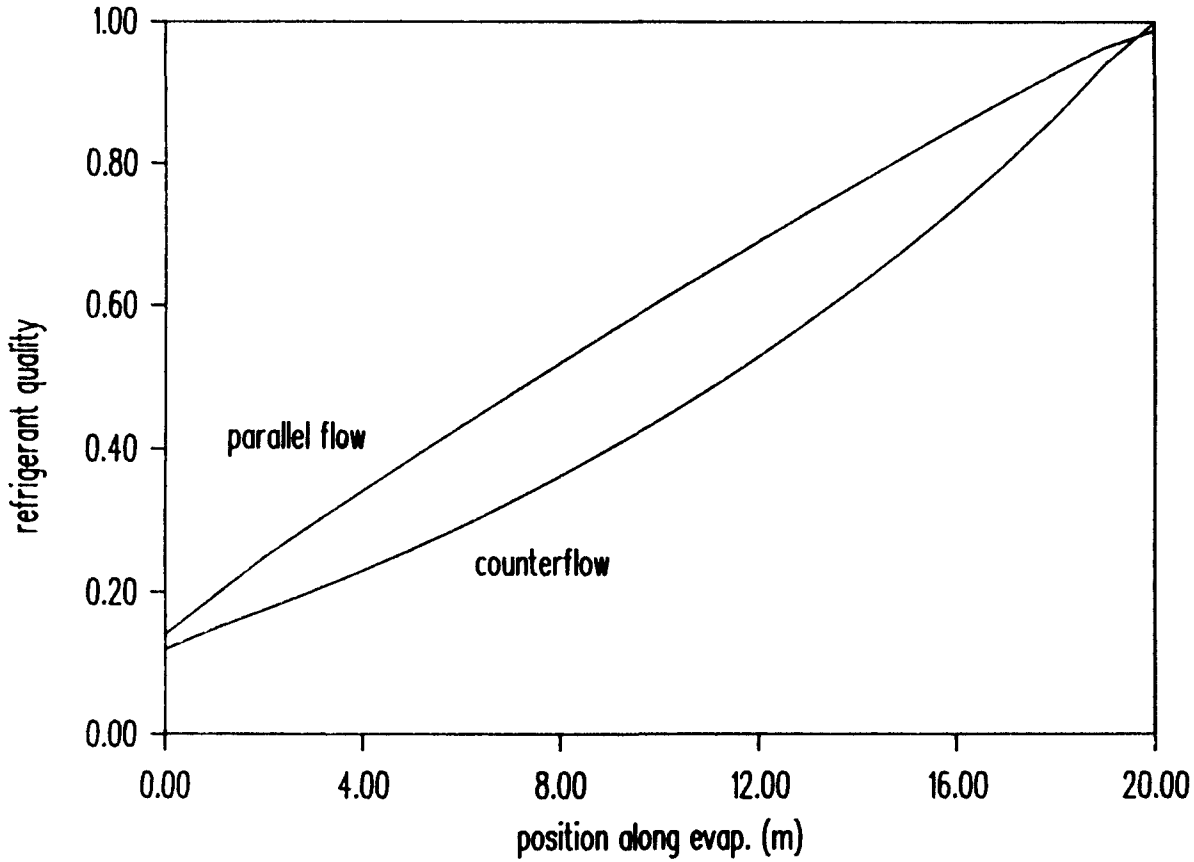

Figure 5.3 Refrigerant quality as a function of position along evaporator for water and refrigerant in counterflow and in parallel flow. The results are shown for a water-source heat pump in steady-state with no water flow reversal and l=20 m, R_o=0.01 m, N=8 and V=4.2x10^{-4} m^3/s.

tables show that the efficiencies of the optimum designs decrease as the operation cycle becomes longer. This decrease in efficiency as a function of time occurs for any heat pump configuration, and is illustrated in Figure 5.4. This figure shows the COP values as a function of time for the optimum water-source heat pump (l=20 m, R_o=0.01 m, and N=8) for the no reversal case. Exergetic efficiency curves show exactly the same shape as COP curves and therefore are not presented. The figure gives three different COP curves, corresponding respectively to a slow flow ($3x10^{-4}$ m^3/s), medium flow ($4x10^{-4}$ m^3/s) and high flow ($5x10^{-4}$ m^3/s).

The figure shows the COP for slow flow starting higher than the other two curves, then decreasing slowly until suddenly a point is reached where the COP falls abruptly, due to ice blockage of the duct. The curves for higher flow rates start at lower performance values, but then the performance shows little time dependence, keeping a nearly constant value.

The curves for lower water flow rate start at a higher performance level because they require less pumping power to pump the water through the 50 m head. However, ice builds faster in the evaporator with lower mass flow rate, producing a faster performance drop. Ice has a double effect in reducing the heat pump performance. Ice in the evaporator insulates the surfaces, reducing the heat pump capacity. This effect is responsible for the slight drop

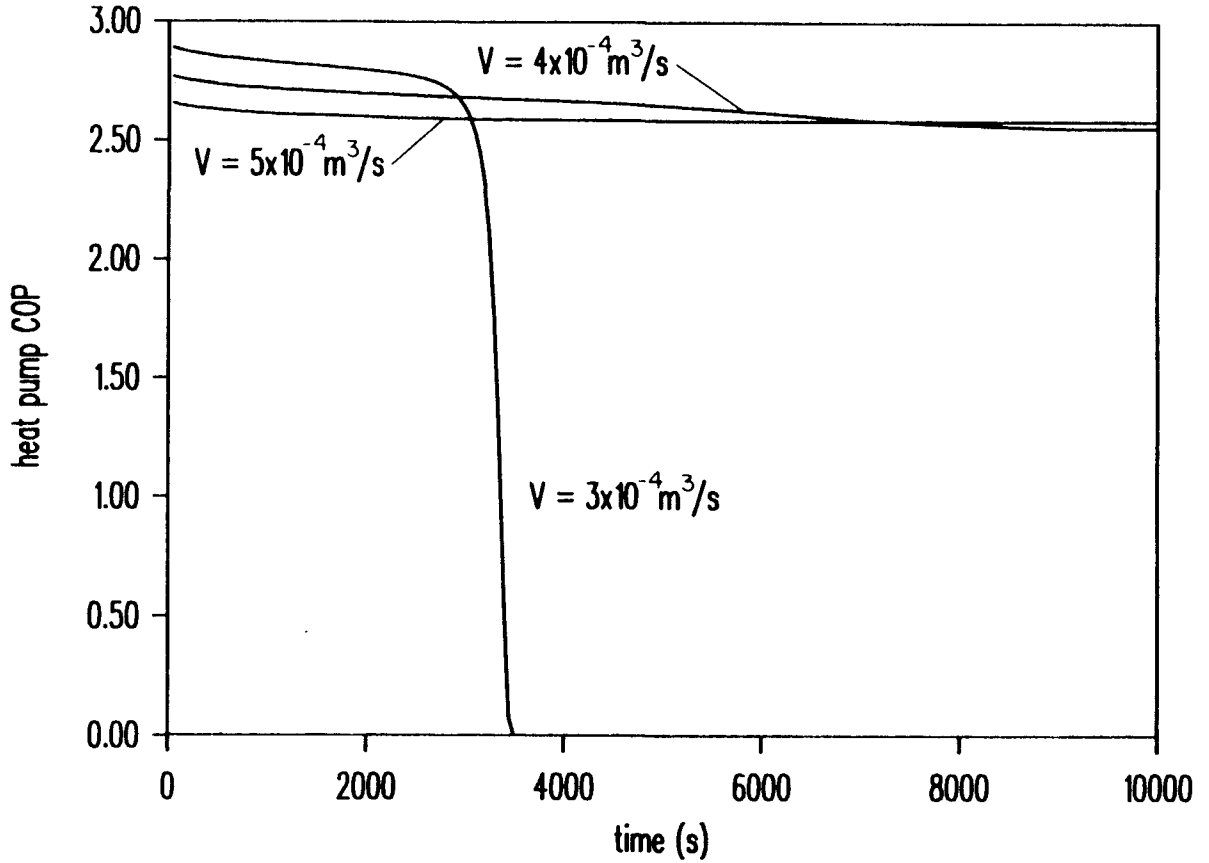

Figure 5.4 Heat pump COP as a function of time for three different water flow rates ($3x10^{-4}$ m^3/s, $4x10^{-4}$ m^3/s and $5x10^{-4}$ m^3/s). The results are shown for a heat pump with no water flow reversal and l=20 m, R_o=0.01 m, and N=8.

in COP for small values of time, and is completely analogous to the case presented in Chapter 2 and illustrated in Figure 2.3. Ice buildup also has the effect of reducing the flow area of the evaporator, increasing the water pressure drop. Excessive blockage produces abrupt drops in performance, as that shown in Figure 5.4 for $V=3x10^{-4}m^3/s$.

Figure 5.5 shows the effect of water flow reversal on heat pump performance. Water flow reversals have the effect of partly deicing the evaporator, increasing the efficiency of the water-source evaporator with respect to the no-reversal case. This partial deicing is also responsible for delaying the blockage of the duct, as shown in the figure for $V=3x10^{-4}$ m^3/s. See Section 5.5.6 for a more complete discussion on duct blockage.

5.5.4 Effect of Evaporator Dimensions: This section analyzes the effect of three evaporator dimensions on heat pump performance. These are the duct length, the number of evaporator circuits in parallel and the duct radius. Each effect is studied separately as follows.

a) Effect of the length: Figure 5.6 illustrates the effect of the duct length on heat pump COP. The figure is for a water-source heat pump at steady-state with no reversal at the optimum conditions (Ro=0.01 m, N=8 and V=4.2x10-4 m3/s). The figure shows an increase in COP as a function of length. This behavior is expected, because the COP is a performance factor, and does not take into account the cost

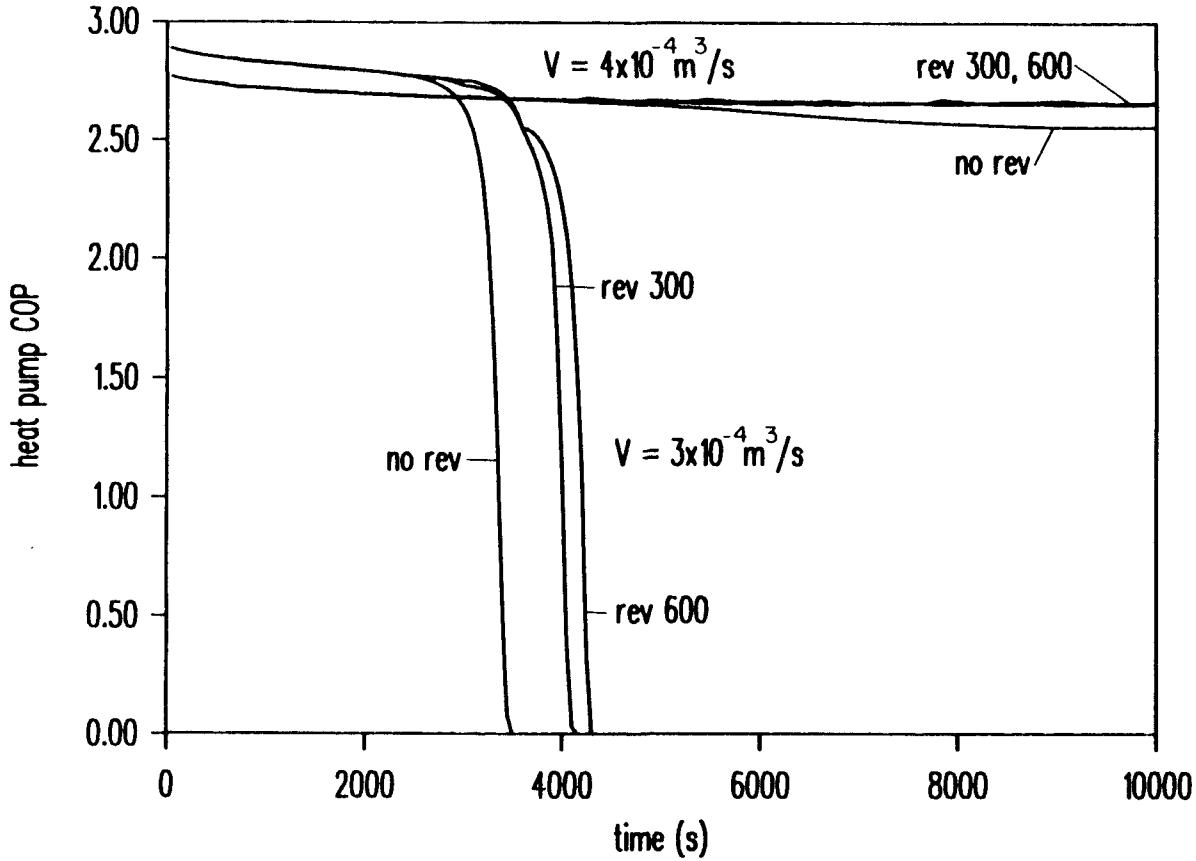

Figure 5.5 Heat pump COP as a function of time for two different water flow rates ($3x10^{-4}$ m^3/s, and $4x10^{-4}$ m^3/s) for three cases, no water flow reversal, reversal every 300 s, and reversal every 600 s. The results are shown for a heat pump with l=20 m, R_o=0.01 m, and N=8.

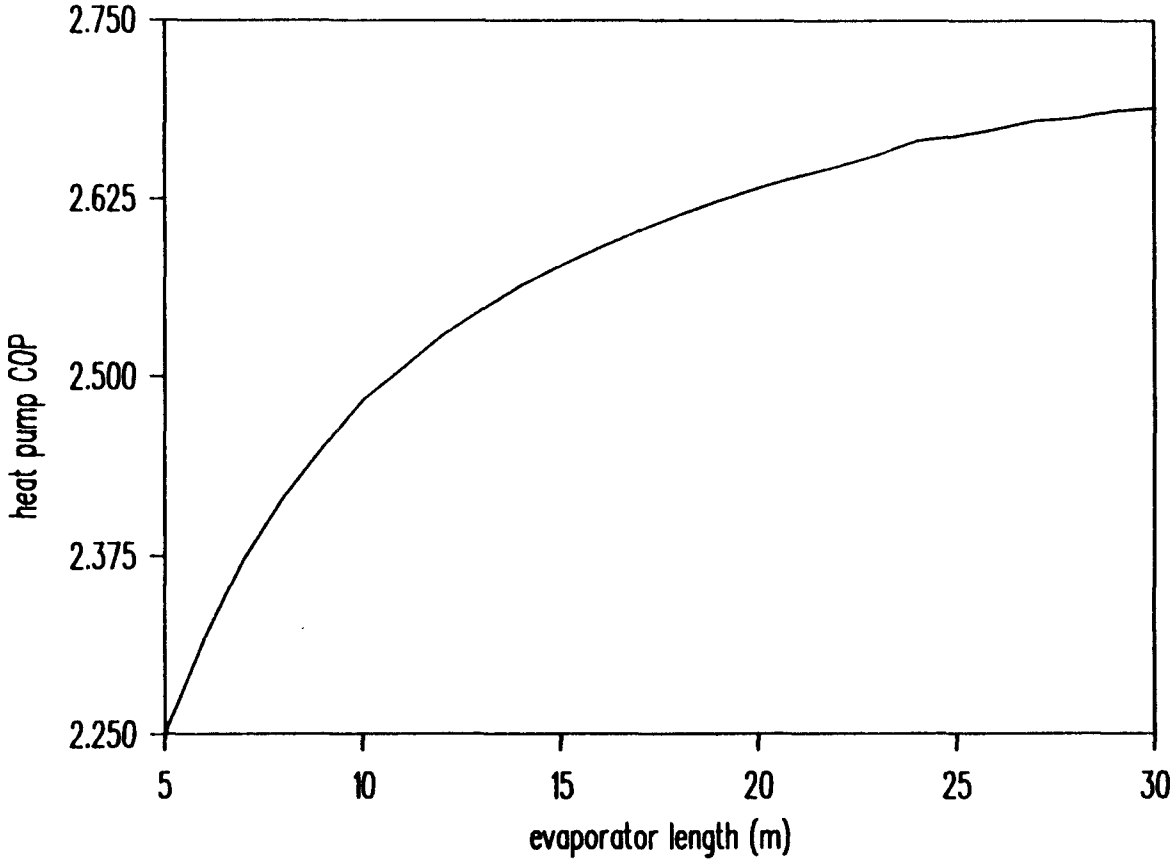

Figure 5.6 Heat pump COP as a function of evaporator duct length. The results are shown for a water-source heat pump at steady-state with no reversal and R_o=0.01 m, N=8 and V=4.2x10^{-4} m^3/s.

of area. Therefore, the optimum length is very large, and it would be infinity if the water could flow without pressure drop.

However, the COP curve levels off after a fast increase for small values of evaporator length. Therefore, there is a length at which the additional performance gain obtained by increasing the length does not justify the extra expense of installing additional area. However, finding this length requires the assignment of costs to the area. See Section 5.5.5 for an analysis that includes area costs.

b) Effect of the number of evaporator circuits in parallel: Figure 5.7 shows the effect of varying the number of evaporator circuits in parallel (N) in an evaporator with l=20 m, R_o=0.01 m, and V=4.2x10^{-4} m^3/s for a water-source heat pump in steady-state with no reversal. The effect of increasing N is an increase in the heat pump COP, in exactly the same way as that shown in Figure 5.6. Again, the optimum heat exchanger is unreasonably large, unless the analysis takes into account the cost of area (see Section 5.5.5).

c) Effect of the radius: As can be seen from Tables 5.1-5.5, the radius is the only evaporator dimension for which the performance optimum is not always reached at the maximum size. The tables indicate optimum results for a radius of 0.01 m for short cycle length. The optimum then shifts to 0.015 m and then to 0.02 m as the operation cycle

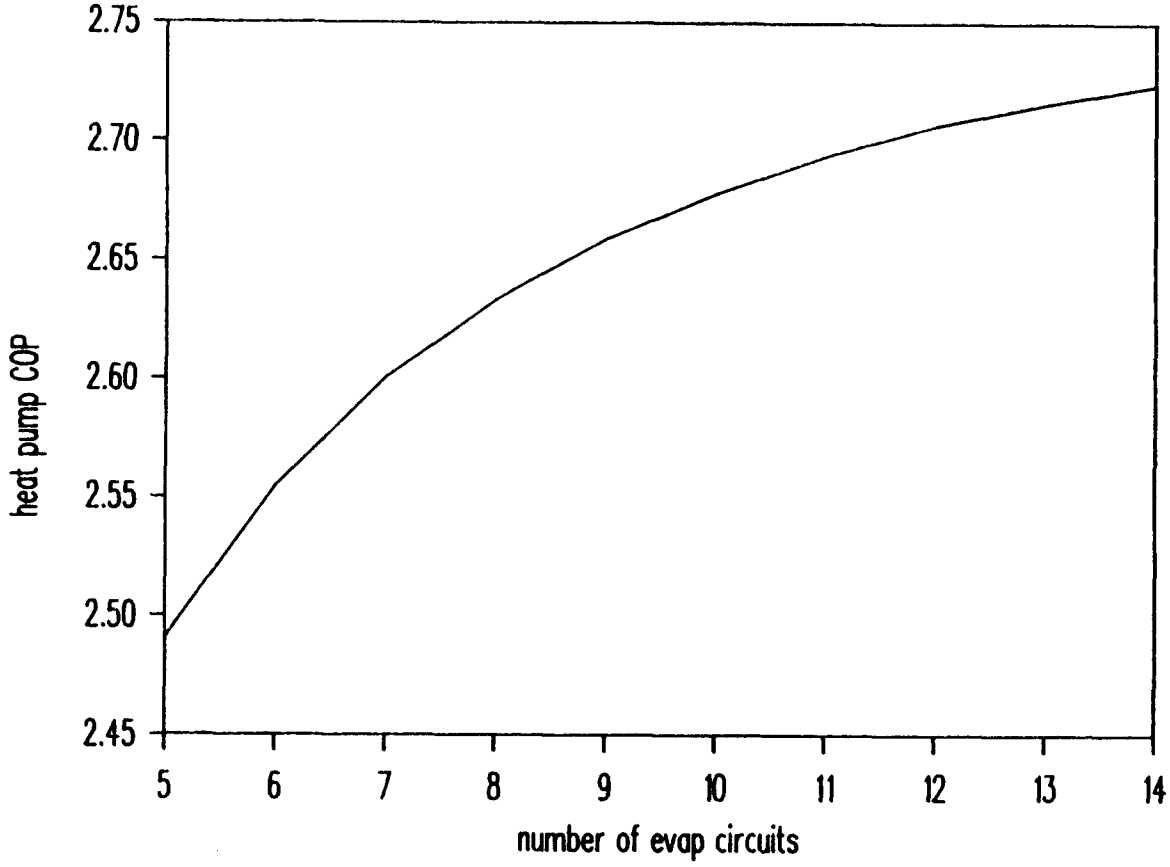

Figure 5.7 Heat pump COP as a function of the number of evaporator circuits in parallel. The results are shown for a water-source heat pump at steady-state with no reversal and l=20 m, R_o=0.01 m, and V=4.2x10^{-4} m^3/s.

length increases. However, at steady-state, the optimum is 0.01 m again.

This variation of the optimum radius with cycle length is the result of two competing effects. The first one is the resistance of the water to heat transfer and the second is the time for blockage of the duct.

The major resistance to heat transfer between the refrigerant and the water is on the water side. The boiling of the refrigerant causes high heat transfer coefficients, and the copper evaporator wall presents a negligible resistance to heat transfer. Therefore, the evaporator performance is heavily influenced by the water-side heat transfer coefficient.

The best way to increase the heat transfer coefficient is to increase the velocity of the fluid. At a constant mass flow rate, the only way to increase the velocity is to decrease the flow area (decrease the radius of the duct). Therefore, selecting a small radius increases heat transfer performance. This is illustrated in Figures 5.8 and 5.9, which show respectively the exergetic efficiency and the COP as a function of time for three different R_o values at the optimum conditions for a steady-state water-source heat pump ($V=4.2 \times 10^{-4}$ m^3/s, l=20 m and N=8), and no reversal. The curves in the figures show small oscillations in performance around an average performance. These oscillations are caused by the necessity to use finite tolerance values in the simulation code, and do not

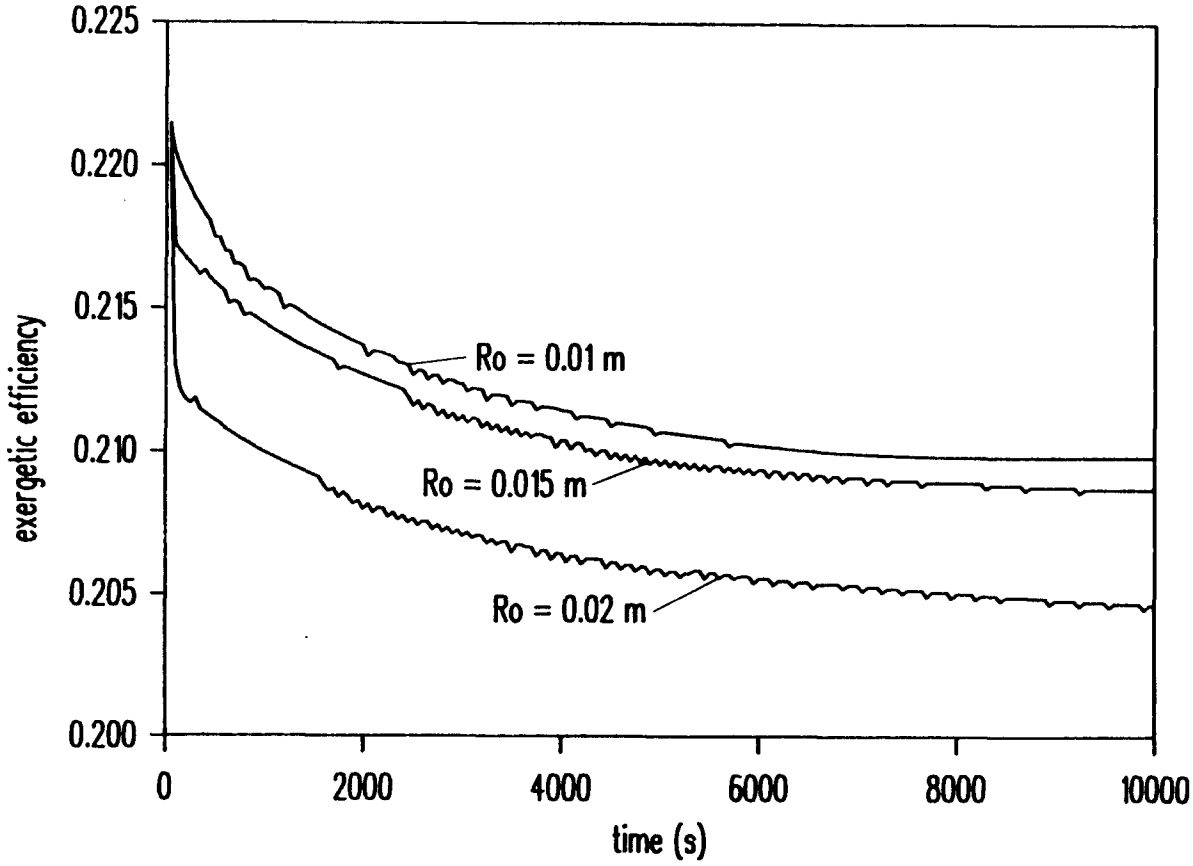

Figure 5.8 Exergetic efficiency as a function of time for three values of the external duct radius (R_O=0.01 m, R_O=0.015 m and R_O=0.02 m). The results are shown for a heat pump with no reversal and l=20 m, N=8, and V=4.2×10^{-4} m^3/s.

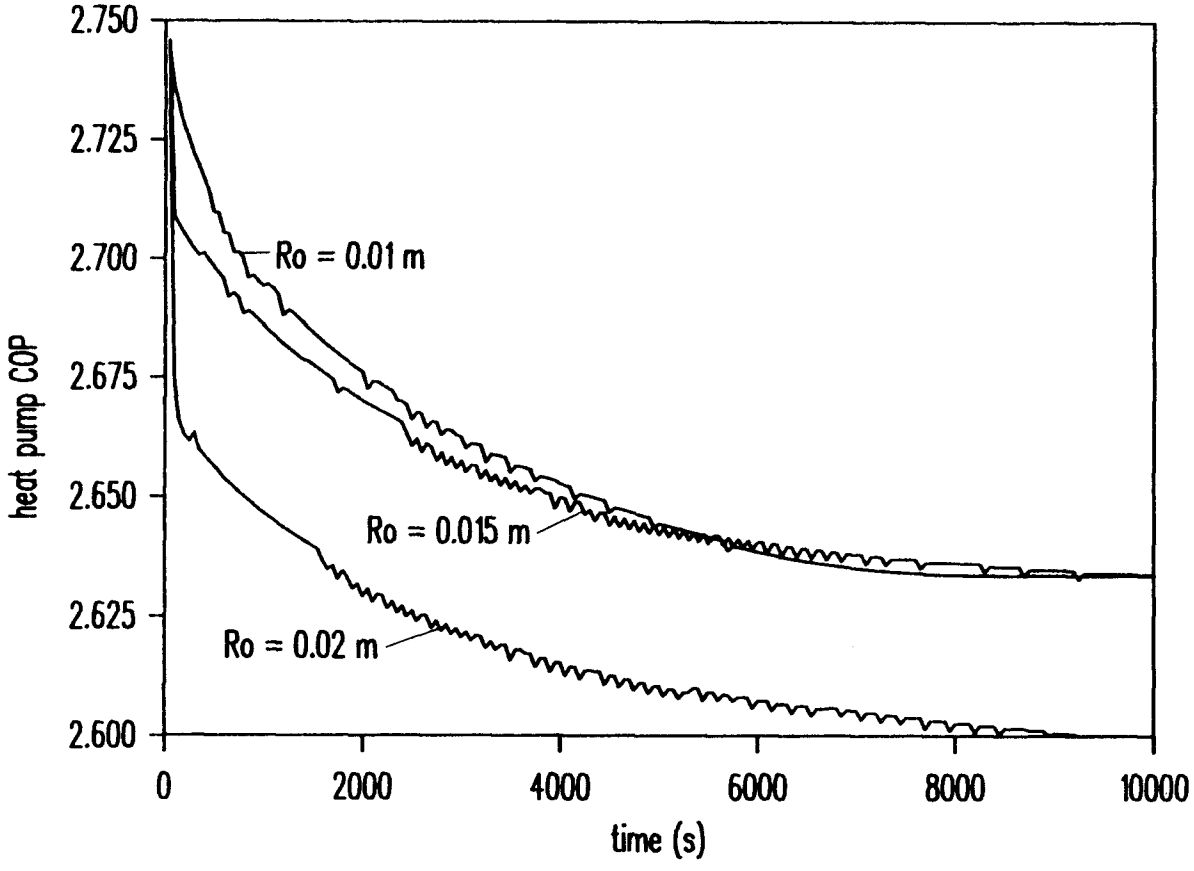

Figure 5.9 COP as a function of time for three values of the external duct radius (R_o=0.01 m, R_o=0.015 m and R_o=0.02 m). The results are shown for a heat pump with no reversal and l=20 m, N=8, and V=4.2x10^{-4} m^3/s.

represent anything physically realistic. The figures show that small values of the radius result in a higher performance, at least in high-flow situations, like the one presented here, where there is no duct blockage.

On the other hand, large-sized ducts take longer to block with ice, and a larger size is then appropriate to delay ice blockage in ice-maker heat pumps. Figure 5.10 illustrates this by showing COP curves for very low flow rates ($V=2x10^{-4}$ m^3/s, l=20 m and N=8), and no reversal. As before, the curve for a smaller radius starts at a higher value, but then the duct is blocked with ice much earlier than the larger ducts.

As a conclusion, a duct with a small radius performs better in any situation, except those for which duct blockage has an effect. This explains the results observed in the Tables 5.1-5.5. In Table 5.1, the operation time of 1800 s is short enough that there is no duct blockage, and therefore the best efficiency is obtained for the smallest radius. For longer operation times, ice starts blocking the ducts with small values of the radius, and therefore the optimum shifts to higher values of the radius. In steady-state there is again no duct blockage, and therefore the optimum is the smallest radius.

5.5.5 Effect of Area Cost: Figures 5.6 and 5.7 show that the optimum evaporators correspond to the maximum allowable duct length and number of evaporator ducts in parallel. This is a natural consequence of using the exergetic

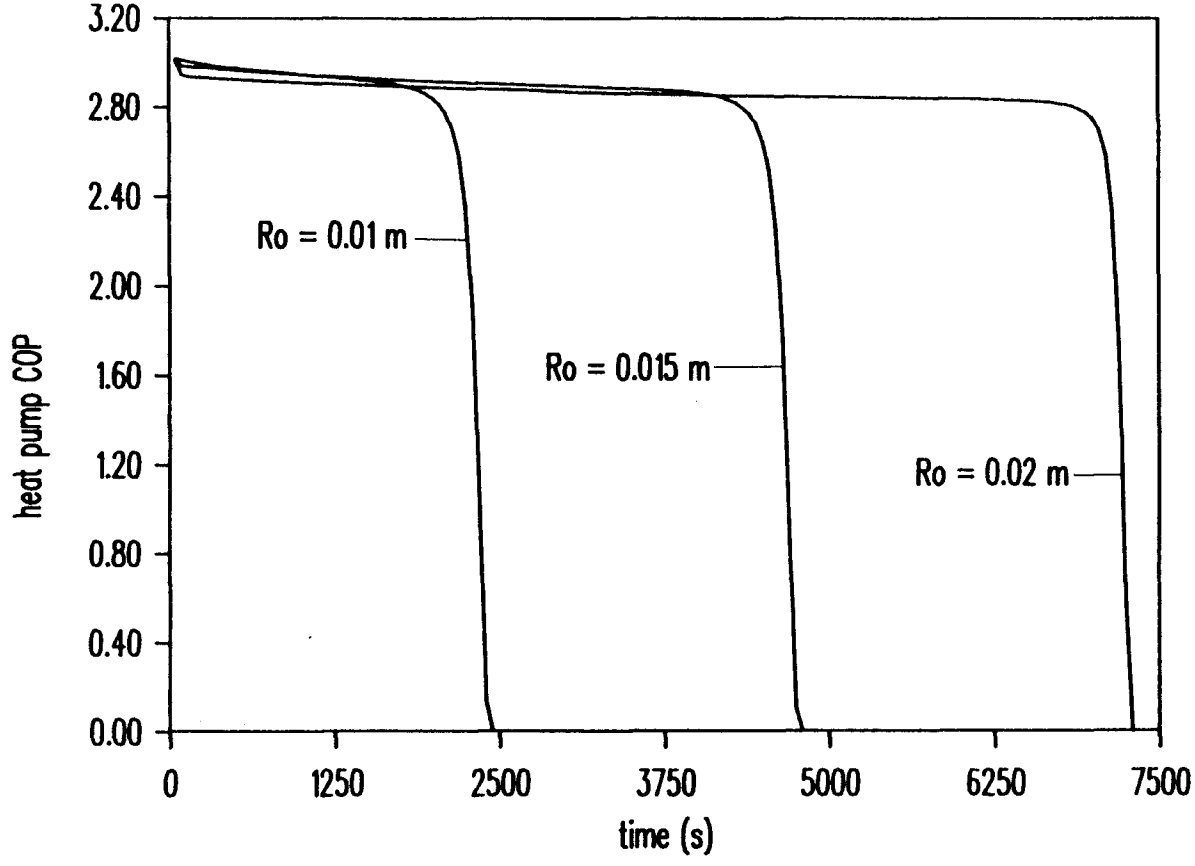

Figure 5.10 COP as a function of time for three values of the external duct radius (R_o=0.01 m, R_o=0.015 m and R_o=0.02 m) for a low-flow case. The results are shown for a heat pump with no reversal and l=20 m, N=8, and V=2x10^{-4} m^3/s.

efficiency as an objective function, since this parameter does not take into account the cost of area.

The analysis in this section includes the cost of area. Taking into account the cost of area results in optimum heat exchangers of reasonable size, with no need for imposing restrictions in the dimensions. Two different methods have been used in the past to account for the area. One is an economic analysis and the other is the material exergy analysis. Economic analyses take into account the cost of the area, but the parameters required for the calculations are always uncertain and subjected to variations. The second method is known as the material exergy analysis. Material exergy analyses take into account the cost of area in terms of parameters that are less subjected to change than those required for economic analyses. Therefore, they are more useful to establish non-changing performance limits in the design. This is the method used for this application.

In a material exergy analysis (Aceves-Saborio et al., 1989b), the cost of area is taken into account by considering the exergy value of the heat exchanger. The exergy value of a heat exchanger, EX_m, is calculated as the exergy of the heat exchanger materials with respect to a dead state, or in different words, the amount of exergy required to build the heat exchanger from a given dead state under reversible conditions. If the heat exchanger has a finite application life, t_{ap}, then it can be

considered that the exergy of the heat exchanger has been "used up" after the application life. This corresponds to having an extra irreversibility source, given as,

$$I_m = \frac{EX_m}{t_{ap}} \tag{5.4}$$

However, processes in real life are not reversible, and building a heat exchanger requires much more energy than just the exergy value of the heat exchanger. The total energy expense is taken into account here, because including it in the analysis adds to the practicality of the results. The total exergy spent in building the heat exchanger can be estimated if the overall efficiency of the manufacture process, Φ_m, is known. With this parameter, Equation (5.4) can be rewritten to take into account the total exergy expense, as follows,

$$I_{m,i} = \frac{EX_m}{\Phi_m \, t_{ap}} \tag{5.5}$$

and this irreversibility production is added to the power consumption in the heat pump, so that the expression for the exergetic efficiency (Equation (5.2)) can be written as,

$$\Phi = \frac{EX_{air}}{W_{comp} + W_{fan} + W_{pump} + I_{m,i}} \tag{5.6}$$

The value of EX_m depends only on the dead state selected, the type of material being used and the size of the heat exchanger. Kotas, 1985, lists material exergy values respect to a dead state. The value listed for

copper is 2115 kJ/kg. Multiplying this value by the heat exchanger mass yields the value of EX_m.

However, the other two parameters appearing in Equation (5.5) are subjected to uncertainties. The application life, t_{ap}, is selected here as 2 years, this value being chosen as an average economic life. The efficiency of the manufacturing process, Φ_m, can be calculated from the data given by Chapman and Roberts, 1983. They estimated values for energy consumption through the main steps associated with copper processing, like mining, concentrating, smelting, refining and fabrication. Their results give best estimates for all the values, but they also show ranges in which the energy consumption may fall, depending on particular conditions in each production site. The results give Φ_m=0.0154 as the best estimate, with a range of possible values of Φ_m between 0.014 and 0.027.

Figure 5.11 shows the effect of using Equation (5.6) to calculate the exergetic efficiency. The figure shows exergetic efficiencies for a water-source evaporator in steady-state with R_o=0.01 m, N=8, and V=4.2x10^{-4} m^3/s. The figure shows curves for three different values of Φ_m, corresponding respectively to the lower end of the range, the best estimate, and the upper end of the range (Φ_m=0.014, 0.0154 and 0.027). The figure also shows the exergetic efficiency for the base case, in which no material exergy is taken into account. The squares in the

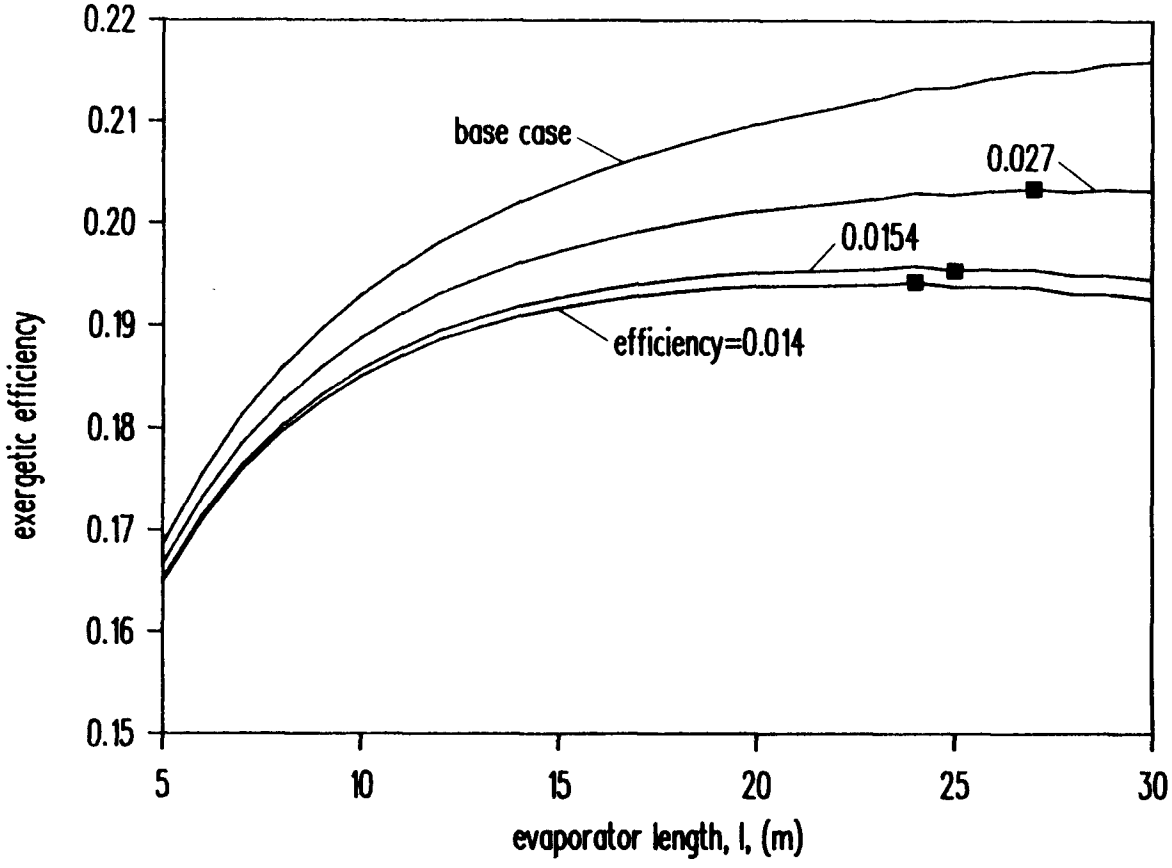

Figure 5.11 Exergetic efficiency calculated including the material exergy as a function of evaporator duct length, for three different exergetic efficiencies of the manufacturing process (0.014, 0.0154, and 0.027) and for the base-case, for which no material exergy is taken into account. The results are shown for a water-source heat pump in steady-state with no reversal and R_o=0.01 m, N=8, and V=4.2x10^{-4} m^3/s.

figure indicate the optimum lengths for each efficiency. From the figure it can be seen that the optimum length changes only between 24 m and 27 m, even though the value of Φ_m is allowed to vary in a wide range.

The material exergy analysis just shown takes into account the cost of the area. However, it does not take into account additional costs that appear in an economic analysis, like labor and profits. Therefore, the method underestimates the cost of the area, and the optimum lengths shown in the figure are larger than those resulting from an economic analysis. However, the optimum lengths obtained in the figure are valuable in the design process, because they establish a non-changing upper limit to the maximum size that a heat exchanger should reach.

5.5.6 Effect of Water Flow Rate. Blockage: It is well known that water flow rate has an important effect on heat pump performance. Water flow rate must be kept high enough to avoid excessive pressure drop due to ice blockage of the duct, while at the same time it must be kept as low as possible, due to the high energy investment required to pump the water through a 50 m head.

Ice blockage of the ducts is caused by excessive ice build-up on the surfaces, due to a slow water flow. However, duct blockage, as used in this chapter does not mean total duct blockage. Some free area must always remain to allow the circulation of a given water flow rate, since the water pump is assumed to be powerful enough to

pump a constant mass flow rate against any pressure drop (Section 3.4).

However, there are cases in which the pressure drop becomes so large that the efficiency of the heat pump decreases abruptly, due to the smallness of the free area that is left for the fluid to circulate. This condition of quasi-blockage is illustrated in previous figures of this chapter (Figures 5.5 and 5.10). This quasi-blockage corresponds to total blockage in any real application, since no pump can provide a constant flow for any pressure drop. Therefore, the quasi-blockage condition is simply referred to as blockage in this chapter.

Tables 5.1 to 5.4 show blockage times for all the optimum heat pump designs, for no water flow reversal, water flow reversal every 300 s and reversal every 600 s. The results show that, in general, reversing the water flow direction delays duct blockage. The tables show some exceptions in which blockage occurs earlier for the heat pumps with reversal. This is an inaccuracy in the calculations caused by the need for using finite tolerances in the iteration process. Periodic water flow reversals are expected to always delay ice blockage. Figure 5.12 also illustrates blockage times as a function of water flow rate for no water flow reversal, reversal every 300 s and reversal every 600 s. The following parameters are used in the figure, l=20 m, R_o=0.01 m and N=8. The figure shows a slow increase in time with an increasing flow rate, until

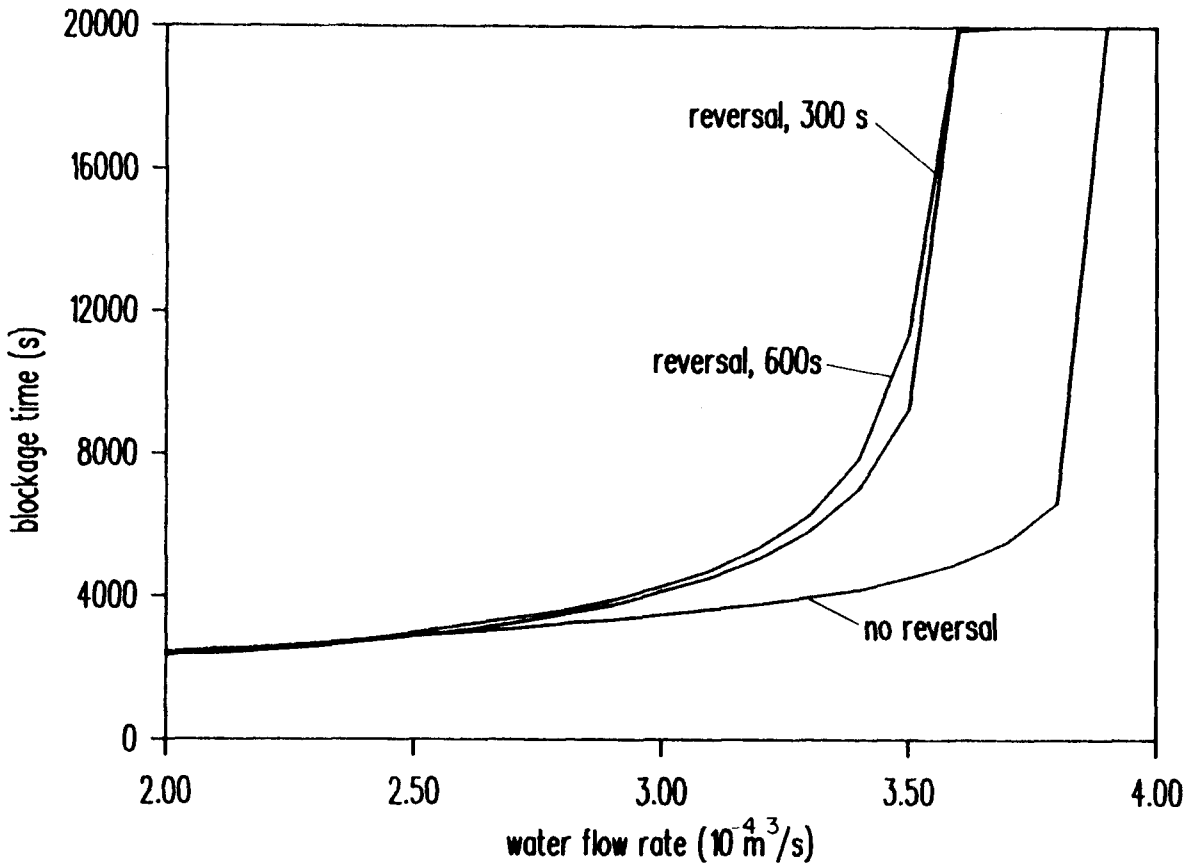

Figure 5.12 Duct blockage times as a function of water flow rate for three cases, no water flow reversal, water flow reversal every 300 s, and water flow reversal every 600 s. The results are shown for a heat pump with l=20 m, R_o=0.01 m, and N=8.

the curve reaches a point where the time increases suddenly. The points where the curve reaches the 20000 s mark are points for which blockage never occurs, and therefore the heat pump can operate as a water-source heat pump, without ever requiring deicing. The figure shows once more the retarding effect on blockage that the flow reversals have, with the 600 s reversal cycle being the most effective in retarding blockage.

Figure 5.13 shows steady-state exergetic efficiencies for water-source heat pumps under the same conditions as those of Figure 5.12. As discussed above, the steady-state exergetic efficiency of a water-source heat pump is greater than zero only for water flow rates at which there is no duct blockage. The figure also shows the optimum exergetic efficiencies for the three cases. The figure shows two major advantages of the curve corresponding to reversal every 600 s. The first was discussed in the previous paragraph, and is the fact that reversal every 600 s retards ice blockage better than the other two conditions. The second advantage is given by the relative position of the optima respect to the blockage flow. It can be seen from the figure that the difference in flow rate between the blockage flow rate and the optimum flow rate is very small both for the no reversal and the reversal every 300 s, while for the 600 s case the difference is substantially larger. Having the two flow rates so close to each other may cause operation problems , because small oscillations

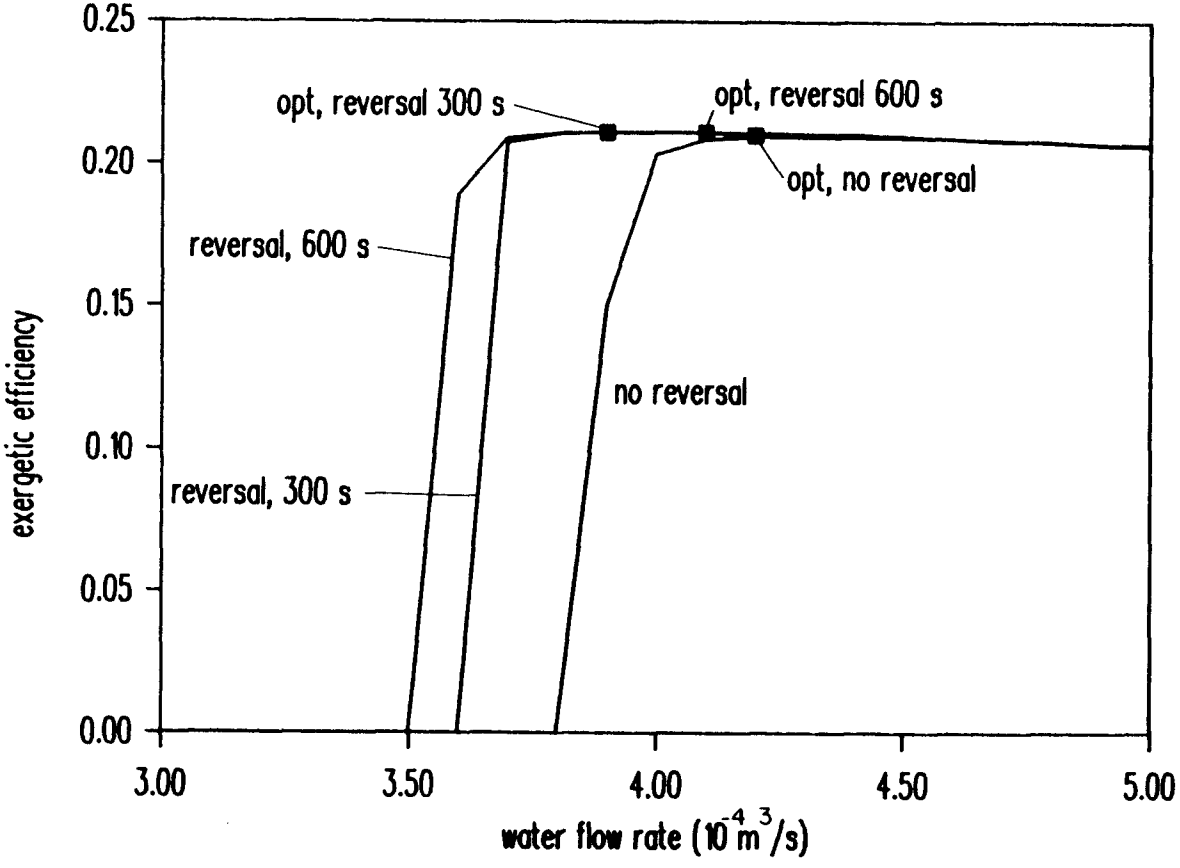

Figure 5.13 Exergetic efficiencies as a function of water flow rate for three cases, no water flow reversal, water flow reversal every 300 s, and water flow reversal every 600 s. The results are shown for a water-source heat pump in steady-state with l=20 m, R_o=0.01 m, and N=8.

in flow rate or water temperature may cause duct blockage. Therefore, the 600 s reversal cycle protects the system better against duct blockage due to changes in conditions.

The small difference between the optimum flow and the blockage flow is due to the high cost of pumping the water. The results indicate that the best designs are those in which the water flow rate is just enough to keep the duct from getting blocked. This result applies to both water-source and ice-maker heat pumps, and agrees with previous studies on water-source heat pumps (Mei, 1983; Reistad et al., 1984), where it was concluded that the high cost of water has an important effect on water-source heat pump designs.

Figure 5.14 shows steady-state ice profiles for no reversal and reversal every 300 s, with l=20 m, R_o=0.01 m, N=8 and V=4x10^{-4} m^3/s. The ice profile for the no reversal case does not change with time. The ice profile for the reversal case changes in form, but it does so cyclically, so that the ice shape at a time t is equal to the ice shape at a time t+600 s. The figure shows ice profiles for the reversal case along one of the cyclical variations. The curves are shown for three times along the cycle, immediately after a reversal, 100 s after the last flow reversal and 200 s after the last reversal. These curves show that, after each reversal, some melting occurs at the entrance of the duct, while some ice forms at the exit. This changes radically the shape of the ice profile, and

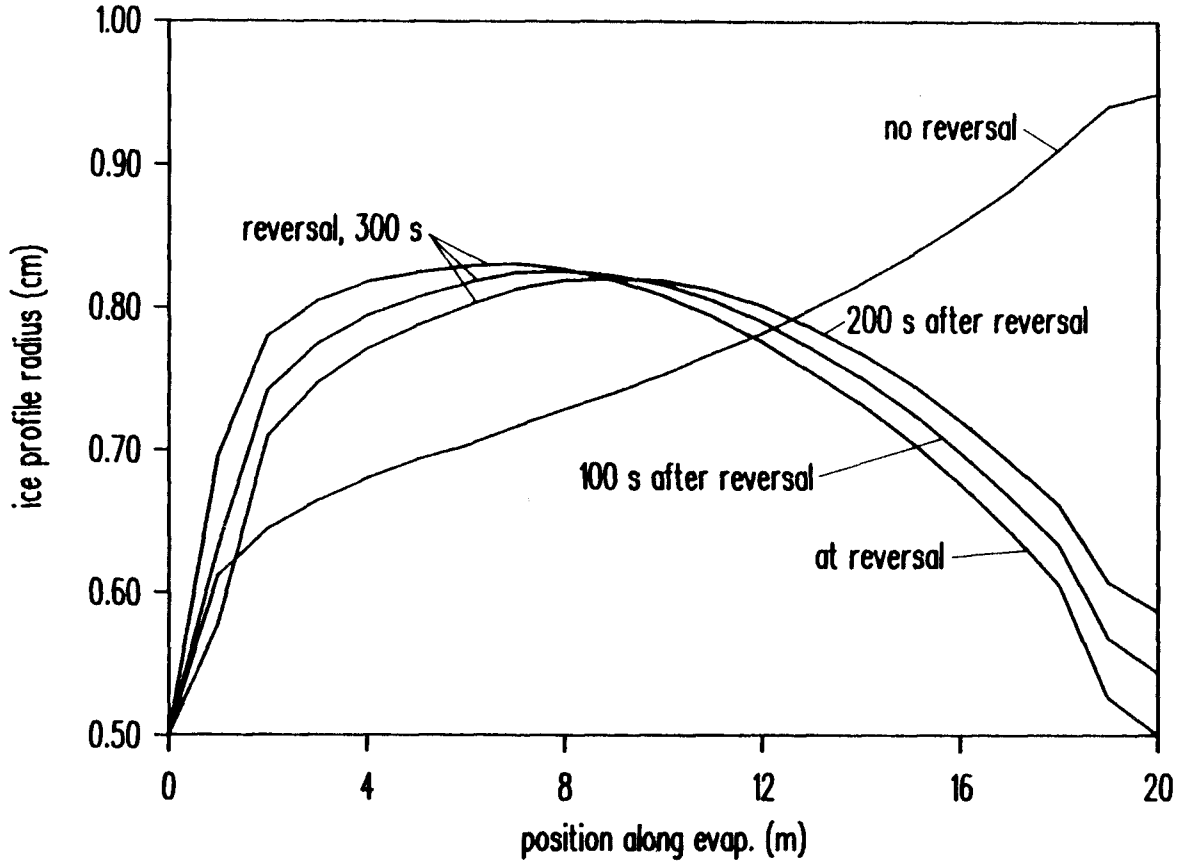

Figure 5.14 Ice profiles along the evaporator for no water flow reversal and for water flow reversal every 300 s, for three different times along the reversal cycle (0 s, 100 s and 200 s after last reversal). The results are shown for a heat pump with l=20 m, R_o=0.01 m, N=8 and V=4x10^{-4} m^3/s.

reduces the duct blockage at the point of maximum blockage. This is very important for reducing the total pressure drop, since pressure drop in a highly blocked annular section is inversely proportional to the cube of the free radial distance. Therefore, in the no reversal case, most of the pressure drop in the duct comes from the segment between 19 and 20 m along the evaporator.

5.5.7 Effect of Pumping Head: Pumping power is the sum of two different contributions. The first is the power required to overcome the pressure drop through the evaporator, and the second is the power required to pump the water through a specified pumping head. This head is considered to be necessary to pump the water from a reservoir to the heat pump. Figure 5.15 shows the total pumping power for different pumping heads, for a water-source evaporator with l=20 m, R_o=0.01 m, N=8, and no reversal. The curve for no head, labeled 0 m, represents the power required to pump the water through the evaporator. This power decreases rapidly with an increase in flow rate, as the blockage conditions disappear. The curve then levels off, the pressure drop reaches a minimum, and then there is a very slight pressure drop increase. This increase is due to the high water flow rate being circulated. The curves for other pumping heads show very notorious minima, as pumping the fluid becomes more costly. The minimum point represents a balance point. Decreasing the flow rate from the minimum point causes a growth in the

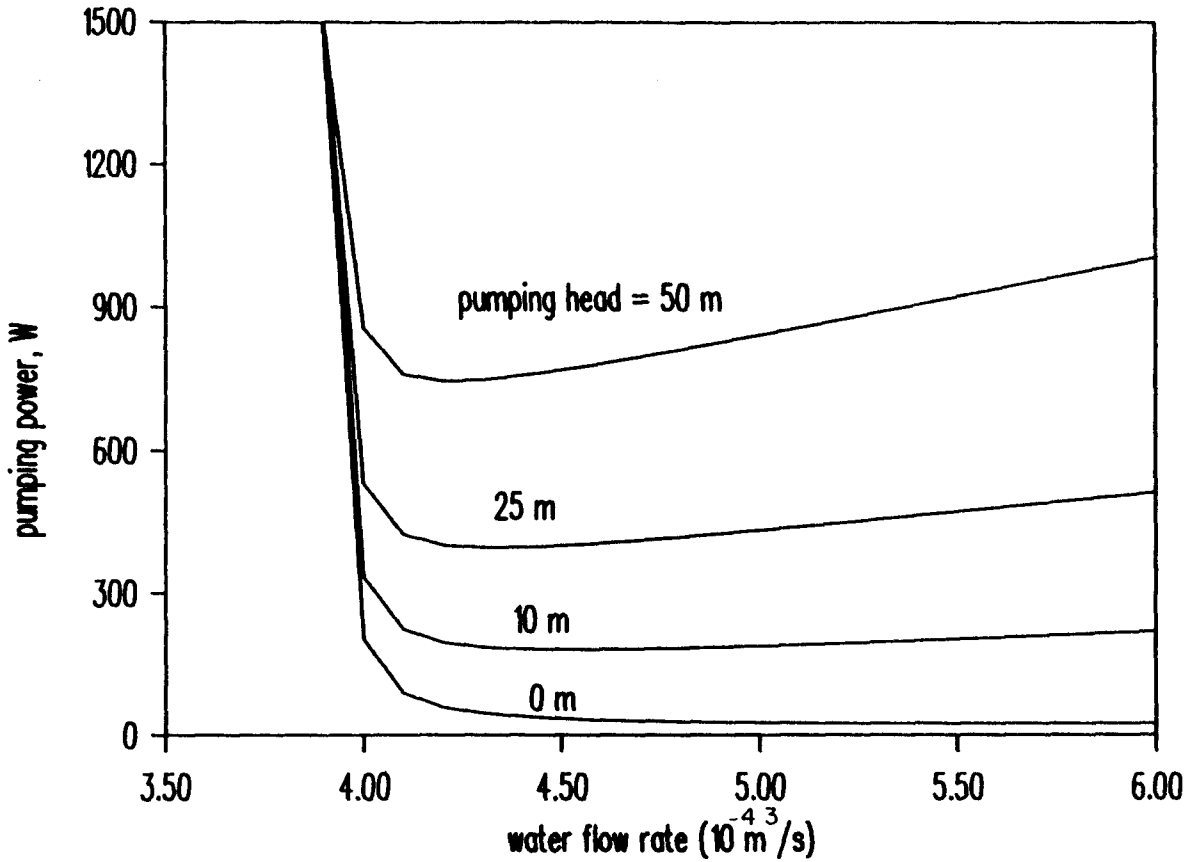

Figure 5.15 Total pumping power as a function of water flow rate for different values of the pumping head. The results are shown for a water-source heat pump in steady-state with no water flow reversal and l=20 m, R_o=0.01 m, and N=8.

ice thickness that produces an aditional pressure drop. Increasing the flow rate from the minimum produces an additional pressure drop due to the need to pump the extra fluid through the given head.

Figure 5.16 shows the COP values for the same evaporator and the same heads used for Figure 5.15. The curve for zero head shows no optimum in the range of water flow rate being used. The COP keeps increasing with an increasing water flow, due to the low cost of pumping the water. There may be an optimum for this case, as the pressure drop keeps increasing with water flow rate, but it would be reached only at extremely high water flow rates. The COP curves corresponding to heads larger than zero present a maximum, and then a slow decrease as the water flow rate increases. It can be observed from the figure that the optimum COP shows a wide variation as a function of the pumping head, from 3.09 with a head of 10 m, to 2.63 with a head of 50 m. Therefore, the pumping head has an important effect on the heat pump COP, and may determine whether a heat pump is competitive as compared with other technologies. However, although the COP varies substantially as a function of the head, the optimum flow rate does not vary much, from 4.2×10^{-4} m^3/s to 4.6×10^{-4} m^3/s for values of the head between 10 m and 50 m. The reason for this is that, even with a small pumping head, the cost of pumping the water is high enough to affect substantially the heat pump COP. Therefore, the conclusion

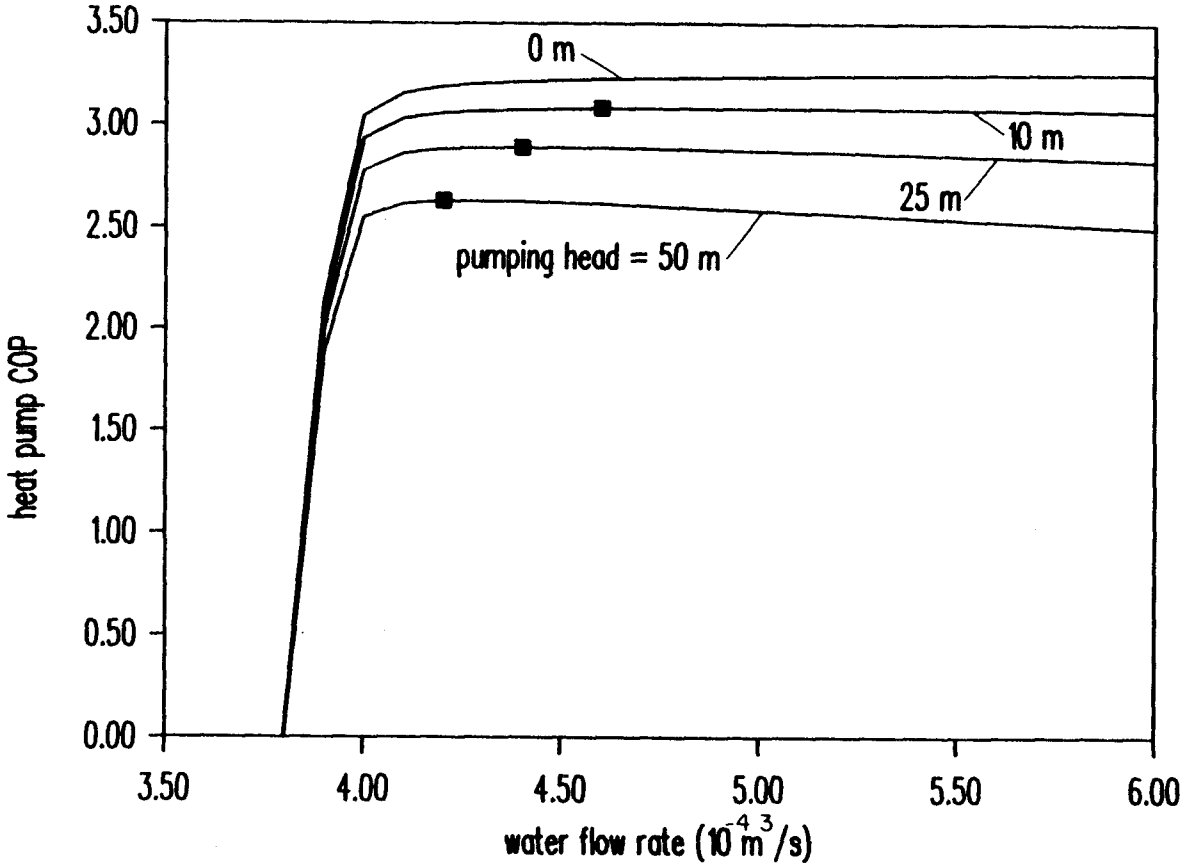

Figure 5.16 Heat pump COP as a function of water flow rate for different values of the pumping head. The squares indicate the optimum COP for each head. The results are shown for a water-source heat pump in steady-state with no water flow reversal and l=20 m, R_o=0.01 m, and N=8.

reached in the previous section, that the optimum flow rate always corresponds to rates just high enough to avoid duct blockage, holds for any reasonable pumping head.

5.5.8. Effect of the frequency of water flow reversals: The work shown up to this point indicates that periodic water flow reversals improve the heat pump efficiency and delay the blockage of the ducts. This improvement has been explained in previous sections as due to a partial deicing caused by the reversal of the liquid.

Every water reversal cycle cause some duct deicing. Therefore, it may be thought that heat pump performance increases as the reversing period decreases, with an optimum period length corresponding to almost instantaneous reversals, making long water reversal cycles undesirable. However, a reversal cycle is not useful to deice the evaporator if the water does not have time to melt some of the ice at the duct entrance before a new reversal occurs. This is shown in Figure 5.14. This figure shows the ice profiles for reversal every 300 s. The curves show that, although some change in the ice profile takes place along the cycle, more ice melting at the entrance of the duct could be possible. In contrast, Figure 5.17 shows ice profiles for the same conditions used in Figure 5.14 for a reversal cycle of 600 s (water-source heat pump in steady-state, with l=20 m, R_o=0.01 m, N=8 and V=4x10^{-4} m^3/s). The profiles not only show a substantial melting at the entrance of the duct, but also a better distribution of the

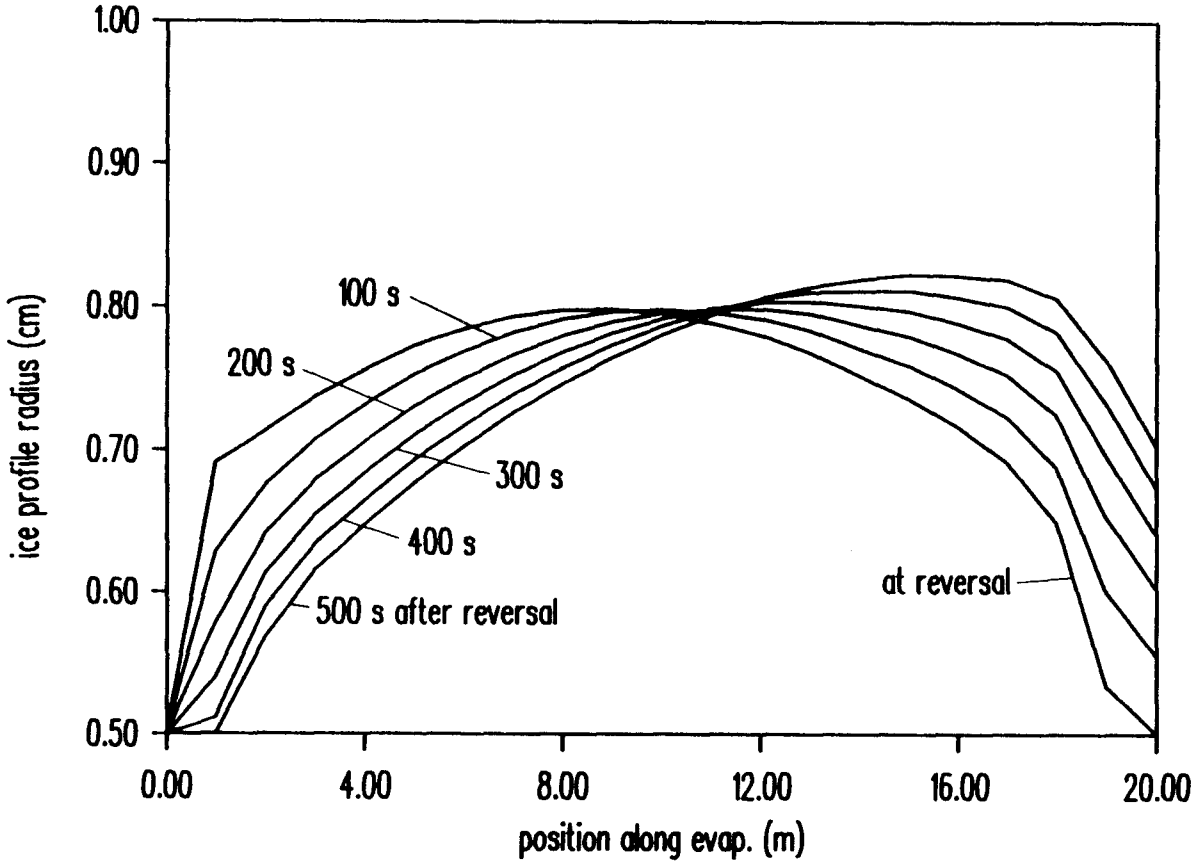

Figure 5.17 Ice profiles along the evaporator for water flow reversal every 600 s, for six different times along the reversal cycle (0 s, 100 s, 200 s, 300 s, 400 s and 500 s after last reversal). The results are shown for a heat pump with l=20 m, R_o=0.01 m, N=8 and V=4x10^{-4} m^3/s.

ice along the duct that reduces the total pressure drop and delays ice blockage as compared to those of Figure 5.14. As a consequence of this, a reversal cycle every 600 s is more useful to delay ice blockage in the ducts, as previously shown in Figure 5.12.

Reversal cycles of extremely long duration do not cause any improvement in efficiency either, since the ice profiles approach the shape of the no reversal case, causing a premature duct blockage and increased pressure drop. Therefore, there may be a duration of the reversal cycle that provides an optimum protection against blockage, and therefore a maximum efficiency at low water flow rates.

Figure 5.18 illustrates the existance of this optimum. The figure shows blockage times as a function of water flow rate for an evaporator with l=20 m, R_o=0.01 m and N=8, and for different durations of the reversal cycle. The results indicate that 600 s is the optimum reversal cycle length, because it delays duct blockage for the longest time. Shorter and longer cycles do not perform so well in delaying blockage, due to the reasons previously discussed. However, they still delay blockage for a long period of time when compared to the no reversal case.

5.6 Conclusions

This chapter has presented the optimization of water-source and ice-maker heat pumps. Five different optimizations are performed. The objective function is

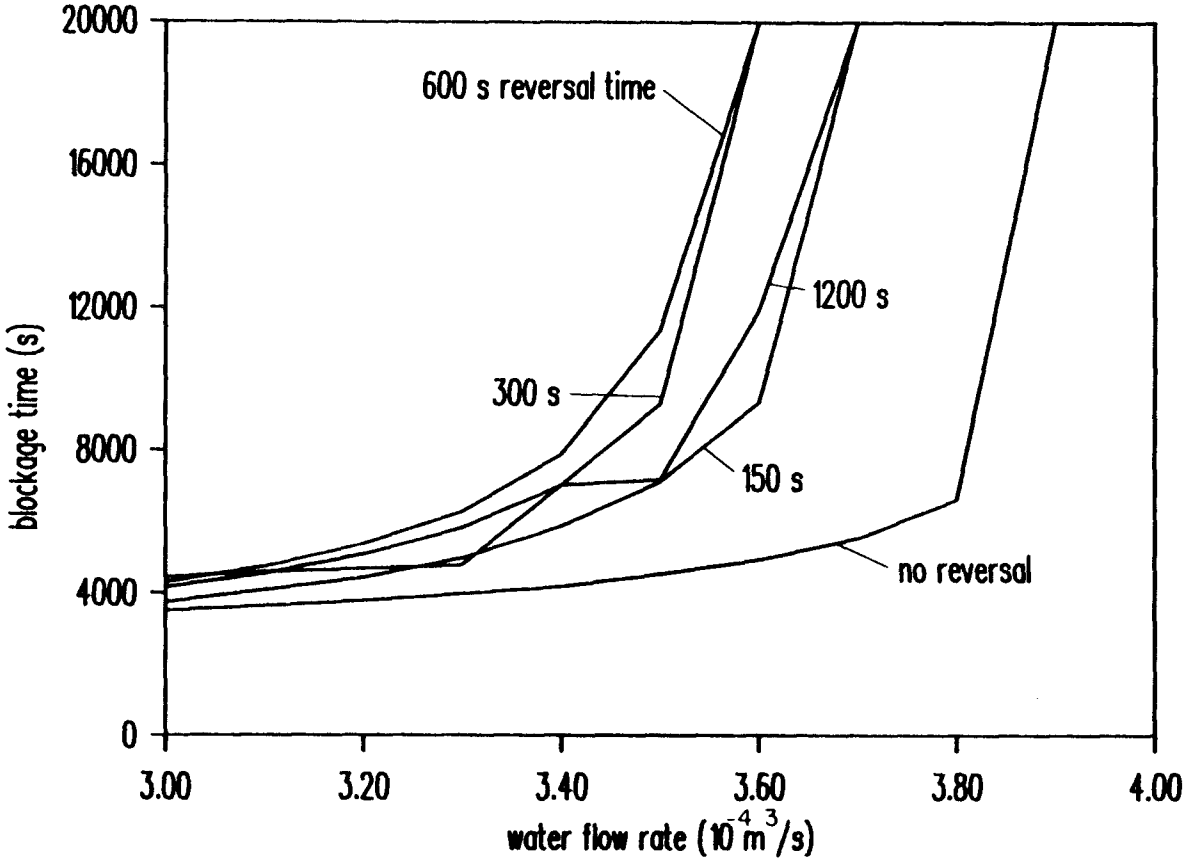

Figure 5.18 Blockage times as a function of water flow rate for different water reversal cycle lengths. The results are shown for a heat pump with l=20 m, R_o=0.01 m, and N=8.

always the exergetic efficiency, but this is evaluated for a water-source heat pump operating in steady-state, as well as for four different operation cycle lengths (30 min, 1 hour, 2 hours and 4 hours) for ice-maker heat pumps. The results show sets of optimum designs for each one of the five objective functions being used. All the calculations were done for three different cases, water flow direction reversal every 300 s, reversal every 600 s and no reversal, to appreciate the effect of water flow reversals on the heat pump performance.

This analysis is concerned mainly with improving the evaporator design. Therefore, the optimization is conducted by using only evaporator parameters as decision variables. All the high-pressure-side parameters of the heat pump are kept fixed during the optimization. The decision variables are the number of evaporator circuits in parallel, the length and radius of an individual evaporator duct, and the water flow rate.

The use of the exergetic efficiency as objective function makes it necessary to establish maximum allowable values for the evaporator dimensions, otherwise the optimum designs would be unreasonably large.

Water cost is a very important factor in water-source heat pump analyses. This analysis takes into account this cost by considering that the water has to be pumped from a water reservoir, and that the total head required to pump the water from the reservoir to the heat

pump is 50 m. The effect of varying the pumping head is also analyzed (Section 5.5.7).

Many important conclusions were pointed out earlier in this chapter. These conclusions are summarized in the next part of this section, as follows.

1. The results shown in Table 5.1 are designs for heat pumps that operate mainly as ice-maker heat pumps. Some desirable characteristics of ice-maker heat pumps as indicated from the table are low water flow rate and a large duct radius.

2. Heat pumps obtained from Table 5.5 operate as water-source heat pumps, with no ice formation once the steady-state is reached. The table indicates that some desirable characteristics for water-source heat pumps are a high water flow rate and a small radius.

3. Heat pump efficiency is different for the two water flow directions relative to the refrigerant flow direction. The efficiency for the counterflow case is higher than the efficiency for the parallel flow case.

4. Heat pump efficiency decreases as a function of time due to ice formation. Ice formation on the surfaces reduces the efficiency in two different ways. Ice on the surfaces insulates the evaporator, reducing its heat transfer performance. Ice buildup also decreases the flow area, causing an increase in pressure drop.

5. All the optimum designs have the maximum allowable number of evaporator circuits in parallel and duct length,

because the objective function does not take into account the cost of area. However, the radius has optimum designs at the minimum allowable dimension for some periods of time. The reason for this is that a small radius is desirable to enhance the heat transfer in the water side.

6. Section 5.5.5 shows a material exergy analysis for the evaporator. The material exergy analysis takes into account the cost of area in terms of parameters that, unlike economic parameters, are not subjected to wide variations. The analysis is used to fix upper bounds on evaporator dimensions. These upper bounds limit the maximum evaporator size that can be obtained from economic analyses.

7. The results show that the optimum water flow rate is barely high enough to avoid duct blockage during the heat pump operation cycle. This is caused by the high cost of pumping the water, and holds true for any reasonable pumping head.

8. The results show that there is an optimum frequency of water flow reversals. This optimum frequency causes the maximum delay of ice blockage and the maximum efficiency. If the water flow reversals take place more frequently than the optimum, the reversal does not have time to cause substantial evaporator deicing. If the water flow reversals take place less frequently than the optimum, the ice profile starts approaching its value for no reversal, causing substantial pressure drop and early blockage.

9. Water flow direction reversals have two major effects. The first effect is an increase in efficiency with respect to the no reversal case, and the second is a delay in the evaporator duct blockage. This delaying effect may be of such magnitude as to avoid blockage altogether for some water flow rates. While an efficiency increase has a big importance on its own, a delay in duct blockage is of extreme importance for ice-maker heat pumps (Table 5.1), because a delay allows them to operate for a longer time without the need for costly cycle reversals that reduce performance and may damage the compressor. For water-source heat pumps (Table 5.5), reversing the water flow direction increases the difference between the optimum water flow rate and the flow rate that causes blockage. This is of great importance, because in the no reversal case this difference is so small ($3x10^{-5}$ m^3/s), that it would not be safe to operate with the optimum flow rate, since small variations in water flow rate or temperature could cause duct blockage. So the efficiencies shown in Table 5.5 for water-source heat pumps with no reversal cannot be reached in a practical case. Higher flows have to be used to avoid the possibility of blockage.

VI. IRREVERSIBILITY ANALYSIS

6.1 Introduction

Irreversibility analyses (second law analyses) have been used in the past to search for possible ways to improve heat pump performance (Wepfer et al., 1979). Second law analyses present a different, complementary, viewpoint from that given by a conventional energy analysis. Therefore, second law analyses can be used in conjunction with energy analyses to point more readily to design improvements.

This chapter presents an irreversibility analysis of the water-source heat pump described in the previous chapters. The study is concerned exclusively with the steady-state behavior of the heat pump, but the analysis could be easily extended to cover the transient state.

The chapter starts by showing a summary of first law magnitudes (energy inputs and heat losses) that exist in the heat pump. Then, the chapter includes a description of the procedure used for calculating exergies and irreversibilities in the heat pump components. After this, a section presents an optimization of the evaporator as an individual (isolated) component. This is done by using two different evaporator-only objective functions. Both of these objective functions are based on second-law parameters. The first is a non-dimensional form of the

total irreversibility generation in the evaporator, and the second is a weighted sum of the irreversibilities, also written in a non-dimensional form. While both objective functions are evaporator-only parameters, the weighted irreversibility equation takes into account the interaction of the evaporator with other components. The effect of taking into account these interactions is studied and discussed.

A later section shows the irreversibility generation in each heat pump component, as well as local irreversibility generation rates in the evaporator. The last section presents the conclusions that can be drawn from the analysis.

6.2 Heat Pump Energy Values

The heat pump model used for this analysis (ORNL model; see Fischer et al., 1988) allows the user to specify the work input in the fan, as well as the heat losses in the different components and connection lines. The values used for this analysis are obtained from a sample file of the program (EXAMPLE1.HET), and are listed next,

fan energy input, W_{fan} = 575 W

discharge line heat loss, Q_{disln} = 443 W

liquid line heat loss, Q_{liqln} = 436 W

suction line heat loss, Q_{sucln} = -275 W

compressor can heat loss, Q_{can} = 9.5% of compressor power inlet.

The negative sign in Q_{sucln} indicates that heat transfer takes place from the environment to the refrigerant. The compressor energy consumption is calculated from a performance map as a function of the inlet and outlet compressor saturated temperatures. The water pump energy consumption is calculated assuming a constant efficiency equal to 0.3. Pump work is required for two purposes. The first is to pump the water through the evaporator duct. The energy consumption required for this is calculated from the basic fluid mechanics equation for the water (Chapter 3). The second purpose is to pump the water from a water reservoir to the heat pump. This power is taken into account by assuming that the pump has to overcome a total head of 50 m to pump the water into the heat pump.

6.3 Irreversibility and Exergy Calculations

Two alternative methods to calculate irreversibilities have been used in the past. The first method is to use the Gouy-Stodola relation. This relation establishes that the irreversibility is proportional to the rate of generation of entropy, with the proportionality constant being equal to the temperature of the dead state (see discussion below). The second method consists of using an exergy balance method. Since irreversibility represents the destruction of useful work (exergy), the irreversibility can be calculated as the difference between inlet and

outlet exergies. While both the Gouy-Stodola and the exergy balance methods are perfectly equivalent, the exergy balance method has been applied extensively in the past to heat pump analysis (Reistad, 1973; Tsaros et al., 1987; Crawford, 1988), and is the method used in this analysis.

All exergy and irreversibility calculations require the selection of a dead state. An appropriate dead state temperature for a water-source heat pump is that of the inlet water, since this acts as a low-temperature reservoir. The water being fed into the heat pump is at atmospheric pressure, and therefore this is used for the dead state pressure. Wepfer and Gaggioli, 1980, recommend the use of a dead state pressure equal to the saturation pressure of the refrigerant at the dead state temperature. However, the dead state pressure does not appear in the irreversibility results, since it cancels out in the exergy balances, and therefore the selection of a dead state pressure has no effect on the results of this analysis.

The irreversibilities in the heat pump components are calculated by using the following expression (Crawford, 1988),

$$I = W + \Sigma(m_{in}\ EX_{in}) - \Sigma(m_{out}\ EX_{out}) + \Sigma(1-T_o/T_i)Q_i \quad (6.1)$$

in this equation, I is the irreversibility generation rate, W is the work rate, m is the mass flow rate, Q is the heat transfer rate, T_o is the dead state temperature, and EX is

the flow exergy, given as,

$$EX = (h-T_o s) - (h_o-T_o s_o) \tag{6.2}$$

Equation (6.1) takes the following forms when applied to the different heat pump components.

For the compressor,

$$I_{comp} = W_{comp} + m_r\ (EX_{comp,in} - EX_{comp,out}) \tag{6.3}$$

For the condenser and fan,

$$I_{cond} = W_{fan} + m_r\ (EX_{cond,in} - EX_{cond,out}) + m_{air}\ (EX_{air,in} - EX_{air,out}) \tag{6.4}$$

For the expansion device (considered adiabatic),

$$I_{exp} = m_r\ (EX_{exp,in} - EX_{exp,out}) = m_r\ (s_{exp,out} - s_{exp,in}) \tag{6.5}$$

For the evaporator and connecting lines from the water reservoir to the heat pump,

$$I_e = m_r\ (EXe,in - EX_{e,out}) + m_f\ (EX_{f,pump,out} - EX_{f,e,out}) \tag{6.6}$$

For the water pump,

$$I_{pump} = W_{pump} + m_f\ (EX_{f,pump,in} - EX_{f,pump,out}) = (1-\cap)\ W_{pump} \tag{6.7}$$

For the connecting lines,

$$I_{line} = m_r\ (EX_{line,in} - EX_{line,out}) \tag{6.8}$$

in this last expression, the subscript line can represent

either the suction, discharge or liquid lines.

Heat losses to the environment do not appear in the equations, because energy losses to the environment are not recoverable as work, and therefore are considered as irreversibilities.

The present analysis also divides the irreversibilities in the evaporator as pressure drop irreversibilities and heat transfer irreversibilities. Although the exergy balance method of irreversibility calculation is not as convenient for separating both irreversibility components as the Gouy-Stodola relation, the separation can still be accomplished by using a method outlined by Ranasinghe et al., 1989. In this method, the total irreversibility is first calculated. Then, the pressure drops are made equal to zero and the irreversibility calculations are repeated. The irreversibility calculated with no pressure drop is the thermal irreversibility. Once the total and thermal irreversibilities are calculated, the pressure drop irreversibility can be calculated by using the following expression,

$$I_{dp} = I - I_{dT} \tag{6.9}$$

This method is expected to give exact results in the case of incompressible fluids. However, when any of the fluids is compressible, or if one of the fluids evaporates or condenses, the results are only approximate. This is

because there are two components of pressure drop. Frictional pressure drop and acceleration pressure drop (Chapter 3). The pressure drop irreversibility is only caused by the frictional pressure drop, since the acceleration pressure drop is recoverable as work. Making equal to zero the total pressure drop is equivalent to neglecting the acceleration pressure drop compared to the friction pressure drop. Fortunately, this is not a bad assumption in this case, since friction pressure drops were found to be at least an order of magnitude higher than acceleration pressure drops.

Heat transfer irreversibilities can also be calculated by a method given by Tsaros et al., 1987. This method calculates heat transfer irreversibility by evaluating the exergy lost by the refrigerant due to heat transfer and the exergy gained by the water due to the same heat transfer. The difference between the exergy lost by the refrigerant and the exergy gained by the water is the heat transfer irreversibility in the heat exchanger.

The two methods were used to calculate the total heat transfer irreversibility for the overall optimum water-source heat pump (l=20 m, R_o=0.01 m, N=8 and V=4.2x10^{-4} m^3/s). The results are shown in Figure 6.1. The results show a good agreement in the whole range, with small differences caused by acceleration pressure drops and errors in calculating average temperatures (the method by Tsaros et al. requires the calculation of average heat

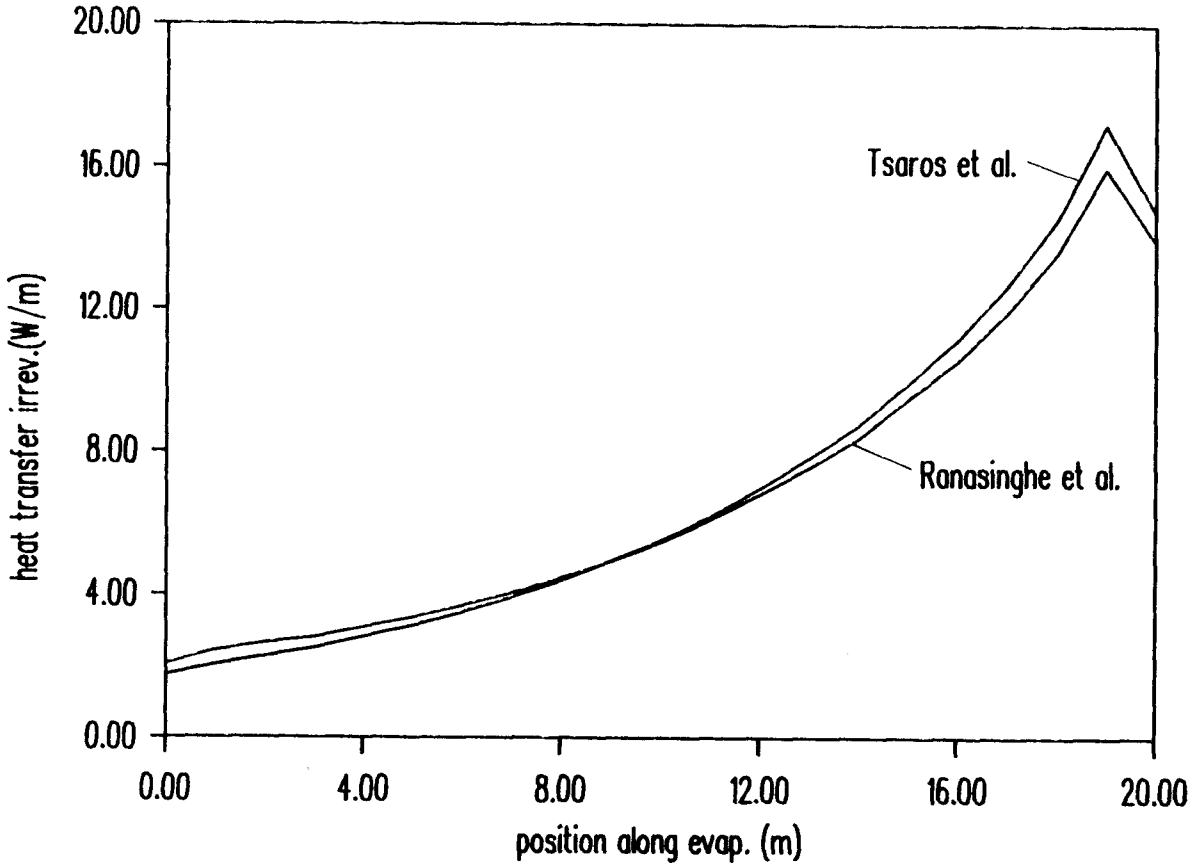

Figure 6.1 Comparison of the thermal irreversibility obtained by using the exergy balance method (Ranasinghe et al.) to that obtained by using the entropy generation due to heat transfer (Tsaros et al.)

transfer temperatures). Therefore, the two methods are considered equivalent.

6.4 Second-Law Optimization of the Heat Pump Evaporator

This section shows an optimization of the water-source heat pump evaporator described in the previous chapters. Chapter 5 presented the optimization of the overall water-source heat pump. All the decision variables used for the optimization were selected as evaporator parameters. Therefore, the results in Chapter 5 give a set of evaporator parameters that maximizes the efficiency of the overall heat pump.

This section shows a restricted (single degree of freedom) optimization of the water-source evaporator. The objective functions used in this section are not overall heat pump performance factors, but rather evaporator irreversibility generation rates. Therefore, this section shows an "isolated" optimization of the evaporator. The optimization is done with respect to two objective functions, one of which does not take into account the interaction of the evaporator with other components and another one that does. The purpose of this section is to present the methodology and compare the results of these optimizations with the design that optimizes the overall heat pump obtained in chapter 5. This section describes first the objective functions used, the design variable and other dimensions, and then the optimization results.

6.4.1 Objective Functions: Two objective functions are used for this optimization. Both of these are evaporator-only irreversibility generation rates, and are presented next.

a) Irreversibility generation rate: The first objective function used here is the total irreversibility generated in the evaporator. Since the evaporator duty (heat transfer rate) is not constant, the total irreversibility generation rate is scaled by dividing it by the evaporator duty. This gives a non-dimensional irreversibility generation rate, similar to that defined by Bejan, 1978, as the number of entropy generation units.

Irreversibility generation in the evaporator includes pressure drop irreversibilities in the water and refrigerant sides, as well as a heat transfer irreversibility. The heat transfer irreversibility in the evaporator can be written as the result of substracting the exergy gained by the water from the exergy lost by the refrigerant as both fluids circulate through the evaporator. The total irreversibility generated in the evaporator can then be written as,

$$I = I_{dpr} + I_{dpf} + (EX_{e,in} - EX_{e,out}) - EX_{f,out} \quad (6.10)$$

In Equation (6.10), the initial exergy of the water is zero. Therefore, the exergy gained by the water is equal to the outlet water exergy. The objective function is given by Equation (6.10) divided by the evaporator duty.

As can be seen, all the parameters included in the analysis are evaporator variables, and therefore this method does not account in any way for interactions between the evaporator and other components.

b) Weighted irreversibility generation rate: In this method, the total irreversibility generation rate, given by Equation (6.10) is modified by introducing weight factors, as follows,

$$I_w = I_{dpr} W_{dpr} + I_{dpf} W_{dpf} + (EX_{e,in} - EX_{e,out}) W_{dtr} - EX_{f,out} W_{f,out} \quad (6.11)$$

The weight factors have the purpose of taking into account the interactions of the evaporator with the other heat pump components. The weight factors have been used by London and Shah, 1983, to take into account the cost of each irreversibility in the overall system. The weight factor associated with each type of irreversibility represents the additional irreversibility generation in the whole system caused by an extra unit of the given type of irreversibility. Therefore, W_{dpr} represents the added irreversibility generation in the overall system caused by a unit increase in I_{dpr}, and the same applies for all the other weight factors in Equation (6.11).

Some of the weight factors can be determined immediately from the system structure. The pressure drop irreversibility in the water side is overcome by a pump that has an efficiency equal to 0.3. Therefore, an extra unit of pressure drop irreversibility causes an increase in

pumping power equal to 1/0.3 = 3.33. Since all this pumping power is spent in overcoming pressure drops or pumping heads, all the added energy fed to the pump eventually becomes a system irreversibility. Therefore, Wdpf=3.33. The exergy of the cold water that flows out of the evaporator has some value because it could be used for seasonal thermal storage, where the cold water is stored to provide air conditioning during the summer months (Fischer and Nephew, 1976). However, seasonal thermal storage requires substantial extra hardware, like a big storage tank and control instruments, and this option is not considered here. Therefore, the value of this exergy is considered equal to zero for this analysis, and $W_{f,out}=0$.

The weight factors for the refrigerant pressure drop and the refrigerant thermal exergy loss depend on interactions with the rest of the heat pump components, and therefore cannot be evaluated directly. However, the existence of a simulation code for the overall heat pump makes it possible to use the method presented by Ranasinghe et al., 1989, to evaluate these weight factors. This method is basically a numerical calculation of the weight factors. To calculate W_{dpr} by using this method, a small additional pressure drop is introduced arbitrarily in the simulation code. This causes an increase in the refrigerant-side pressure drop irreversibility, and also an increase in overall heat pump irreversibility. Dividing the increase in overall heat pump irreversibility by the

increase in refrigerant-side pressure drop irreversibility yields the value of the weight factor for pressure drop. Doing this calculation results in W_{dpr}=2.45.

Introducing a small pressure drop in the simulation code causes an increase in pressure drop irreversibility in the refrigerant side, and an increase in overall system irreversibility. However, it also causes changes in the thermal irreversibility and in the water-side pressure drop irreversibility. The method used to calculate W_{dpr}, described in the previous paragraph, assumes that these changes in other irreversibility sources are small compared to the changes in pressure drop irreversibility in the refrigerant side and overall heat pump irreversibility. Although this is true in the calculation of W_{dpr}, it is not the case in the calculation of W_{dtr}. The calculation of W_{dtr} requires correcting the change in total irreversibility generation to take into account the changes in other irreversibility sources, as discussed next.

To calculate W_{dtr}, the inlet water temperature is reduced by a fraction of a degree. This produces a change in thermal irreversibility and a change in total heat pump irreversibility. However, reducing the water temperature also produces an increase in pressure drop irreversibility in the water side (an increase in pumping power). This increase exists because reducing the water temperature increases the duct blockage by ice in the duct. Therefore, more power is required to pump the water through the duct.

This increase in pumping power is not negligible. In this case, the increase in overall heat pump irreversibility has to be corrected by substracting to it the increase in pumping power. The result of this substraction is then divided by the change in thermal irreversibility to obtain W_{dtr}. The resulting value for W_{dtr} is 0.84. With these values for the weight factors, the objective function becomes,

$$I_w = 2.45\ I_{dpr} + 3.33\ I_{dpf} + 0.84\ (EX_{e,in} - EX_{e,out}) \quad (6.12)$$

The objective function is Equation (6.12) divided by the evaporator duty.

6.4.2 Decision Variable and Evaporator Parameters: This analysis presents a single-degree-of-freedom optimization of the evaporator. The decision variable is the water flow rate into the evaporator. There is necessarily an optimum value of the water flow rate, because low water flow rates produce duct blockage by ice and this increases substantially the pressure drop. Increasing excessively the water flow rate also causes a decrease in heat pump performance, due to the high pumping power necessary to pump the water through the 50 m head and through the evaporator (see Chapter 5).

The other evaporator parameters are fixed at the values obtained for the optimum evaporator, as calculated in Chapter 5 and given in Table 5.5. These values are

l=20 m, R_o=0.01 m, and N=8. Other heat pump parameters are fixed at values given in Section 4.4.

6.4.3 Optimization Results: Figures 6.2 and 6.3 show respectively the total irreversibility generation and the weighted irreversibility, as given by Equations (6.10) and (6.12). The curves have about the same shape. In the low-flow range, ice blockage in the duct dominates, producing a substantial increase in pressure drop. High flow rates cause increases in pumping power. The optimum point is a balance between these two factors. The optimum points are equal for the two figures, and also coincide with the flow that optimizes the overall heat pump (4.2×10^{-4} m^3/s).

Dividing Equations (6.10) and (6.12) by the evaporator duty results in the non-dimensional irreversibility curves shown in Figure 6.4. The evaporator duty is fairly constant throughout the range of water flow rates, and therefore dividing both equations by the duty does not change the shape of the curves or the optimum point. The optimum points again correspond with the design that optimizes the overall heat pump.

Figure 6.5 shows the ratio between pressure drop and heat transfer irreversibilities in the evaporator. This ratio has been titled irreversibility distribution ratio by Bejan, 1979. Bejan also pointed out that this ratio should have a value close to unity at the optimum point. This is true here. In addition to this, the irreversibility distribution ratio has its minimum value at the optimum

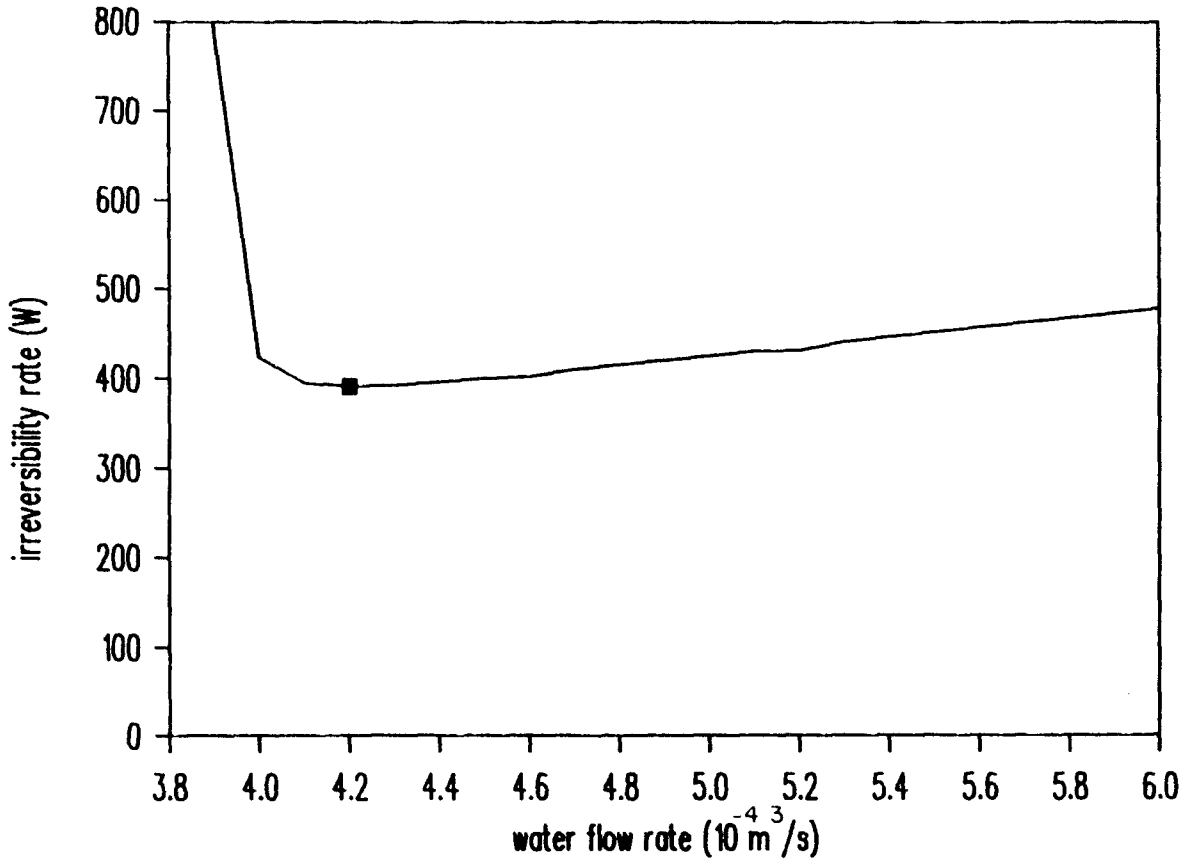

Figure 6.2 Total irreversibility generation in the evaporator as a function of water flow rate. The optimum point is indicated by a block.

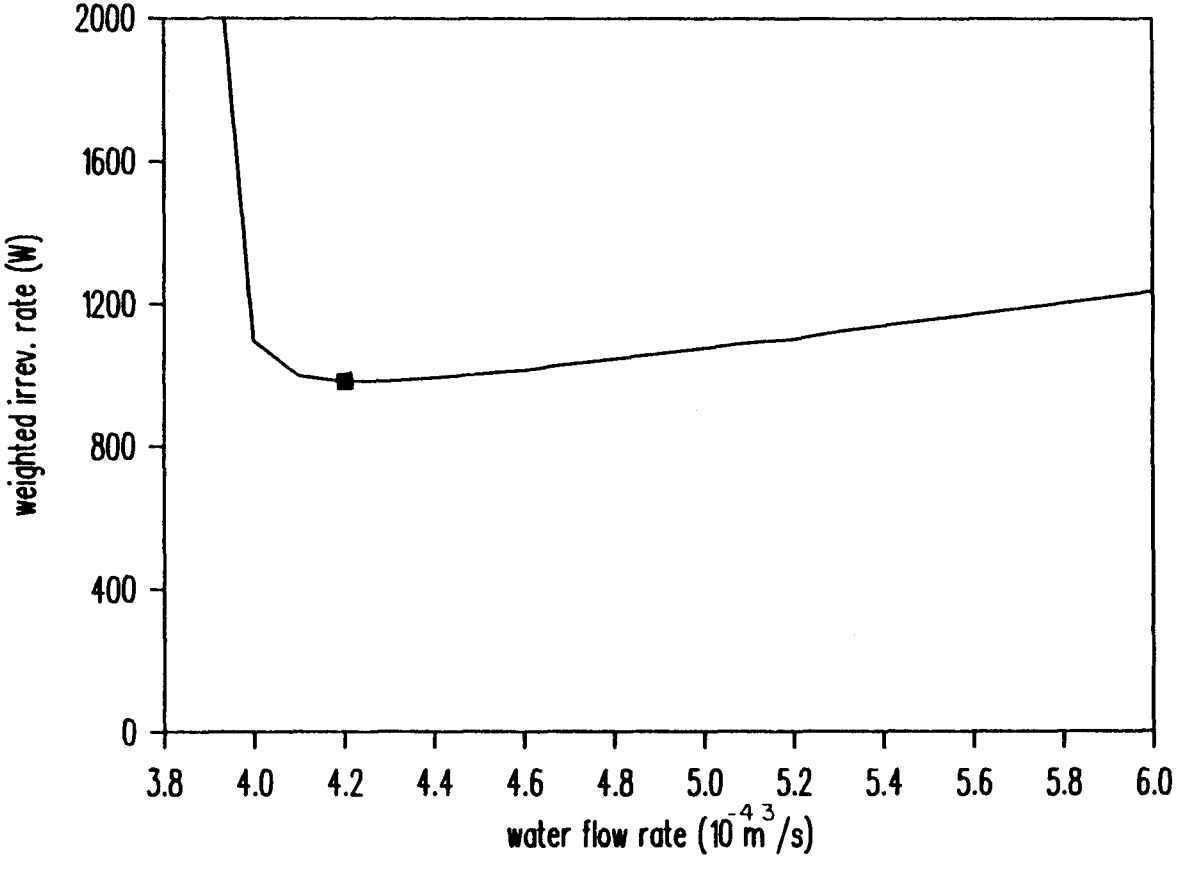

Figure 6.3 Weighted irreversibility generation in the evaporator as a function of water flow rate. The optimum point is indicated by a block.

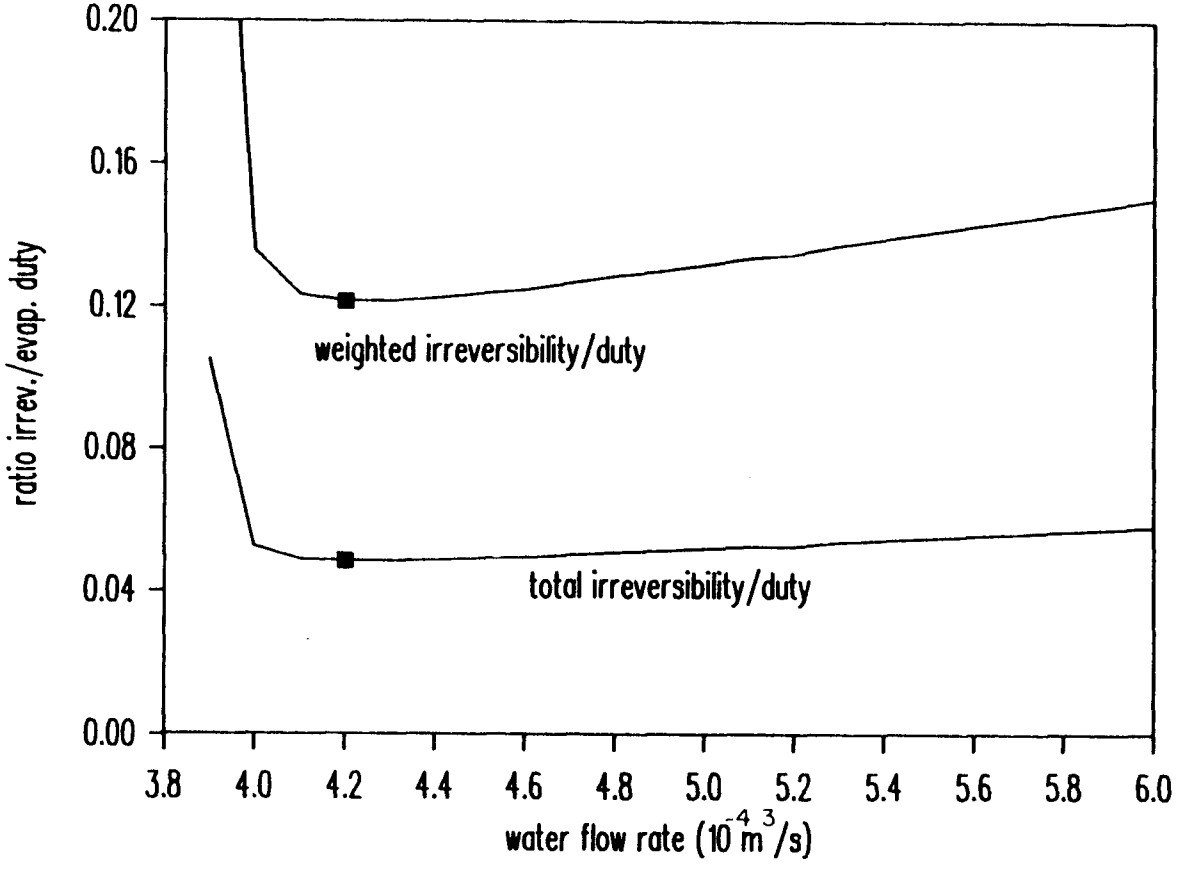

Figure 6.4 Objective functions (total irreversibility divided by duty and weighted irreversibility divided by duty) as a function of water flow rate. The optimum points are indicated by blocks.

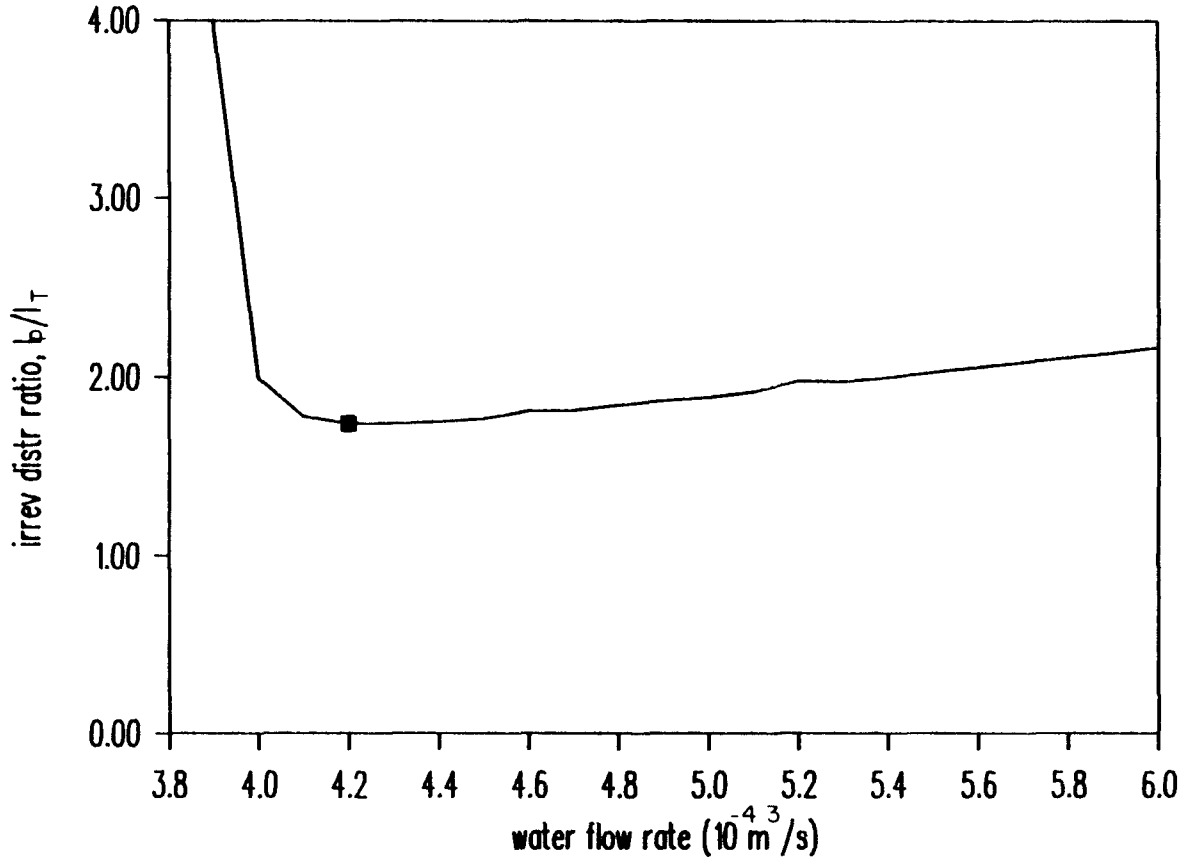

Figure 6.5 Irreversibility distribution ratio (pressure drop irreversibility divided by heat transfer irreversibility) as a function of water flow rate. The optimum point is indicated by a block.

point. This can be expected in a system like the one analyzed here, where the trade-off that determines the optimum is between two different sources of pressure drop, and thermal irreversibility does not have much effect in determining the optimum.

The results presented here show that both objective functions yield an optimum evaporator that coincides with the evaporator that optimizes the overall heat pump. This result is expected for the weighted irreversibility objective function, since this takes into account the interactions with other heat pump components. The use of the weighted irreversibility objective function should always yield designs that optimize the overall system for a variety of complex systems. The use of the irreversibility objective function also resulted in the design that optimized the overall system. However, this is not the case in most instances, because the irreversibility objective function does not take into account any interaction of the evaporator with other components. The optimum design coincided in this case with the optimum for the overall system because the operation conditions of the heat pump are not greatly affected by changes in the water flow rate, and therefore the interactions that would deviate the irreversibility optimum from the overall optimum are small.

Even though both methods were equally successful in calculating the optimum for the overall system, Figure 6.4

shows that the weighted irreversibility objective function reflects more accurately the real cost of irreversibility. Figure 6.4 shows that the irreversibility generated in the evaporator increases very slowly for water flow rates higher than the optimum. Therefore, a designer may think that operating the heat pump with a very high water flow rate, like $6x10^{-4}$ m^3/s, is almost as good as operating at the optimum flow rate. The weighted irreversibility objective function takes into account pump inefficiencies, and therefore shows that operating the water at high water flow rates produces a significant decrease in performance.

6.5 Irreversibility Analysis of the Optimum Heat Pump

This section shows the results of the irreversibility analysis of the optimum heat pump obtained in the previous section. The heat pump model (ORNL model) uses lumped analyses for the compressor, condenser, expansion device, and connecting lines. Therefore, only overall irreversibility generation values are reported for these components. The evaporator irreversibility calculations include an evaluation of local irreversibility rates along the circuits.

Table 6.1 shows second-law values for the heat pump. The table includes energy input to components, exergy gain rates and irreversibility values. All values are expressed in Watts, and then as a percentage of the total work input. The table also includes two different exergetic

Table 6.1 Second-law values for the optimum water-source heat pump. The table shows power consumption rates, exergy gain rates, irreversibility generation rates, and two different exergetic efficiencies for the system, one that takes into account the exergy of the water, and another that does not. All energy and irreversibility rates are expressed both in Watts and as a percentage of the total work input.

energy inputs	W	%
compressor	2600	66.4
fan	574	14.7
water pump	743	19.0
exergy gains	**W**	**%**
compressor air	821	21.0
evaporator water	82	2.1
irreversibility generation	**W**	**%**
compressor	978	25.0
discharge line	106	2.7
condenser[1]	934	23.8
liquid line	31.4	0.8
flow control device	60.8	1.6
evaporator[2]	391	10.0
water pump	522	13.3
suction line	4.7	0.2
exergetic efficiencies		**%**
including water exergy		23.0
not including water exergy		21.0

[1] Includes fan power

[2] Includes irreversibility in the lines connecting the water reservoir with the heat pump.

efficiencies for the system. The first includes both the exergy of the water and the air, and the second takes into account only the exergy of the air. The results show that using the exergy of the water for cool storage results in an increase in efficiency of 2%.

As can be expected, the compressor is the main contributor to the total irreversibility. The heat exchangers also contribute substantially to the irreversibility, with the condenser producing most of the irreversibility (the irreversibility generation in the evaporator is only about 40% of that generated in the condenser). This is caused by the differences in temperatures between these components and the dead state. The evaporator interchanges heat at a temperature close to that of the dead state, while the condenser temperature is substantially higher than the dead state temperature. The high irreversibility generation rate in the condenser calls for increased condenser area.

For the evaporator, the irreversibility distribution ratio, I_{dp}/I_{dT} (Figure 6.5), gives valuable indications on possible improvements. In general, a very low irreversibility distribution ratio indicates that it is convenient to use fins, or some other heat enhancement device (Liang and Kuehn, 1988). However, in this case, the ratio has a high value. This indicates that pressure drop irreversibilities play the main role in the heat pump performance. Therefore, it would be convenient to reduce

pressure drop irreversibilities in the evaporator, either by avoiding duct blockage due to ice or by reducing the 50 m head existing between the water reservoir and the evaporator.

The irreversibility generated by the water pump is also significant, and the possibility of using a pump with a higher efficiency for this type of application should be explored.

Figure 6.6 shows local pressure drop irreversibility generation rates and thermal exergy losses in the evaporator as a function of the position along the duct. The thermal exergy loss in the refrigerant side shows a sharp peak near the end of the duct. This peak exists because at this point most of the refrigerant becomes vapor. This causes a substantial decrease in the heat transfer coefficient. The pressure drop in the refrigerant side increases substantially near the end of the duct, again because most of the refrigerant has boiled into vapor. Vapor flows at a higher speed than liquid, producing an increase in pressure drop. The pressure drop irreversibility in the water side increases sharply at the end of the duct (water and refrigerant flow countercurrent, so the entrance of the duct for the refrigerant is the end of the duct for the water). This sharp increase is due to duct blockage by ice. The ice profile inside the duct has been shown in the previous chapter. The thermal exergy loss in the water side is

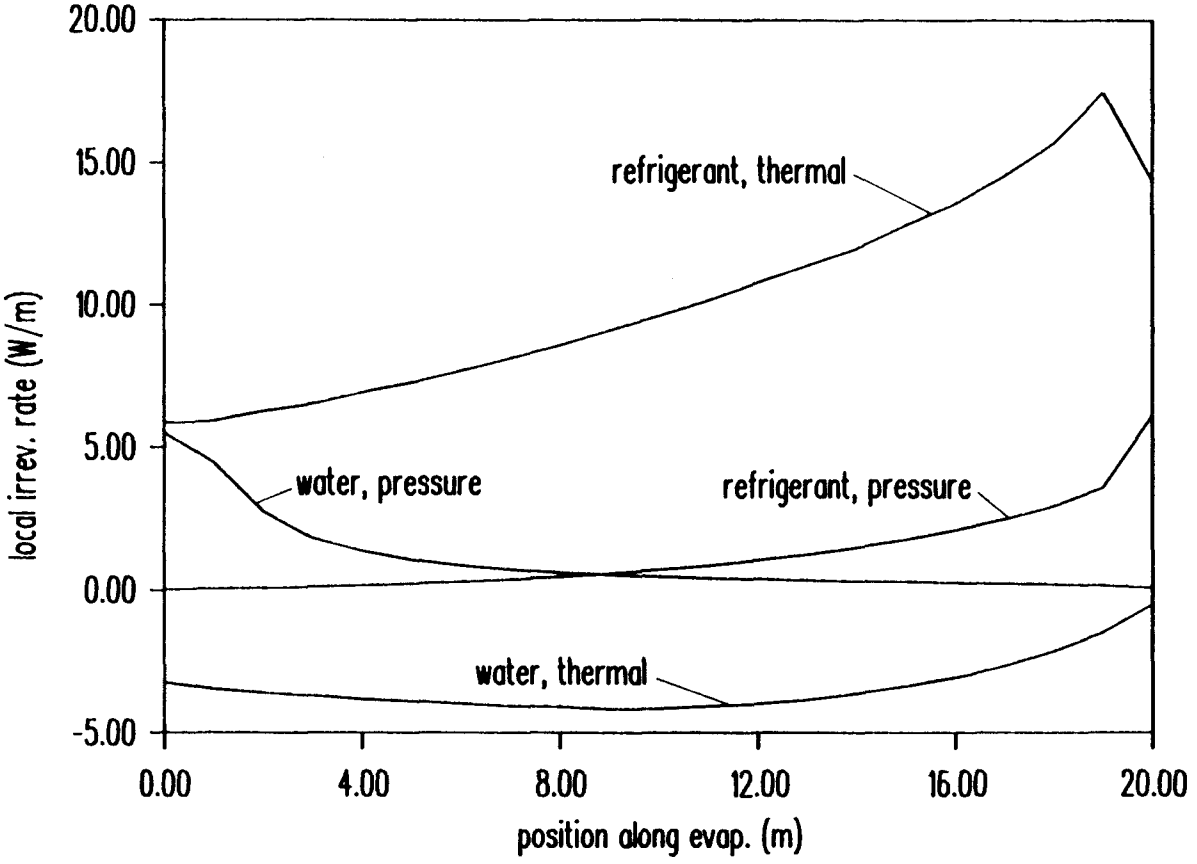

Figure 6.6 Local pressure drop irreversibility and thermal exergy loss in the two fluids circulating in the evaporator.

negative, because the water gains exergy along the evaporator.

6.6 Conclusions

This chapter has presented an irreversibility analysis of the water-source heat pump described earlier in the thesis. The chapter includes a second-law optimization of the evaporator with respect to two different objective functions. The purpose of this optimization is to illustrate the methodology and compare the optimum results with the optimum design obtained previously in an overall heat pump optimization (Chapter 5). Once the optimum design is obtained, irreversibility and exergy values are calculated for the optimum heat pump system.

The two objective functions used for the optimization are the total irreversibility generation in the evaporator divided by the evaporator duty, and a weighted evaporator irreversibility rate, also divided by the duty. While the irreversibility objective function does not take into account interactions of the evaporator with other heat pump components, the weighted irreversibility objective function takes into account these interactions through the use of the weight factors. The weight factors are calculated either directly from the system structure or by using the heat pump simulation program, according to a procedure shown in the chapter.

The results of the optimization yield optimum designs

for both objective functions that coincide with the optimum for the overall system. While this is expected for the weighted irreversibility objective function, it is unusual for the total irreversibility objective function, since this does not take into account interactions with other heat pump components. The reason for these two optimum designs being equal is that the optimization is restricted to a single decision variable, and changes of this variable in the whole range do not change substantially the operation conditions in other heat pump components. This limits the interactions that would otherwise deviate the minimum irreversibility evaporator from the overall system optimum.

The results also show the ratio of pressure drop irreversibility to heat transfer irreversibility in the evaporator (irreversibility distribution ratio). This ratio has a fairly high value for the whole range of conditions. This high value exists because the trade-off that determines the optimum is not between heat transfer irreversibility and pressure drop irreversibility, but rather between pumping power caused by duct blockage by ice and pumping power due to excessive water flow. The high ratio indicates that it would be very convenient to reduce the ice blockage in the duct or the pumping head required to pump the water from the water reservoir to the evaporator. However, neither of these options may be feasible in most cases.

The irreversibility analysis of the optimum heat pump indicates a very high condenser irreversibility and a fairly low evaporator irreversibility. While this is due partly to the temperature differences at which each of these components interchange heat with respect to the dead state, the result indicates that an increase in condenser area may help improve efficiency. The water pump is also a major source of irreversibility in the heat pump. Therefore, there is a substantial potential for improvement in this system by using a more efficient water pump.

VII. CONCLUSIONS AND RECOMMENDATIONS FOR FUTURE WORK

7.1 Conclusions

This thesis has presented a theoretical and numerical evaluation of water-source evaporators with freezing. The purpose of the thesis is to obtain improved heat pump performance by using the flow reversal method and selecting appropriate evaporator geometries. The thesis includes an introduction and literature survey, a theoretical and numerical evaluation of ice-maker evaporators, a description of a water-source/ice-maker heat pump simulation model, an optimization based on the heat pump model previously described, and an irreversibility analysis of the water-source heat pump. This section summarizes the main conclusions reached in each one of the parts of this thesis.

The theoretical analysis of the ice-maker evaporator uses a simplified model of a flat-plate evaporator immersed in a water reservoir. The purpose of this section is to find the water temperature in the reservoir that minimizes the total cost of operating the evaporator. The optimization is carried out with the cost of deicing the evaporator as a parameter. The calculation of evaporator performance as a function of water temperature and deice cost is then repeated for an overall heat pump system by using a detailed heat pump simulation code. This heat pump

simulation model is used to test the generality of the conclusions obtained from the theoretical analysis.

Even though there are great differences between the theoretical and the numerical evaporator models, the results obtained from both analyses agree in three important aspects. First, the heat pump simulation results indicate that heat pumps operating with no penalty for deicing should have a short operation cycle (operate as an ice-maker heat pump), in agreement with the results obtained from the evaporator analysis. Second, the heat pump simulation results and the evaporator results show a close relationship between water temperature and optimum operation cycle length. Third, the results obtained from both analyses indicate that the optimum heat pump corresponds in almost every case to either an ice-maker heat pump (frequent evaporator deicing) or to a water-source heat pump (no evaporator deicing). Intermediate conditions (heat pumps with a long operation cycle that require deicing) should be avoided, because they only rarely correspond to the optimum. In this way, all the main conclusions obtained from the theoretical analysis are true also for a detailed heat pump simulation. Therefore, these conclusions are expected to have a very extended validity.

Two evaporator geometries are analyzed for application to the overall heat pump simulation. Both evaporators are tube-in-tube heat exchangers with the water circulating in

the annulus and the refrigerant circulating in the inner tube. The difference between the two geometries is that one evaporator has four fins uniformly spaced in the water side, and the other evaporator has no fins. While the finned duct is expected to perform better than the evaporator with no fins, difficulties with the simulation code make it impossible to use this model for the overall heat pump model. Therefore, the heat pump simulation is based on the evaporator model with no fins.

The heat pump simulation uses the evaporator model previously described along with a steady-state model that simulates the high-pressure side of the heat pump. The steady-state model allows calculation of time-dependent heat pump performance during normal operation, because the heat pump can respond very fast to changes in evaporator conditions, so that it operates practically at steady-state all the time (quasi-steady-state). However, the model cannot be used to predict heat pump performance in highly time-dependent situations, such as deice cycles. Therefore, the heat pump model used here cannot be used to predict efficiency losses due to deicing.

The heat pump optimization calculations include an extensive evaluation of the effect that evaporator parameters have on heat pump performance. In addition, the calculations evaluate the advantages of using the flow reversal method. The results indicate that water flow direction reversals have two major effects. The first

effect is an increase in efficiency with respect to the no reversal case, and the second is a delay in the evaporator duct blockage by ice. This delaying effect may be of such magnitude as to avoid blockage altogether for some water flow rates. While an efficiency increase has a big importance on its own, a delay in duct blockage is of extreme importance for ice-maker heat pumps, because a delay allows them to operate for a longer time without the need for costly cycle reversals that reduce performance and may damage the compressor. For water-source heat pumps, reversing the water flow direction increases the difference between the optimum water flow rate and the flow rate that causes blockage. This is of great importance, because in the no reversal case this difference is so small ($3x10^{-5}$ m^3/s), that it would not be safe to operate with the optimum flow rate, since small variations in water flow rate or temperature could cause duct blockage. So the efficiencies shown in Table 5.5 for water-source heat pumps with no reversal cannot be reached in a practical case. Higher flows have to be used to avoid the possibility of blockage.

The irreversibility analysis performs two main tasks. The first is an overall heat pump irreversibility analysis that is helpful to indicate possible improvements in the overall system. The second one is an evaporator optimization. This optimization uses two objective functions. One is the total evaporator irreversibility

generation rate, and the other is a modified form of the total irreversibility generation rate, where weight factors have been included to take into account the interactions between the evaporator and other heat pump components. The purpose of this optimization is to illustrate the methodology and compare the optimum results with the optimum design obtained previously in an overall heat pump optimization.

The results of the optimization yield optimum designs for both objective functions that coincide with the optimum for the overall system. While this is expected for the weighted irreversibility objective function, it is unusual for the total irreversibility objective function, since this does not take into account interactions with other heat pump components. The reason for these two optimum designs being equal is that the optimization is restricted to a single decision variable, and changes of this variable in the whole range do not change substantially the operation conditions in other heat pump components. This limits the interactions that would otherwise deviate the minimum irreversibility evaporator from the overall system optimum.

7.2 Recommendations for Future Work

This thesis has shown that the flow reversal method can be used to improve heat pump efficiency in low-temperature water-source and ice-maker heat pumps.

However, two additional tasks are still left to be performed. The first task is to search for situations in which the flow reversal method offers higher performance improvements than those obtained here. The second is a validation of the results presented here. These two tasks warrant additional research. This thesis suggests the following areas of research to accomplish these tasks.

1. Evaluate other evaporator geometries besides the tube-in-tube evaporator with no fins used in this thesis. This evaluation may include, but is not limited to, the finned annulus model. Different evaporator geometries may prove more advantageous for the flow reversal method than the tube-in-tube evaporator considered here.
2. Evaluate experimentally the flow reversal method. This evaluation is useful for validating the results presented here. Also, an experimental evaluation may be useful to obtain improved conditions for the evaluation of the flow reversal method.

BIBLIOGRAPHY

1. S.M. Aceves-Saborio: "Analysis of Ice Formation for Application to an Ice-Maker Heat Pump," MS Thesis, Oregon State University, Corvallis, OR, 1987.

2. S.M. Aceves-Saborio, G.M. Reistad and H. Nakamura: "Analysis of Ice Formation With Flow Reversal for Application to a Water-Source Heat Pump," ASHRAE Transactions, Vol. 95, part 2, 1989a.

3. S.M. Aceves-Saborio, J. Ranasinghe and G.M. Reistad: "An Extension to the Irreversibility Minimization Analysis Applied to Heat Exchangers," Journal of Heat Transfer, Vol. 111, 1989b, pp. 29-36.

4. K.E. Atkinson: An Introduction to Numerical Analysis, John Wiley and Sons, New York, NY, 1978.

5. V.D. Baxter: "Intermediate Report on the Performance of Plate-Type Ice-Maker Heat Pumps," Oak Ridge Station Paper # ORNL/CON-23, Oak Ridge, TN, 1978.

6. V.D. Baxter: "Ice-Maker Heat Pump Development: Final Report," Oak Ridge Station Paper # ORNL/CON-50, Oak Ridge, TN, 1980.

7. V.D. Baxter: "Ice-Maker Heat Pump Harvesting Scheme Development and Ice-Packing Density," ASHRAE Transactions, Vol. 87 part 1, 1981, pp. 1429-1444.

8. A. Bejan: "General Criterion for Rating Heat Exchanger Performance," International Journal of Heat and Mass Transfer, Vol. 21, 1978, pp. 655-658.

9. A. Bejan: "Second-Law Analysis in Heat Transfer," Proceedings of the Workshop on The Second Law of Thermodynamics, Washington, DC, August 14-16, 1979.

10. H.S. Carslaw and J.C. Jaeger: Conduction of Heat in Solids, Oxford University Press, London, 1959.

11. J.B. Chaddock and J.A. Noerager: "Evaporation of

Refrigerant 12 in a Horizontal Tube with Constant Wall Heat Flux," ASHRAE Transactions, Vol 72, part 1, 1966, pp. 90-103.

12. P.F. Chapman and F. Roberts: Metal Resources and Energy, Butterworths, London, 1983.

13. J.C. Chen: "A Correlation for Boiling Heat Transfer to Saturated Fluids in Convective Flow," I & EC Process Design and Development, Vol. 5, 1966, pp. 322-329.

14. J.G. Collier: Convective Boiling and Condensation, 2nd. ed., Mc Graw-Hill, New York, 1981.

15. J. Crank: "How to Deal with Moving Boundaries in Thermal Problems," in R.W. Lewis, K. Morgan, and O.C. Zienkiewicz, editors: Numerical Methods in Heat Transfer, John Wiley and Sons, New York, NY, 1981.

16. R.R. Crawford: "An Experimental Laboratory Investigation of Second-Law Analysis of a Vapor-Compression Heat Pump," ASHRAE Transactions, Vol. 94, part 2, 1988, pp. 1491-1505.

17. D.F. Elger: "Design and Optimization of a Heating-Only Heat Pump for Western Pacific Northwest Applications," MS Thesis, Oregon State University, Corvallis, OR, 1983.

18. EPRI: Heat Pump Manual, EPRI EM-4110-SR, Electric Power Research Institute, Palo Alto, CA, 1985.

19. H.C. Fischer and E.A. Nephew: "Application of the Ice-Maker Heat Pump to an Annual Cycle Energy System", ASME paper 76-WA/Ener-4, 1976.

20. S.K. Fischer, C.K. Rice and W.L. Jackson: "The Oak Ridge Heat Pump Design Model: Mark III Version Program Documentation," ORNL/TM-10192, 1988.

21. S.D. Goldstein: "On the Calculation of R-22 Pressure Drop in HVAC Evaporators," ASHRAE Transactions, Vol. 85, part 2, 1979, pp. 122-131.

22. T.G.N. Haldane: "The Heat Pump, an Economical Method of Producing Low-Grade Heat From Electricity," J.I.E.E.E., 1930, p.666-675.

23. P. Juhola: "Method and Equipment for Utilization of the Freezing Heat of Water as a Source of Heat of a Heat Pump," Canadian Patent 1233330, 1988.

24. T.J. Kotas: The Exergy Method Of Thermal Plant Analysis, Butterworths, London, 1985.

25. F. Krauss: "The Heat Pump in Theory and Practice," Power, Vol. 54, 1921, p. 298-300.

26. H.G. Landau: "Heat Conduction in a Melting Solid", Quarterly of Applied Mathematics, Vol. 8, 1950, p. 81- 94.

27. J.H. Lee: "Analysis and Simulation of Dual-Source Heat Pumps with Three-Fluid Evaporators," Ph.D. Thesis, Oregon State University, Corvallis, OR, 1989.

28. H. Liang and T.H. Kuehn: Irreversibility Analysis of a Water to Water Mechanical Compression Heat Pump," in F.C. Chen, V.C. Mei and Z. Lavan, eds. Analysis and Applications of Heat Pumps, ASME AES-Vol 8, 1988, pp.31-36.

29. A.L. London and R.K. Shah: "Costs of Irreversibilities in Heat Exchanger Design," Heat Transfer Engineering, Vol. 4, 1983.

30. J.W. MacArthur and E.W. Grald: "Prediction of Cyclic Heat Pump Performance With a Fully Distributed Model and a Comparison With Experimental Data," ASHRAE Transactions, Vol. 93, part 2, 1987, pp.

31. V.C. Mei: "Laboratory Tests of a Residential Low-Temperature Water Source Heat Pump," ASHRAE Transactions, Vol. 89, part 2, 1983, pp.

32. M.J. Moran: Availability Analysis: A Guide to Efficient Energy Use, Prentice-Hall, Englewood Cliffs, 1982.

33. H. Nakamura, G.M. Reistad and S. Aceves-Saborio:

"Numerical Solutions for Laminar Heat Transfer in Parallel Plates with Freezing and Thawing by Using Periodic Flow Reversals," Proceedings of the 1989 International Symposium on Cold Regions Heat Transfer, Sapporo, Japan, 1989.

34. S.V. Patankar: Numerical Heat Transfer and Fluid Flow, Mc Graw-Hill Book Co. New York, NY, 1980.

35. G.B. Rackliffe and K.B. Schabel: "Groundwater Heat Pump Demonstration Results for Residential Applications in New York State," ASHRAE Transactions, Vol. 92, part 2A, 1986, pp. 3-19.

36. J. Ranasinghe, S.M. Aceves-Saborio and G.M. Reistad: "Irreversibility and Thermoeconomics-Based Optimization of a Ceramic Heat Exchanger," Journal of Engineering for Power and Gas Turbines, accepted for publication.

37. G.M. Reistad: "Availability Analysis of the Heating Process and a Heat Pump System," Symposium Paper, ASHRAE Annual Meeting, June 1973.

38. G.M. Reistad, J.G. Griffiths and S. Lang: "Evaluation of Dual-Source Evaporator for Residential Heat Pumps," ASHRAE Transactions, Vol. 90, part 1, 1984.

39. C.K. Rice, S.K. Fischer, R.D. Ellison and W.L. Jackson: "Design Optimization of Conventional Heat Pumps: Application to Steady-State Heating Efficiency," Contract W-7405-ENG-26, Oak Ridge National Laboratory, Oak Ridge, TN, 1981.

40. G.M. Rinaldi, L.W. Bonnell and C.T. Geary: "Supercooling of Water in ACES Heat Exchanger", Oak Ridge Station paper # ORNL/MIT-263, 1977.

41. P. Sampson and R.D. Gibson: "A Mathematical Model of Nozzle Blockage by Freezing," International Journal of Heat and Mass Transfer, Vol. 24, 1981, pp. 231-241.

42. W.M. Shah: "A New Correlation for Heat Transfer During Boiling Flow Through Pipes," ASHRAE Transactions, Vol. 82, part 2, 1976, pp. 66-86.

43. W.E. Stewart and C.L.G. Dona: "Development of Improved

Ice-Making Techniques for Storage Heat Pumps," ASHRAE Transactions, Vol. 94, part 2, 1988, pp. 419-431.

44. J.R.S. Thom: "Prediction of Pressure Drop During Forced Circulation Boiling of Water," International Journal of Heat and Mass Transfer, Vol. 7, 1964, pp. 709-724.

45. W. Thomson: "On the Economy of the Heating and Cooling of Buildings by Means of Currents of Air," Glasgow Philosophical Society Proceedings, 1852, p. 269-272.

46. T.L. Tsaros, R.A. Gaggioli and P.A. Domanski: "Exergy Analysis of Heat Pumps," ASHRAE Transactions, Vol. 93, part 2, 1987, pp. 1781-1797.

47. W.J. Wepfer, R.A. Gaggioli and E.F. Obert: "Proper Evaluation of Available Energy For HVAC," ASHRAE Transactions, Vol. 85, part 1, 1979, pp. 214-230.

48. W.J. Wepfer and R.A. Gaggioli: "Reference Datums for Available Energy," in R.A. Gaggioli, editor: Thermodynamics: second law analysis, American Chemical Society Symposium Series No. 122, Washington, D.C., 1980, pp. 77-92.